A MOLECULAR MODEL OF CLASSICAL COMPLEMENT ACTIVATION BY AQUAPORIN-4 AUTOANTIBODIES IN NEUROMYELITIS OPTICA AND PATHWAY-SPECIFIC CONTRIBUTIONS TO CENTRAL NERVOUS SYSTEM INJURY

By

JOHN NORBERT SOLTYS

B.S., University of Vermont, 2009

A thesis submitted to the

Faculty of the Graduate School of the

University of Colorado in partial fulfillment

of the requirements for the degree of

Doctor of Philosophy

Neuroscience Program

2016

This thesis for the Doctor of Philosophy degree by

John Norbert Soltys

has been approved for the

Neuroscience Program

by

Wendy Macklin, Chair

Jeffrey L Bennett, Advisor

V Michael Holers

Angeles Ribera

Ken Tyler

Date: August 19, 2016

Soltys, John Norbert (PhD, Neuroscience Program)

A Molecular Model of Classical Complement Activation by Aquaporin-4 Autoantibodies in Neuromyelitis Optica and Pathway-Specific Contributions to Central Nervous System Injury

Thesis directed by Professor Jeffrey L Bennett

ABSTRACT

Neuromyelitis optica (NMO) is a central nervous system autoimmune disorder that primarily affects the spinal cord and optic nerve, with worldwide representation and impact. Current therapeutics only marginally combat the aggressive morbidity and mortality of NMO, and effective treatment requires therapies that can specifically target mechanisms of the destructive autoimmune response. Aquaporin-4 autoantibodies (AQP4-IgG) are specific to NMO, and are pathogenic. Binding to CNS tissue causes astrocyte cell death with secondary demyelination. Human lesions display features of cytotoxic immune activation including IgG and complement deposition, and heavy immune cell infiltrate. Disrupted cellular homeostasis is also observed. It is critical to unravel at the molecular level how AQP4 autoantibodies coordinate CNS autoimmune destruction.

Clinical and experimental data have consistently distinguished AQP4-IgG mediated complement-dependent cytotoxicity as a coordinating effector mechanism in NMO lesion pathogenesis. AQP4-IgG activates complement to directly damage the CNS, and complement activation is necessary for lesion propagation to secondary demyelination. Understanding how AQP4-IgG activates the complement system to initiate lesion formation, and the sources of complement protein throughout lesion formation would provide significant insight into the molecular mechanisms driving lesion formation. The goal of my studies is to construct a molecular model of AQP4-IgG mediated effector complement activation and to characterize

the sources of complement protein during lesion formation.

The form and content of this abstract are approved. I recommend its publication.

Approved: Jeffrey L Bennett

DEDICATION

for my family - your continued support in my personal and professional endeavors is never taken for granted ($p<.05$)

ACKNOWLEDGEMENTS

I would like to first thank Dr. Jeffrey Bennett for providing an outstanding training environment. Your guidance as a research advisor and mentor has shaped how I approach scientific inquiry and function as a professional. You have inspired confidence to entertain any thought and step into the unknown with a healthy dose of humor, skepticism, and reason.

I also thank Dr. Gregory Owens for his support as a close collaborator. Your continuous presence in the laboratory and conversation at seminars and conferences was invaluable in developing my communication and critical thinking skills.

I would like to thank the past and present members of the Bennett & Owens laboratories: David Baldwin, Kevin Blauth, Kaitlyn Hickey, Markus Kowarik, Chiwah Lam, Yiting Liu, Adeline Matschulat, Andre Navarro, Cory Reiter, Alanna Ritchie, Kristin Schaller, Hannah Schumann, and Scott Wemlinger. It is a blessing to work in an environment with an entourage of friends. You have all made significant and essential contributions to the proceeding body of scientific knowledge and I thank you all for selflessly sharing the fruits of your labor. I extend a special thanks to Kevin Blauth and Alanna and the entire Ritchie family. The significant time and conversation that you have (both voluntarily and involuntarily) shared has kept me grounded and balanced, and continues to inspire my future motivations.

Thank you to Drs. Emily Gibson, Stephanie Meyer, and Diego Restrepo for your contributions to the STED imaging project. I also thank members of my committee – Drs. V. Michael Holers, Wendy Macklin, Angeles Ribera, and Ken Tyler - for continually pushing

me and providing avenues to participate in the scientific community at the highest possible level. Thank you for your encouragement and for generously sharing your time.

Thanks are also extended to the Neuroscience and Medical Scientist Training Programs and the Neurology Department for tremendous administrative and professional support: Matthew Bishop, Jodi Cropper, Emily Dailey, Leah Lleras, Diane Strong, and Deanne Sylvester, thank you.

Lastly, I thank my mice (IACUC Protocol #47213(05)1E) and above all, the patients who have generously shared a piece of themselves. It is an extreme honor and privilege to have shared in your story. I hope that your sacrifice will live on forever immortalized as something larger than life in the hearts you allow to beat, the eyes you give vision to, and the lungs you give breath to. Thank you.

TABLE OF CONTENTS

LIST OF TABLES

LIST OF FIGURES

LIST OF ABBREVIATIONS

ADCC: antibody-dependent cellular cytotoxicity

ADEM: acute disseminated encephalomyelitis

AQP4: aquaporin-4

AQP4-IgG: aquaporin-4 immunoglobulin G antibody

ASA: antibody spatial arrangement

BBB: blood brain barrier

BSA: bovine serum albumin

C1ql: C1q-like

C3aR: C3a receptor

C5aR: C5a receptor

CaAM: calcein-acetoxymethyl

CDC: complement-dependent cytotoxicity

CSF: cerebrospinal fluid

CH: constant heavy

CHO: chinese hamster ovary

CNS: central nervous system

CRISPR: clustered regularly interspaced short palindromic repeats

DABCO: 1,4-diazabicyclo[2.2.2]octane

DNA: deoxyribonucleic acid

DNP: dinitrophenol

EAE: experimental autoimmune encephalitis

EGFP: enhanced green fluorescent protein

ELISA: enzyme-linked immunosorbent assay

EM: electron microscopy

fB: factor B

Fc: fragment crystallizable

FcR: fragment crystallizable receptor

FITC: fluorescein isothiocyanate

FWHM: full width half maximum

GFAP: glial fibrillary acidic protein

HBSS: Hank's balanced salt solution

HEK: human embryonic kidney

HIV: human immunodeficiency virus

HLA: human leukocyte antigen

Ig: immunoglobulin

IHC: immunohistochemistry

IL: interleukin

LDH: lactate dehydrogenase

M1-AQP4: aquaporin-4 isoform beginning translation on methionine 1

M23-AQP4: aquaporin-4 isoform beginning translation on methionine 23

mAb: monoclonal antibody

MAC: membrane attack complex

MASP: mannose-associated serine protease

MBL: mannan binding lectin

MBP: myelin basic protein

MEM: minimal essential media

MS: multiple sclerosis

nAChR: nicotinic acetylcholine receptor

NGS: normal goat serum

NMDAR: n-methyl-d-aspartate receptor

NMO: neuromyelitis optica

NMO-SD: neuromyelitis optica spectrum disorders

OAP: orthogonal array of particles

PALM: photoactivated localization microscopy

PBS: phosphate buffered saline

PFA: paraformaldehyde

PI: propidium iodide

PKC: protein kinase C

PLP: proteolipid protein

PSF: point spread function

rAb: recombinant monoclonal antibody

SNP: single nucleotide polymorphism

STED: stimulated emission depletion

STORM: stochastic optical reconstruction microscopy

TBI: traumatic brain injury

Th: T helper

CHAPTER I

INTRODUCTION

Introduction

The work herein tests mechanisms of immune complement protein activation in the central nervous system (CNS) disorder neuromyelitis optica (NMO). Specifically, I will build a molecular model describing how aquaporin-4 autoantibodies activate the classical complement pathway to initiate astrocyte injury. I will then demonstrate how classical pathway cross-activation of the alternative complement pathway may contribute to CNS injury in *ex vivo* and *in vivo* NMO experimental lesions.

To provide background for the studies, I will first provide a broad overview of NMO (Section II), the autoimmune target aquaporin-4 (AQP4; Section III), and the complement system (Section IV). A more rigorous dissection of AQP4 autoantibodies (Section V) and lesion pathogenic mechanisms (Section VI) is then presented, concluding with an introduction of my hypotheses (Section VII). Figures are at the end of this and all chapters.

An Overview of Neuromyelitis Optica

Early History

In 1894, Eugene Devic (1858-1930) described a series of 17 patients with co-existing monophasic optic neuritis and transverse myelitis [1, 2]. He suggested that the cohort shared a novel syndrome labeled *"neuromyelitis optique."* Additional reports preceding and proceeding Devic's label introduced the possibility for a broader spectrum of clinical presentations [3-7]. For example, a relapsing clinical course was reported as early as 1829,

with vision loss and spinal pain accompanied by intractable vomiting [8, 9]. Reports, including one by the first physician to Louis XVII, also emphasized the mysterious anatomic predilection towards the spinal cord and optic nerve while the brain itself was generally unaffected [10]. In 1907, Peppo Achiote proposed to unify the syndromes to the *Societe de Neurologie de Paris* by making Devic the eponym of NMO: "*maladie de Devic"* [7].

The nosology of *neuromyelitis optique* would be debated for over a century to follow. Technologic and scientific advances fueled novel studies to understand if partially overlapping clinical presentations in fact reflected unique pathogenic mechanisms or instead represented variable presentations of a common mechanism. An intimate knot was tied between Devic's disease and "*disseminated sclerosis*", what is today appreciated as multiple sclerosis (MS). The two demyelinating disorders shared significant clinical and histopathologic findings [11]. In a seminal 1930 report [12], Russell Brain (1895-1966) concluded that "the clinical and pathological differences between *neuromyelitis optique* and *disseminated sclerosis* appear to be differences in acuteness and intensity only…there seems no justification for separating them." In decades to follow, the term neuromyelitis optica (NMO) was nevertheless applied to patients with simultaneous bilateral optic neuritis and transverse myelitis in attempts to better distinguish the disorders [13-17]. Although both MS and NMO may follow a monophasic or relapsing clinical course, NMO attacks were both more aggressive and clinically disabling. Longitudinally extensive spinal lesions spanned more than 3 vertebrae, an atypical finding of MS lesions. A high percentage of NMO patients, but not MS patients, died of respiratory failure [17]. However, the knot remained tied in the absence of definitive clinical criteria, laboratory testing, neuroimaging and histopathologic findings.

Diagnostic Criteria & The NMO Spectrum

A key breakthrough in understanding NMO came in 2004 with the discovery of a putative immunoglobulin (Ig) biomarker, NMO-IgG [18]. The Ig fraction of NMO patient serum, but not of MS and other myelopathies, was recognized to bind murine CNS tissue microvessels, pia, subpia, and Virchow-Robin space in a unique pattern detected via indirect immunofluorescence. AQP4, the predominant homeostatic water channel of the CNS, was recognized as the candidate autoantigen in 2005 [19] with AQP4-IgG serology incorporated into revised diagnostic criteria in 2006 [20]. The criteria facilitated the recognition of NMO as a distinct clinical disorder. AQP4-IgG was found to be highly sensitive and specific for NMO, and pathogenic (Chapter 1, Section V: AQP4-IgG). High specificity to NMO also allowed for the recognition of supporting laboratory and neuroimaging findings [21, 22], and an expanded appreciation for both more restrictive and more global clinical presentations including syndromes of the area postrema (irretractable nausea and vomiting >48 hours) [23-25], brainstem [26, 27], diencephalon (sleep disturbances including narcolepsy) [28, 29], and cerebrum [30, 31]. Peripheral involvement is absent.

Both historical and contemporary clinical presentations are now unified as neuromyelitis optica spectrum disorders (NMO-SD) [32]. Diagnosis requires at least 1 discrete core clinical attack affecting the spinal cord, optic nerves, area postrema, brainstem, diencephalon, or cerebrum; all may represent the initial presenting event at variable frequencies. AQP4-IgG serology and neuroimaging features supportive of NMO may facilitate the diagnosis. Clinical judgement is also required as no clinical feature is pathognomonic for NMO. The revised criteria aim to facilitate early diagnosis including the

recognition of inaugural forms, with the goal of reducing disease burden as early and aggressive clinical deficit is not recovered.

Additional Biomarkers

Beyond AQP4-IgG, other diagnostic biomarkers do not exist [33]. Furthermore, several caveats preclude the use of AQP4-IgG as a marker of active CNS injury (Chapter 1, Section V: AQP4-IgG). NMO is broadly appreciated as a disorder of pathologic autoimmunity whereby inflammatory, demyelinating lesions cause CNS tissue injury [34, 35]. The clinical utility for biomarkers of CNS injury including damaged astrocyte, neuron, and blood brain barrier (BBB) protein remains unclear [33]. Immune complement system analyses indicate variable alterations in pathway activation [36-38], and the pro-inflammatory cytokine/chemokine footprint is supportive of a dysregulated B cell response [39], promotion of a T helper (Th) 17 response [40, 41], and granulocytic activation [40]. While the array of CNS/immune proteins hold promise for greater diagnostic accuracy and individualized care, the markers are non-specific and more research is needed to delineate their clinical and diagnostic utility for NMO-SD.

Lesion Pathology

NMO patient spinal cords display diffuse swelling and softening at multiple spinal segments, variable myelin and axon loss, and necrosis of both gray and white matter. Vascular fibrosis and hyalinization coincides with an increased density of blood vessels [42, 43]. Multiple studies support that AQP4 and glial fibrillary acidic protein (GFAP) immunoreactivity loss occur early in lesion formation and indicate the rapid destruction of

perivascular astrocyte populations [44-46]. Myelin loss is secondary; myelin integrity ranges from normal to demyelinated in regions of astrocyte loss. Oligodendrocytes in early lesions display nuclear chromatin condensation indicative of apoptosis [44, 47]. Variable neuronal damage has been reported [42, 47]. A population of unipolar and bipolar GFAP+ AQP4- progenitors initiates reparative gliosis [44]. Chronic lesions of spinal cord and optic nerve are gliotic with cystic degeneration, cavitation, and atrophy [42] [43].

Morphologically, patterns of AQP4 and GFAP are not uniform between and within lesions [47]. This may reflect that multiple destructive mechanisms drive tissue injury, and/or that multiple temporal stages of lesion progression are being captured. Immunologically, heavy macrophage and microglial infiltration, and prominent but variable eosinophillic and granulocytic perivascular infiltrate are observed in early active lesions [42, 47-49]. Few but present CD3+ and CD8+ T-lymphocytes, and a paucity of NK cells, are also noted [42, 50]. Perivascular IgG, IgM, and C9neo deposition are observed in what is generally described as a "rim and rosette" pattern [42]. The immunologic profile supports a large pathogenic role for humoral immunity. Lesions may also display evidence glutamate toxicity and disturbed water homeostasis [51, 52].

Prognosis

NMO-SD may follow monophasic or relapsing clinical courses [32]. Relapses are unpredictable, with most patients having secondary attacks anywhere between months to years after the initial attack. Relapse is common (~60% of all patients) within 1 year of developing a longitudinally extensive spinal cord lesion [53]. Overall, the clinical course is aggressive and deficit is incremental. Approximately half of all patients have severe visual

loss and motor issues after 5 years [54-57]. Respiratory failure by ascending myelitis is the most frequent cause of death. Historical estimates of mortality were approximately 30% at 5 years, although more recent estimates are close to 10% at 5 years [57, 58].

Epidemiology

Epidemiologic studies in NMO are challenging as population-based studies are difficult to perform for rare disorders and available data likely represents a non-uniform cross-study population given evolving diagnostic criteria. Disease prevelance is estimated at .053-.4/100,000 from studies in Japan, Cuba, Denmark, Mexico, and French West Indies [59-62]. NMO is estimated to account for 1-2% of all demyelinating disease in the United States, impacting 4000-8000 individuals [63]. NMO constitutes a higher percentage (20-48%) of demyelinating disease in the West Indies and Asia [64]. Cohorts from Mayo Clinic, John Hopkins, and University at Texas Southwestern had an average onset age of 41.1 (range 3-81), female to male ratio of approximately 7:1, and although patients were predominantly of white and African descent, ~10% of all disease was found in Latin Americans, Asians, and native Americans combined [63].

Pediatric NMO exists. Pediatric disease is similar, and the NMO-SD diagnostic criteria are considered sufficient for diagnosis [65]. However, differences are present and largely concern clinical observation and management. A greater percentage of cases are monophasic and may display a lesser female predominance [66, 67], recurrent cerebral symptoms are more common [68], and extensive spinal cord lesions are less specific for NMO [67]. Longitudinal observation of the clinical course may be required for a confident diagnosis.

Co-Existing Autoimmunity

Co-existing autoimmunity is not uncommon in NMO, with up to 1/3 of patients having additional autoimmune complications [69, 70]. Systemic lupus erythematosus (SLE), Sjogren's syndrome, and myasthenia gravis are most common amongst the 19 additional reported co-existing conditions [71]. The relationship is largely of clinical and diagnostic concern. As NMO displays restricted CNS involvement, the onset of peripheral involvement may warrant a more comprehensive diagnostic evaluation. The relationship between NMO and these disorders is unknown. NMO clinical onset has both preceded and proceeded that of alternate autoimmune disorders.

NMO Etiology

The etiology of NMO remains unknown. A common, clear genetic and/or environmental exposure has not been identified.

Familial Genetics**:** Cases of NMO in identical twins and in female family members have been reported, but represent only a small fraction (1-3%) of all cases [72-77]. Thus, any genetic association appears complex. This is not necessarily surprising as all inherited genes are collectively thought to contribute less than half of autoimmune susceptibility, even in genetic twins [78]. Curiously, a Caucasian mother-daughter pair developed NMO at different stages of life [75]. It is therefore possible that an environmental exposure over an underlying genetic susceptibility may cause NMO. Indeed, NMO patients may have a common genetic background that predisposes to pathologic autoimmunity. Autoimmune disease is present at a higher rate in the family trees of NMO patients compared to the general population, and

NMO patients may harbor additional anti-self antibodies in addition to AQP4-Ig [74, 79]. A common autoimmune background could also explain the high percentage of co-existing autoimmunity found in NMO patients.

Immune Genetics: Few studies have investigated human leukocyte antigen (HLA) alleles. In Japan, optical-spinal multiple sclerosis, now appreciated to be NMO, is associated with the DPB1* 0501 allele [80, 81]. However, approximately 60% of the population expresses the allele [81]. In Caucasian populations, HLADRB1*03 appears associated with AQP4-IgG seropositive NMO [82-84]. Associations with other immune regulatory genes and epigenetic modifications have not been reported. Complement genetic associations may be of particular interest given the plethora of pathogenic roles complement may play [85, 86], particularly any genetic profiles that may increase susceptibility for pathway activation. Investigations into NMO patient "complotype" may offer novel insights in this regard [87, 88]. Individual complement protein single nucleotide polymorphisms (SNPs) are thought to be of little consequence. However, combinations of complement protein SNPs (coined as one's "complotype") may predispose towards a more active or inactive complement system. More studies are needed to understand mechanisms linking immune genetic profiles to the development of NMO.

AQP4 Genetics: Genetic variations in AQP4 do not appear to be associated with NMO. 8 SNPs were found in a cohort of 177 NMO cases, of which only one was uncommon compared to the general population (R19I and R19T) [89, 90]. When introduced into human

AQP4, the SNP does not influence AQP4 assembly, membrane organization, or AQP4 autoantibody binding [91]. It is unknown if SNPs influence immune system development.

AQP4 polymorphisms are also found in the general population and have been reported in other neurologic conditions including sudden infant death syndrome [92], migraine [93], temporal lobe epilepsy [94], and stroke-associated brain edema [95]. Loss of function and gain of function polymorphisms have been reported in normal subjects, although functional conclusions require confirmation that the polymorphism does not impact surface expression and membrane organization [96]. Compelling evidence for a role of AQP4 SNPs in NMO is therefore lacking.

Environmental Exposures: Experimental evidence supports a possible role of molecular mimicry - whereby an immune response to a pathogen may elicit cross-reactivity to self antigens that share structural or sequence homology – in exposing a molecular determinant that may promote immune cross-reactivity with AQP4 [97]. AQP4-reactive T cells were found in the periphery of adult NMO patients at an increased prevalence compared to healthy controls . When collectively exposed to the entirety of the AQP4 sequence via a library of small peptides, the peptide spanning amino acids 61-80 (p61-80) induced a large, Th17-biased T cell response. p61-80 corresponds to a span of extracellular loop amino acids recognized by AQP4-IgG. Curiously, this amino acid span shares 90% sequence homology with amino acids p204-217 in *Clostridum perfringens* ABC-transporter, and 60-70% homology with ABC transporters in other clostridum species. *C. perfringens* is a ubiquitous commensal bacterium more frequently associated with enterotoxin-mediated food poisoning [98]. To test the potential for molecular mimicry, T cells were first primed by exposure to the

ABC p204-217 with a recall response tested by exposure to the AQP4 p61-80, and vice-versa. Significant cross-reactivity was observed [97].

Pediatric T cells have not been tested for cross-reactivity to *C. perfringens*, but cases may follow a viral prodrome [99]. A multivariate analysis on early life environmental exposures in a smaller pediatric population identified that breastfeeding and daycare may be protective against NMO, while exposure to Epstein-barr virus, cigarette smoking, or delivery via cesarean section did not infer a greater odds ratio [100]. In Japan, *Helicobacter pylori* or *Chlamydophila pneumonia* may be associated with AQP4-IgG [101]. Mechanistic explanations linking the exposure to AQP4 autoimmunity are unclear.

Treatment

Given the aggressive clinical course with accumulating disability, treatment goals are 1) to prevent future clinical activity and 2) to recognize a clinical relapse and administer rescue therapy as rapidly as possible to limit CNS damage [85, 86]. Assays that recognize early clinical activity and predict prognostic metrics are greatly needed to achieve these goals. It is not currently possible to predict when a clinical attack will occur. A detectable AQP4-IgG titer remains the greatest risk for a clinical attack: patients are at risk of relapse indefinitely and prolonged treatment is required, even with clinical remission [65].

There is no currently approved therapy; common approaches include immunosuppression and immunomodulation. Available agents – azathioprine, mycophenolate mofetil, rituximab, and corticosteroids – have been reviewed in significant detail [85, 86]. Overall, treatments are noncurative, only partially effective, and carry an undesirable safety and/or side-effect profile. The need for prolonged treatment may therefore

cause significant burden to the patient. Novel therapeutic strategies have been proposed to specifically combat some pathogenic molecular mechanisms driving CNS injury. Some – for example, complement therapeutics – have demonstrated early successes in clinical trials [102, 103]. More research into the efficacy of these approaches and better models of lesion molecular pathogenesis are needed. Treatments directed at lesion repair do not exist.

Aquaporin-4

Introduction

AQP4 was cloned from rat lung in 1994 based on sequence homology with other aquaporin proteins [104]. AQP4 is most abundantly expressed in the CNS, but is also expressed in kidney collecting duct epithelial cells, stomach parietal cells, airways, glands, and skeletal muscle [105, 106]. Structurally, 6 helical membrane-spanning domains and 2 shorter helical membrane domains surround an aqueous pore (Figure 1.1A) [107]. 3 extracellular loops are interweaved and of variable size. The N-terminus and C-terminus are both intracellular. The N-terminus plays a role in organizing AQP4 on cell membranes [108], and the C-terminus is involved in protein-protein interactions [109, 110]. Similar to other aquaporins, AQP4 is expressed as a tetramer on the cell surface (Figure 1.1B) [111, 112]. Tetramers are assembled in the endoplasmic reticulum and are then transported to the cell surface. Each monomer within the tetramer functions as a bidirectional water-selective channel that enables water flow across membranes in response to osmotic gradients [107].

Membrane Organization

The intracellular N-terminus plays a key role in the membrane organization of AQP4. Alternative splicing creates 2 isoforms, initiating translation at Met1 or Met23 to generate M1-AQP4 and M23-AQP4 isoforms respectively (Figure 1.1A) [113-115]. A longer isoform (Mz) has been reported in rat, but not mouse or human [116]. Early freeze fracture electron microscopy (EM) studies demonstrated that M1-AQP4 tetramers repel and are therefore isolated on cellular membranes, while M23-AQP4 tetramers organize into large arrays comprised only of AQP4 protein termed orthogonal arrays of particles (OAP; Figure 1.1C) [117]. AQP4 is the only known aquaporin to aggregate in large complexes on the cell membrane [118].

Super resolution PALM/STORM imaging using novel single molecule labeling approaches has begun to dissect the biochemical drivers and kinetic properties of AQP4 membrane assemblies. M1-AQP4 tetramers are highly mobile on plasma membranes while the larger M23-AQP4 OAPs are immobile [119-121]. Astrocyte protein machinery assembles M1- and M23-AQP4 into heterotetramers at variable isoform ratios [112]. In OAPs, the M1-AQP4 isoform forms a larger wall surrounding an inner donut of M23-AQP4 isoforms [122]. The membrane fluidity of AQP4 and the number and size of OAPs is therefore regulated by the ratio of M1:M23 isoforms within each tetramer. In primary glial cultures, N-terminus palmitoylation of M1-AQP4, calcium elevations, and protein kinase C (PKC) signaling impact AQP4 surface organization [112].

Significant questions remain as to what the homeostatic regulators of AQP4 membrane expression and organization are at the tissue level. The functional significance of membrane organization, and the more general biologic function of OAP assembly, are also

unknown. Presumably, AQP4 membrane organization is tightly regulated as AQP4 expression varies widely both between and within tissues [123, 124].

AQP4 in the CNS

AQP4 is polarized to astrocyte foot processes surrounding CNS vasculature, pial and ependymal surfaces in contact with the CSF in the subarachnoid space and ventricles, and retinal Muller cells [118]. OAP formation is higher in the spinal cord and optic nerve compared to other brain regions [125]. The mechanisms driving and functional purpose for the anatomic specificity of membrane organization are unclear. Functional proposals include regulated AQP4 water transport and cell-cell adhesion [126-129].

AQP4 function within the CNS has been largely characterized using AQP4 knock out (-/-) mice [118, 130]; humans lacking AQP4 have not been identified. At baseline, AQP4 -/- mice are generally normal in appearance, survival, growth, and neuromuscular function [131-133], although electrophysiologic and/or behavioral studies have deduced partial impairments in visual [134], auditory [135], and olfactory signaling [136]. Proposed mechanisms generally involve an impaired homeostatic regulation of extracellular ion concentration. The ability of AQP4 to function as a bidirectional water channel helps maintain normal CNS homeostasis as demonstrated by altered stress phenotypes in various experimental models of vasogenic and cytotoxic edema, and obstructive hydrocephalus [131, 132, 137, 138]. Impaired water permeability is also proposed to cause increased seizure duration [139], attenuated experimental autoimmune encephalitis (EAE) [140], and hamper glial scarring [141]. The impact that AQP4 isoform and membrane organization has on these processes is unknown.

The Complement System

Early Recognition

In 1891, Hans Buchner (1850-1902) and colleagues discovered a heat labile factor in blood capable of killing bacteria [142-144]. The substance was named alexin, the Greek translation being 'to ward off.' Jules Bordet (1870-1961) expanded the theory in 1895 to propose that in addition to an alexin-like factor, a heat-stabile substance referred to as sensitizer was required to prime bacteria for cell lysis [142, 145]. *Vibrio cholerae*, usually lysed within minutes of serum addition, were not lysed when serum was heat-inactivated at 56°C. However, bacteria were still coated with the substance sensitizer, and addition of non-activated serum to the pre-coated bacteria was sufficient to cause cell lysis. At the end of the century, Paul Ehrlich (1854-1915) proposed that amborecepters attached to the surface of specific pathogens, permitting an interaction with the sensitizer - which he termed complement - to lyse the target cell. Amboreceptors are recognized today as antibodies. Ehlrich's refined theory gave birth to complement nomenclature and recognized the system's key role in innate immunity [144-146].

Composition

The complement system is now recognized to comprise ~30-50 germline-encoded proteins including activating proteins, receptors, inhibitors and regulators that play a myriad of key homeostatic roles beyond lysing foreign cells [142, 147]. The high degree of protein phylogenetic conservation amongst both invertebrates and mammals may underscore the physiologic significance of system [148]. Complement participates in innate immunity, bridging innate and adaptive immunity, organ and immune system development, and in

maintaining physiologic homeostasis. Example processes include bone and cartilage development [149], angiogenesis [150], hematopoietic stem cell engraftment [151], liver regeneration [152], amphibian limb and eye regeneration [153], the clearance of apoptotic cells and debris [154], the development of the natural autoantibody repertoire [155], and multiple roles within the CNS as described later.

Activation occurs along a proteolytic cascade, with each sequential step building upon a previously exposed substrate [142, 156]. Activating proteins are largely synthesized by the liver and are circulate as inactive precursors. Complement activating surfaces may activate complement along three traditionally recognized pathways: the classical, alternative, and lectin pathways (Figure 1.2, Star 1). The surface features recognized by each pathway and early activated pathway proteins differ as briefly introduced in the following sub-sections (Figure 1.2, Black Boxes). All pathways converge to activate the common pathway, a proteolytic cascade that begins at protein C3 and ends with the inclusion of C9 into a membrane attack complex (c5b-9) that can lyse a targeted cell (Figure 1.2, Star 2/3). In addition to direct deposition on the target surface, activated common pathway complement products include soluble, diffusible fragments. C3a and C5a can serve as chemotoxins to recruit immune cells expressing C3a and C5a receptors (C3aR, C5aR; Figure 1.2, Star 4). Cell-cell interactions may be further facilitated by additional membrane receptors that interact with deposited activated fragments, for example C3b (facilitating cell opsonization) and C1q (Figure 1.2 Star 5). In a tissue environment, the binding of soluble proteins to neighboring cells may also modulate native tissue physiology (Figure 1.2, Star 6). Complement activation therefore has the potential to act directly on the targeted cell, promote

an inflammatory environment via immune cell recruitment and activation, and modulate the local tissue environment.

The array of functional roles highlight that a balance between complement activation and inhibition is critical to maintain normal physiology: in any given environment, the level of activation is finely tuned to maintain physiologic homeostasis and reflects both the local activation of specific pathway proteins and the local expression of complement inhibitors to prevent destructive, runaway activation. A clear distinction between activation at sublytic levels and lytic levels is appreciated. Indeed, the system is regulated at multiple levels along the activation cascade, allowing for the directed activation of select components (Figure 1.2, red X's). The large number of fluid phase and membrane bound regulators and inhibitors are reviewed elsewhere [142, 147, 157]. Of note, although spontaneous complement activation occurs throughout the body, the presence of complement inhibitors generally limits self-directed damage. This balance is of clinical significance as disruptions in either activation capabilities or inhibitory functions may promote a chronic inflammatory environment [147, 158]. Activation on foreign pathogens and subsequent elimination is highly efficient and tightly regulated.

Classical Pathway Activation

Bordet and Ehrlich's studies characterized what is today recognized as the classical complement pathway. Binding of the complement protein C1q to IgG- and IgM-bound antigens, B-amyloid, C-reactive protein, DNA, or apoptotic bodies can trigger C1 activation [147, 159]. Subsequent activation of the proteins C4 and C2 generate a convertase to activate C3 (Figure 1.2). C1q has a stem and tulips structure, with each stem supporting one globular

head capable of contacting the targeted surface [159-161]. The mechanism triggering C1q activation upon target binding remains unclear, as do the unique features of the target that facilitate high affinity C1q binding.

Classical Pathway Activation by IgG

An *in vivo* molecular model of C1q activation by IgG does not exist. Establishing a model is of considerable interest given the potential implications in autoimmunity and therapeutic design. Significant insight has been provided via studies largely directed at optimizing therapeutic monoclonal antibody (mAb) effector activity (examples include anti-CD20 and anti-HIV mAbs) [162, 163]. Early work first mapped the C1q binding site and later work recognized key organizational requirements to facilitate multivalent IgG:C1q interactions [162-170].

The IgG C1q binding site is located in the Fc CH2 domain (Figure 1.3A bottom) [165, 171]. Although the general location of the binding pocket is consistent between IgG subclasses, variations in amino acid composition impact C1q affinity [172]. *In vitro* and *in vivo* studies have recognized K322 as a key IgG1 amino acid contact [164, 169]. IgG1 mutagenesis studies and computer modeling indicate additional interacting residues including charge-charge, polar, and nonpolar contacts [168-170]. The contact site on C1q is located on a globular head (Figure 1.3A top) [160]. Therefore, each of the 6 globular heads of C1q has the potential to interact with IgG. Furthermore, each globular head likely contacts 2 antibodies [173, 174].

A low-level of activation may always occur in the bloodstream where IgG circulates as a monomer [175]. However, the affinity of C1q for monomeric IgG is very low [176,

177]; presumably, a high affinity multivalent interaction directs high level activation on IgG coated surfaces. The findings that antigen membrane fluidity and epitope exposure may limit activation further support that the geometric organization of multiple CH2 C1q binding sites is critical for high level activation [178-187]. Curiously, IgG crystallized into hexamers [171, 188-190]. The biologic function of IgG hexamers was thought to represent an evolutionary conserved functional relationship between IgG and IgM [191]. In contrast to IgG, IgM circulates as a pre-formed Ig multimer and activates C1q at high levels. The pre-formed multimeric platform would expose multiple C1q contact sites after IgM binds target antigen. IgG hexamers were thought to accomplish the same end-goal but via monomer assembly upon binding to a targeted surface. In support of this hypothesis, K322 was well exposed on IgG hexamers and patterned to engage all C1q globular heads [163, 171]. Indeed, a recent study spontaneously hexamerized IgG via site-directed mutagenesis, resulting in fluid-phase complement activation in the absence of target antigen [163]. Furthermore, cryo-EM modeling localized C1q over an IgG hexamer that was assembled after monomeric antibodies bound to DNP-coated liposomes. The study offers a general model to approach IgG:C1q interactions. Lower stoichiometry IgG:C1q interactions were not examined in the study, nor were the molecular drivers that may facilitate IgG assembly after surface binding.

A question remains how C1q binding to a multimeric IgG platform leads to subsequent C1 activation. Activation occurs by dislodging the C1r2:C1s2 complex that is normally packed within the collagenous stems of C1q [192]. Data favors that an outward movement of C1q collagenous stems dislodges the complex to expose the proteolytic active site [159, 160, 192]. Presumably, activation is directly stimulated by the IgG platform to ensure high-level activation on an appropriately targeted surface. The observation that

complement activation occurs on fluid-phase IgG hexamers in the absence of target antigen provides experimental support for this [163, 193]. However, the mechanism(s) inciting the mechanical stress remain at large. The C1q binding site needs to be adequately exposed, but this does not necessarily explain why activation may require a globular head contact on 2 neighboring IgG molecules [173, 174]. A consideration comes from mapping key IgG amino acid contacts on the C1q globular head. It is puzzling that amino acids at both the bottom and top of the globular head interact with IgG (Figure 1.3A-C) [160, 194]. Proposed models support that the initial IgG:C1q contact(s) allow a calcium ion to transfer from the globular head to IgG, inducing a change in the globular head electrostatic potential that allows the head to "roll" along IgG to form a thermodynamically favored interaction with a second set of amino acid contacts. This intrinsic molecular motor may inflict a mechanical stress sufficient for activation. Perhaps globular head rolling takes advantage of contacts on neighboring IgG molecules, with an IgG hexamer optimally organizing neighboring Fc domains to facilitate C1q globular head rolling.

The proposed model raises several questions as to what a sufficient IgG platform is that would incite mechanical stress, and how variations in platform organization influence the process. An IgG hexamer may optimally interweave both CH3 domain Fc-Fc interactions and CH2 domain Fc-C1q interactions to facilitate the process. *In vivo* models are needed to understand how IgG hexameric platforms may assemble over protein surfaces, and what molecular variables regulate the process.

Alternative Pathway Activation

The alternative pathway is spontaneously activated by a "tick-over" process from hydrolysis of C3, and does not require a specific protein interaction [147, 158]. However, the process may be accelerated by C3 binding to specific surfaces: gas bubbles, platelet membranes, biomaterials, repeating polysaccharides, endotoxin, IgA-containing immune complexes, C3 nephritic factor, and some immunoglobulin light chains [195]. Pathway activation can also occur via C3 fragments generated from classical and lectin pathway activity. The role of activation, given the non-specific nature, was therefore initially thought to serve as a positive feedback loop to amplify activation of the common pathway and accelerate target destruction [196]. A central role for the alternative pathway in driving clinical disease is now well appreciated [158]. Proposed molecular mechanisms relate to the pathway's potential to continually fuel complement activation and create a chronic inflammatory environment. Ongoing tissue destruction may therefore occur even after the inciting agent has been eliminated.

Lectin Pathway Activation

An interaction between the protein mannan-binding lectin (MBL) with microbial sugars was originally recognized to activate the lectin pathway [142, 197]. MBL shares significant structural homology to C1q; in this regard repetitive patterns of microbial sugars may stimulate high level MBL activation [161]. Ficolins 1-3 and collectin-11 can also activate the pathway [198, 199]. Potential interactions between MBL with IgG containing an agalactosyl (G0) carbohydrate (IgG-G0), IgM, and a bypass pathway that directly activates C3 have been reported [200, 201]. The lectin and classical pathway both activate C4 prior to

activating the common pathway, however, lectin pathway C4 activation occurs via mannose-associated serine protease (MASP) proteins rather than C2 (Figure 1.2).

CNS Complement Expression

CNS cells directly synthesize complement proteins, with neurons and glia capable of expressing the complete C1 through C9 activation cascade [202-205]. Astrocytes, oligodendrocytes, microglia, and neurons all synthesize regulators and receptors. C3aR and C5aR are widespread at the genetic and protein levels on neurons and glia. Unique families of complement proteins have also been discovered in the brain: cerebellins and C1q-like proteins termed C1ql1-3 [206, 207].

In general, complement inhibitors in the brain are not well characterized but expression appears to be low [202, 204]. The potential misbalance of inhibitors vs. activating proteins is puzzling. For example, oligodendrocytes don't generally express inhibitors despite the full potential for C1-C9 expression. Curiously, over half of the 50+ genes encoding putative complement regulatory proteins in the mouse genome are expressed in the CNS [202, 208]. Many of these are uncharacterized, but may offer insight into the apparent misbalance. Astrocytes stand out in expressing high levels of CD59, inhibiting the final step of the common pathway (C9 inclusion into c5b-9) [209]. CD59 expression is notable from the perspective of study design and interpretation. It is possible that high levels of common pathway activation may occur but be undetected, or misinterpreted as activated at lower levels, if c5b-9 is used as a marker to gauge overall pathway activity.

CNS Complement Function

Complement participates in both CNS development and homeostasis, primarily through classical and common pathway proteins. Both C1q and C3 -/- mice show alterations in synapse structure [210-212]. Resident microglia phagocytose C1q and C3b tagged synapses, and microglia-produced C1q may be released to enhance the process [212]. The functions of cerebellins and C1ql1-3 are unknown but may include the regulation of synapse development and synaptic plasticity [207, 213, 214]. Furthermore, neuronal lineage cells proliferate and respond to C3a-C3aR interactions, indicating roles in adult neurogenesis and stem cell maturation [215]. Complement plays a homeostatic role in removing apoptotic cells. C1q binding to apoptotic neuronal cells assists in C3b and C4b generation to facilitate clearance [154]. More global deficits in apoptotic cell removal observed in C1q -/- mouse are proposed to predispose one to autoimmunity. Lastly, sublytic levels of activated complement fragments promote cell survival: C3a, C5a and C1q supplementation promotes enhanced cell survival in culture, attributed to growth factor release [204, 216-218]. Sublytic c5b-9 deposition stimulates oligodendrocyte cell survival [219].

Given the range of roles that complement plays, deleterious activation could significantly disrupt CNS physiology by cross-activating endogenous processes. Complement activation has been observed in a range of neurodegenerative disorders including Alzheimer's, amyotrophic lateral sclerosis (ALS), and Parkinson's [203, 204]. However, elucidating the role of complement in the molecular pathogenesis of these disorders is challenging as it is difficult to distinguish if complement activation is directly causing the damage, or if activation reflects the cross-activation of endogenous processes (for example, synaptic remodeling or cellular waste removal). Pathologic activation may also

contribute to traumatic brain injury (TBI) via the alternative pathway, and amplify CNS vasculature damage in stroke via the lectin pathway [202-204]. Better models to study CNS complement activation are needed to fully elucidate pathway roles in health and disease, and to recognize how activation may tip from homeostatic to pathologic levels.

Complement and the Blood Brain Barrier

Preserving a partition between peripheral and central complement protein sources is paramount to maintain appropriate complement protein levels within the CNS. Blood brain barrier endothelial cells are critical in this regard. On one interface, the cells are exposed to peripheral complement proteins; on a second interface, the cells are exposed to intrathecal protein. BBB breakdown – a common observation in many CNS disorders - may allow peripheral proteins to leak into the CNS and disrupt the natural system regulation.

It is perhaps surprising that the endothelial cells themselves may serve as a complement-activating surface and play pro-inflammatory roles to amplify activation and/or promote cross-compartmental immune damage [204]. In response to stress, endothelial cells are primed as a complement-activating surface by exposing damage associated molecular patterns (DAMPs). Subsequent C1q binding may induce expression of adhesion molecules including E-selectin, intercellular adhesion molecule-1 (ICAM-1), vascular cell adhesion molecule-1 (VCAM-1), and release cytokines including interleukin (IL)-8, IL-6, and monocyte chemoattractant protein-1 (MCP-1) [220-223]. MBL may also compete with C1q binding. Cytotoxic roles of lectin pathway activation have been demonstrated in experimental models of oxidative stress, hypoxia, and TBI [204]. Early evidence supports that MBL activation may translate to human disease [224, 225]. The exposed molecules that MBL

binds remain unclear, except for cytokeratin-1 [226]. Endothelial cells also respond to activated complement fragments. MASP1, C3a, and C5a binding can induce NF-kB signaling, p38MAPK activation, and IL-6 and IL-8 cytokine production [227, 228]. C3a and C5a may also promote cytoskeletal modification [229, 230], and in addition to sC5b-9, vascular permeability [231-234]. Thus, while maintaining a wall that effectively divides 2 sources of complement proteins, BBB endothelial cells are active responders to the local environment and can serve as a source of activated complement proteins in CNS disease.

AQP4-IgG

Introduction

Significant efforts have been invested in understanding the relationship between AQP4-IgG and NMO. Initial assays detected serum AQP4-IgG via indirect immunofluorescence and ELISA and reported a mean sensitivity of 63-64%; optimized next generation cell-based serum assays with microscopy or flow-based detection report a mean sensitivity of 77%. [235-237]. AQP4-IgG is essentially 100% specific to NMO [238]. Although AQP4-IgG has been detected in patient serum prior to clinical onset, the natural history of AQP4-IgG is poorly understood [239]. Positive serology requires a clinical attack to diagnose NMO [240].

Pathogenicity

Multiple criteria have been proposed for determining the pathogenicity of putative immunoglobulin responses in human disease [241-244]. The historical rationale lies in a conscious adaptation of Koch's postulates [245]. Although the criteria vary, a general

framework involves: 1) Recognition of putative immunoglobulin antigen, 2) Demonstration of autoantibodies in inflicted population, and 3) Recapitulation of clinical and pathologic disease upon experimental transfer. The third criteria is reviewed below at multiple evidence tiers. The overwhelming consensus is that AQP4-IgG is pathogenic and the inciting agent driving CNS tissue destruction.

Direct Evidence: Direct evidence of pathogenicity can be demonstrated by human-to-human or human-to-animal transfer. Ethical considerations generally limit human-to-human transfer experiments. However, maternal to fetal trans-placental transmission may offer an experiment of natural biology in pregnant AQP4-IgG seropositive females. The pathogenic potential for transplacental transfer exists, as human embryos express AQP4 as early as 20 weeks [246, 247]. However, the transfer of NMO-like CNS pathology has not been documented to date. A caveat is that AQP4-IgG may cause placental damage incompatible with fetal life. 43% of women miscarry after NMO onset, compared to only 7% of total pregnancies (calculated retrospectively) prior to clinical onset [248]. Babies otherwise appear healthy and normal. A complementary experimental investigation in mice offered a putative mechanism for the miscarriages [247]. AQP4 rAb binding to the placenta at high concentrations induced NMO-like pathology that incited placental necrosis, causing fetal death and miscarriage. Lower titers produced inflammation compatible with placental survival and fetal life. AQP4 expression occurs late in developing embryos and is not polarized until P1-P3, precluding CNS studies in pups until after full-term delivery [249].

Human-to-animal transfer reproduces human NMO lesion pathology, with limited success recapitulating clinical phenotype. The latter may reflect the site of CNS damage in

experimental models and delivery method of AQP4-IgG. 3 distinct models have been developed to date: transfer with co-induction of EAE, direct CNS injection/infusion, and peripheral transfer with CNS flux mediated by BBB traumatic injury. Briefly, purified Ig from AQP4-IgG+ NMO patients (disease duration ≥3 years), but not AQP4-IgG- NMO patients, produced NMO like pathology in an EAE transfer model. Cross-absorption of AQP4-IgG supported AQP4 antigen specificity [250]. Bennett and colleagues (2009) also utilized an EAE model; transfer of an AQP4 autoantibody cloned from a human patient (AQP4 rAb, see later sub-section), but not isotype control rAb, recapitulated NMO lesion pathology [251]. Direct co-injection/infusion of AQP4-IgG/rAb with human complement has produced NMO pathology in the brain, optic nerve, and spinal cord [252-257]. Spinal cord pathology may produce clinical deficit [256]. Finally, peripheral administration of AQP4 rAb, but not isotype control rAb, causes CNS NMO pathology after a cortical needle prick to break the BBB [258]. Of note, all models have required the introduction of an inflammatory environment to produce NMO-like pathology. Peripheral or central infusion in the absence of inflammatory modulation does not cause typical CNS lesions despite high levels of bound autoantibody [259, 260]. This may underscore the significant contributions of the pro-inflammatory cytokine/chemokine environment in pre-disposing human tissue for injury. Thus, three distinct models have provided evidence of human-to-animal experimental transfer.

Indirect Evidence: To date, indirect experimental evidence of AQP4-IgG pathogenicity is lacking. One approach would be to recapitulate NMO-like pathology upon immunization with AQP4 protein. However, Ig generated in this fashion may not necessarily reflect a

natural repertoire of AQP4 autoantibodies [261]. A better understanding of how epitope reactivity may drive pathogenicity in NMO is needed to understand the utility of this model or to interpret any model where a lesion is incited using non-patient derived AQP4 antibodies [262]. An alternate approach to acquire indirect evidence would be to induce an NMO lesion upon experimental immune modulation. Indeed, autoimmunity itself is an inherent property of a healthy immune system, whereas autoimmune disease is most generally defined as an aberrant immune response where pathologic reactivity towards self antigen develops after a break in immune tolerance [263]. The origins of the tolerance break have not been studied in NMO; characterization of and experimental induction may facilitate the development of a novel murine NMO model.

Circumstantial Evidence: Finally, human studies provide circumstantial evidence for AQP4-IgG pathogenicity. In some individuals, titers are observed to rise before a clinical attack and reduction of titers with plasma exchange reduces disease activity [264-266]. However, a threshold AQP4-IgG titer cannot be determined for individual patients. AQP4 rAb sequence analyses support that AQP4 reactive autoantibodies represent an active immune response against the causative target [267]. Experimental administration of AQP4-IgG/rAb to *ex vivo* and *in vitro* cultured cells consistently demonstrates cytotoxic potential, and AQP4-IgG localizes to experimental CNS lesions [51, 52, 250, 267, 268]. In conclusion, direct and circumstantial clinical and experimental evidence strongly support that AQP4-IgG is the inciting pathogenic agent causing CNS injury.

The Serology Divide

Serologic testing has divided NMO into AQP4-IgG seropositive (AQP4-IgG+) and AQP4-IgG seronegative (AQP4-IgG-) cohorts. Research efforts have largely focused on the relationship between AQP4-IgG and NMO, leaving AQP4-IgG- NMO poorly characterized. A greater proportion of patients appear to have monophasic disease and present at an earlier age, with less female predominance [65]. A shared NMO diagnosis is currently of clinical value as it guides appropriate treatment. However, a key question is why AQP4 autoantibodies may not be detected in some patients that fit the clinical profile of NMO-SD.

Several hypotheses have been proposed regarding the absence of AQP4-IgG [269]. First, patients are actually AQP4-IgG+ but have a titer below the assay detection limit. Initial serology assays have demonstrated lower sensitivity compared to second generation assays; the sensitivity of state-of-the-art assays is unknown [57]. An implication is that AQP4-IgG-NMO may be less common than initially reported, if present at all. A second hypothesis is that intrathecal plasmablast populations drive disease activity [267, 270, 271]. Therefore, circulating peripheral AQP4-IgG titers would not necessarily be detected unless the pathogenic plasmablast population has established a peripheral niche. Seroconversion and compartmental titers are reported although the interpretation is unclear [272-274].

Alternatively, AQP4-IgG- NMO may actually exist and be incited by a distinct, unrecognized pathogenic agent that shares a downstream CNS inflammatory phenotype with AQP4-IgG mediated injury. An association between anti-MOG antibodies and AQP4-IgG-NMO, but not AQP4-IgG+ NMO, has been reported [275-277]. However, anti-MOG antibodies do not recapitulate NMO-like pathology in animal models and are not specific to NMO [278]. For example, anti-MOG antibodies are found in up to 40% of acute

disseminated encephalomyelitis (ADEM) patients [33]. Perhaps AQP4 itself remains the causative agent; non-humoral AQP4 autoimmune mechanisms have not been rigorously examined nor have AQP4 distress mechanisms in the absence of immune involvement. It is also possible that AQP4-IgG- NMO is a misdiagnosis. A retrospective study that reexamined AQP4-IgG- patients with longitudinally extensive spinal cord lesions reported that an AQP4-IgG- NMO diagnosis may have been correct for only a minority (~6.5%) of patients [279]. Alternate diagnoses including ADEM and post-infectious disorder, amongst other demyelinating disease, better fit the respective clinical picture. Misdiagnosis could also arise in a phenocopy disorder; indeed, the pathology of MOG+ NMO mimics Type 2 multiple sclerosis [278, 280, 281]. More rigorous testing of these hypotheses is required to better understand the serology divide.

Titers and Clinical Activity

An interesting question is why a consistent relationship between AQP4-IgG titers and clinical activity has yet to emerge if AQP4-IgG is responsible for damaging CNS tissue [265, 282]. Correlations between AQP4-IgG titer with disease activity, prognostic measures, and therapeutic response vary [265, 282-284]. Within an individual patient, a threshold titer sufficient for disease activity has not been identified, and clinical improvement may be associated with no change in titer [284]. The titer at relapse also varies widely between patients at the time of clinical relapse. The compartmental localization of titers at the site of CNS damage may partially explain the discordance as CSF titers may better correlate with disease activity and neuroinflammation than peripheral titers [273].

A key limitation of these studies is that polyclonal serum or CSF AQP4-IgG is used to quantify titer. Quantifying absolute levels in a polyclonal titer treats all antibodies as having equal abilities to engage AQP4, however epitope reactivity and post-translational modifications play significant roles in determining how AQP4-IgG interacts with the target antigen and activate immune effector pathways [178, 261, 285-291] (Figure 1.4A/C). Indeed, one study found that the ability of an AQP4-IgG titer to activate complement correlated better with clinical activity than the absolute titer alone, indicating that AQP4-IgG may harbor subpopulations of variable pathogenic potential [283]. Molecular models of effector activation by AQP4-IgG are needed to guide the development of novel assays to characterize these subpopulations.

AQP4 rAb as a Tool to Study AQP4-IgG

Bennett and colleagues (2009) developed an alternate experimental approach to reproduce the AQP4 autoantibodies found in human patients as monoclonal, recombinant antibodies (AQP4 rAb; Figure 1.4). AQP4 rAb are generated using paired antibody heavy and light chain sequences directly amplified from relapsing NMO patient cerebrospinal fluid CD138+ plasmablasts. These cells produce the majority of Ig in inflammatory and infectious disease [292-294]. The antibody variable region sequences are cloned into vectors, which are then transfected into *in vitro* cultures to mass-produce the respective antibody. The vectors contain the remaining IgG1 constant region sequences. Thus, the antibodies maintain the epitope-specificity of AQP4-IgG found in human patients. The only differences in IgG1 sequence that would arise would be due to patient IgG constant region allotype. AQP4-IgG

glycosylation patterns may also differ but have not been rigorously studied in human populations.

AQP4 rAb were first generated from an NMO patient at the time of initial clinical presentation. Characterization of rAb antigen specificity demonstrated that AQP4-reactive rAb are present at similar frequencies (~60%) in NMO patient CSF as rAb targeting the known inciting agent in alternate CNS inflammatory disorders [292]. Sequence analyses revealed a VH2 and VH4 germline bias, and significant intraclonal diversity in both the framework and complementary-determining regions (CDR). AQP4 rAb were also found to be pathogenic and induce NMO CNS immunopathology. The results collectively supported that AQP4 rAb represent disease-relevant autoantibodies, with each rAb recapitulating part of the targeted AQP4 autoimmune response observed in human patients. Multiple rAb from additional NMO patients have since been generated and are undergoing laboratory characterizations (Bennett, unpublished data). Thus, the use of AQP4 rAb allows for rigorous dissections of polyclonal AQP4-IgG and offers a novel approach to build the molecular models needed to recognize pathogenic subpopulations.

A Molecular Dissection

AQP4-IgG represents a heterogeneous population of AQP4-reactive clones predominantly of the IgG1 subclass [51, 267, 270]. Significant efforts have been placed in characterizing the potential array of epitope binding patterns, with a broader goal of understanding how the various patterns may influence antibody pathogenicity.

AQP4-IgG binds to the extracellular domains of AQP4. Although binding specifically to M23-AQP4 was originally reported, more recent studies have demonstrated binding of

AQP4-IgG to both M1- and M23-AQP4 [52, 289, 295, 296]. M23-AQP4 binding is generally observed at a higher avidity. Biochemical studies indicate that this may arise due to altered extracellular loop conformation or epitope stabilization upon OAP assembly [289].

Early studies to identify major extracellular loop epitopes produced disparate results. One study reported the potential for a subgroup of antibodies whose binding is dependent on Loop A amino acids [297] . Two possible loop contact sites were reported. The second group of AQP4-IgG appeared to require contacts on Loop C and Loop E. A second study reported a broader array of epitopes for polyclonal IgG against AQP4 monomers, tetramers, and OAPs [298]. Some of the epitopes included intracellular domain peptide spans that would not normally be exposed on a cell surface. Both studies used polyclonal serum AQP4-IgG, potentially masking some AQP4-reactive subpopulations.

The use of AQP4 rAb to map extracellular loop binding patterns allowed for a more rigorous characterization [299]. All AQP4 rAb bound to the extracellular domains of AQP4 in two broadly characterized patterns. Pattern 1 rAb contacted amino acids on 2 of 3 extracellular loops (Loops C and E), while Pattern 2 rAb contacted amino acids on all extracellular loops (Loops A, C, and E). Within each pattern, a significant and unappreciated microheterogeneity in single amino acid contacts was observed that included differing dependencies on specific amino acids as well differing amino acids within the extracellular loop contacted. AQP4 epitopes can therefore be distinguished by both the extracellular loops contacted, and specific amino acids within each loop. AQP4 rAb do not bind to denatured AQP4, suggesting that the native formation of extracellular AQP4 epitopes may influence pathogenicity. The pathogenic potential of AQP4-IgG that binds denatured AQP4 has not

been tested. The discrepancy could also indicate differing compositions between intrathecal and peripheral AQP4-IgG populations.

AQP4 rAb also have distinct binding affinities for AQP4, variable B_{MAX}, and some epitopes have enhanced abilities to outcompete the binding of other AQP4 autoantibodies [289, 300]. Using AQP4 rAb to establish molecular models of pathologic immune effector activation therefore offers significant promise in unraveling the molecular determinants driving antibody pathogenicity. Indeed, the structural foundation of any multimeric biologic interaction can be potentially crumbled by AQP4 isoform manipulation (Chapter 1 Section 3), and AQP4 rAb of varying epitopes, binding affinities, and absolute binding levels can be used to understand potential variables contributed by AQP4-IgG. To build these models, the key AQP4-IgG mediated cytotoxic mechanisms driving CNS tissue injury require identification.

Lesion Pathogenesis

Introduction

Molecular models of NMO lesion formation are needed to understand how and when the expanse of activated immune and cellular mechanisms observed in human lesions contribute to CNS damage. To date, a spontaneous animal model of NMO does not exist. Multiple experimental AQP4-IgG transfer models have been developed to identify the *in vivo* cytotoxic potential of putative AQP4-IgG mediated destructive mechanisms, and to understand how the activation of additional cytotoxic mechanisms may emanate from activation of the respective mechanism. Here, a molecular model of lesion pathogenesis is

presented. The strengths and limitations of the experimental approaches used to generate the molecular model of lesion pathogenesis are discussed when appropriate.

Lesion Initiation: The Source of AQP4-IgG

The compartmental origin (central vs. peripheral) of inciting pathogenic AQP4-IgG is unclear. The question is of significance in understanding the translational strengths and potential limitations of each experimental lesion model. AQP4-IgG was historically thought to passively flux from the periphery into the CNS. Peripheral titers are approximately 500:1, and traditional methods of monitoring intrathecal Ig synthesis were elevated in only a small fraction of patients [265, 271, 301, 302]. However, intrathecal synthesis may be masked due to technical limitations including the inability to quantify tissue-bound Ig. Furthermore, although influx does not necessarily require significant BBB permeability, investigations into BBB integrity were inconclusive [271, 302].

The observation that NMO lesion pathology can be produced by AQP4 rAb generated from CSF plasmablasts introduced the possibility for an intrathecal origin of AQP4-IgG [303]. Furthermore, a comparison of the peripheral and central Ig transcriptome and proteome during acute NMO clinical exacerbations demonstrated that a significant fraction of CSF Ig is produced by an intrathecal B cell population [304]. The population includes both novel and peripherally-derived clones: 53% of the CSF IgG transcriptome was matched to peptides recovered exclusively in the CNS, 28% was matched to recovered peptides in both the serum and CSF, and 18% were unrecovered in the CSF. AQP4-specificity was also demonstrated. The data propose an alternate model of lesion initiation: BBB disruption may be secondary to initial astrocyte disruption caused from a peripheral B cell population that

transited into the CNS and produced AQP4-Ig. The secondary passive flux of peripheral AQP4-IgG may propagate the lesion to produce clinical deficit.

Each hypothesis poses considerable experimental challenges to test. Although peripherally administered AQP4 rAb has been demonstrated to access CNS tissue and cause NMO-pathology, the models have required traumatic or inflammatory BBB disruption and therefore rely on the controversial assumption that significant BBB disruption is an inciting mechanism in human disease [258, 267, 305]. From the intrathecal perspective, direct injection of AQP4-IgG/rAb breaks the BBB which limits investigations of secondary BBB breakdown [252-254, 260]. Chronic central infusion of AQP4-IgG causes a transient astrocytopathy independent of effector activity that does resemble human NMO [259]. The finding may indicate a pathogenic role for the pro-inflammatory environment in human NMO and represents a limitation in experimental lesion models. A better understanding of the similarities and differences between human and experimental inflammatory lesion environments is needed. In humans, the molecular environment and pro-inflammatory influence on B and T cells have been the subject of recent reviews [35, 39].

Lesion Initiation: Cytotoxic Mechanisms

In vitro, *ex vivo*, and *in vivo* experimental models have recognized multiple AQP4-IgG mediated astrocyte cytotoxic mechanisms that could initiate CNS injury. To date, *in vitro* studies have identified effector complement and immune cell Fc receptor (FcR) activation, induced AQP4 internalization, and altered AQP4 water channel function as possible mechanisms after AQP4-IgG binding [51, 52, 267, 306]. However, *in vitro* studies may not translate in a tissue environment and could also reflect compensatory adaptations to

a cell culture environment. *Ex vivo* and *in vivo* models directly support a pathogenic role of immune effector activation, and largely argue against AQP4 internalization or altered water channel function as primary cytotoxic mechanisms [128, 253, 254, 307]. In intra-cerebral injection models, astrocyte loss - the initiating pathogenic insult - is observed following injection of AQP4-IgG/rAb via complement and/or FcR effector activation but no cytotoxicity is observed in the absence of immune effector activation (Figure 1.5 Star 1) [253, 254, 257, 308, 309]. In a second lesion model where AQP4 rAb is peripherally administered into rat and provided CNS access via traumatic BBB injury, complement effector activation alone causes astrocyte loss. FcR effector activation incites an astrocyte response (decreased AQP4 expression), but causes no cytotoxic damage [258]. The models therefore consistently demonstrate a cytotoxic role of complement effector activation and variable potentials for FcR effector mechanisms in inciting astrocyte loss.

The membrane organization of AQP4 may play a key role in regulating AQP4-IgG effector activation. Complement-dependent cytotoxicity (CDC) is activated by AQP4-IgG and AQP4 rAb on M23-AQP4, but not M1-AQP4 [306]. Antibody-dependent cellular cytotoxicity (ADCC) can be activated on both M1-AQP4 and M23-AQP4. Curiously, NMO pathology has a predilection towards CNS sites where M23-AQP4 is expressed at higher levels [125]. The significance of this observation in driving lesion initiation is unclear. It is also unclear why NMO pathology does not develop in peripheral organs despite AQP4-IgG binding [260], and why destructive cellular-mediated responses are not initiated against these tissues as they may initiate independent of AQP4 membrane organization. Thus, AQP4 membrane organization may play unappreciated regulatory roles in directing human lesion pathology.

An outstanding question is how both complement proteins and immune cells access CNS-bound AQP4-IgG. Experimental models are dependent on providing the respective immune pathways with artificial CNS access. A better understanding of how the pro-inflammatory environment observed in human NMO patients may influence immune activation and CNS access either via peripheral flux (peripheral immune infiltrate and complement protein) or via local production (complement protein) is needed. AQP4-IgG binding to CNS tissue may directly recruit immune cells via astrocyte NF-kB mediated cytokine release, although the mechanism requires clarification [49].

Lesion Propagation

A coordinating role of complement effector activation, but not immune cellular-mediated mechanisms, is proposed to drive lesion propagation to secondary demyelination. In intra-cerebral injection models, a complete demyelinating lesion only occurs when the classical complement pathway is activated by AQP4-IgG/rAb, despite the potential of ADCC to cause astrocyte loss [253, 254]. Importantly, the studies attribute cytotoxic complement activation to a direct interaction between AQP4 rAb and C1q (Figure 1.5 Star 2). For example, a consequence of FcR-mediated astrocyte destruction could be activation of alternative or MBL pathways, or classical pathway activation via the exposure of novel IgM targets. However, this is not observed. AQP4 rAb- FcR interactions are nevertheless acquired to achieve the fullest potential of AQP4 rAb mediated CNS destruction as AQP4 rAb that only activate complement cause limited lesion pathology [254, 257, 258]. AQP4-IgG astrocyte binding activates signaling cascades to recruit and co-stimulate peripheral immune infiltrate. The driving mechanisms and molecules released are unknown but likely include

cytokines and activated complement fragments (Figure 1.5 Star 3). The proteins may also bind directly to neighboring CNS cells to cause damage. For example, the cytokines IL-6 and IL-1b exacerbate CNS damage in *ex vivo* lesion models [268]. The prominent cellular infiltrate of human lesions - macrophages, eosinophils, and neutrophils - all contribute to CNS damage. Target reduction and enhancement, or therapeutic inhibition of each cell type influences the size of experimental lesion formation [257, 310, 311]. T cells and microglia do not appear to contribute to the initiation or propagation of CNS destruction [312, 313].

Temporally, astrocytes are rapidly destroyed within an hour following lesion initiation with complement [309]. Oligodendrocyte cell body apoptosis occurs approximately 3 hours later, although the myelin sheath remains largely intact. The mechanistic link between astrocyte loss and oligodendrocyte cell death may represent direct immune cytotoxicity (Figure 1.5 Star 4) or a loss of CNS cellular homeostasis (Figure 1.5 Star 5) [314]. Myelinolysis coincides with immune cell infiltration, with significant infiltrate observed at 24 hours [309]. The temporal link with neuronal dysfunction has not been readily investigated, nor have any pathogenic contributions from BBB endothelial cells.

A more recent rat experimental lesion observed a region termed a “penumbra” consisting of AQP4 loss but intact GFAP and MBP expression in the absence of complement deposition surrounding NMO lesion cores [257, 258]. Similar pathology was observed when complement-null AQP4 rAb was injected or when endogenous complement was inhibited, but no penumbra was observed when antibodies deficient in both complement and Fc receptor binding were injected. This suggests that an alternate immune effector mechanism, rather than AQP4 internalization, drives the penumbra formation. Although the finding nevertheless emphasizes the destructive consequences that emanate from AQP4 rAb-

mediated classical complement pathway activation, the heterogeneous lesion phenotype may indicate an intricately regulated, simultaneous cross-activation of multiple competing molecular processes. Refined experimental lesion models are needed to build more complete molecular models of lesion pathogenesis.

Lesion Repair

Lesion repair is not well studied. A population of uni- and bipolar astrocytes expressing GFAP and AQP4 are observed in early human lesions [44]. A population of bipolar, elongated astrocytes atypical of post-inflammatory gliotic reactions substantially repopulated an experimental NMO lesion at one week post-initiation [309]. Olig-2 positive oligodendrocyte precursor cells, but not mature NogoA-positive cells, were also abundant and no signs of remyelination were observed. A better understanding of the initial repair response and how the response may be altered in more chronic lesion environments is needed.

Model Translation

AQP4-IgG mediated experimental models of CNS destruction recapitulate the major features of human NMO lesions, including the temporal progression of astrocyte loss to secondary oligodendrocyte loss and demyelination. All models to date emphasize a key role of complement effector activation by AQP4-IgG in inciting and propagating CNS tissue destruction. The models also support that the immune cell infiltrate likely reflects targeted signaling cascades that independently recruit and co-stimulate FcR effector activation. Indeed, a translational strength of the models is that the infiltrating immune cell populations

are quite similar to human lesions. This is particularly notable for the neutrophil response, given a decreased neutrophil response in mice compared to humans and the relative lack of a neutrophil response in other murine models [315-317].

Having established the coordinating cytotoxic role of complement activation by AQP4-IgG, studies are now needed that better characterize the entirety of the complement in NMO lesion pathogenesis. The specific pathways contributing activated complement protein – the classical, alternative, lectin pathways – are unknown. The timing of pathway activation has not been pursued, nor have characterizations of the direct and indirect cytotoxic roles played by the system. These studies are greatly needed to guide the design and delivery of novel therapeutics that may directly combat lesion pathogenesis at multiple molecular stages.

Introduction of Hypotheses

Overwhelming clinical and experimental evidence supports that complement effector activation by AQP4-IgG plays a key role in inciting and propagating CNS tissue destruction in NMO. A better understanding of how and when complement may be activated by AQP4-IgG subpopulations, and the sources of complement protein fueling lesion formation, are needed to better detect disease activity in the clinic. My studies are therefore founded on the underlying hypothesis that AQP4-IgG effector complement activation plays a key pathogenic role in NMO lesion formation.

By building a molecular model of classical complement pathway activation, I will test the hypothesis that AQP4 membrane organization, in addition to AQP4-IgG epitope specificity, constrains the geometric organization of AQP4 autoantibodies to promote or limit effector complement activation. The aim involves imaging AQP4 autoantibodies at super

resolution. The experiments performed to develop and validate an imaging analysis algorithm are first presented in Chapter 2. The data is currently under peer review. The imaging technique is combined with functional studies using AQP4 rAb and patient serum AQP4-IgG to build a molecular model of classical pathway activation in Chapter 3. The chapter is formatted as a manuscript suitable for peer review.

I will then test the hypothesis that multiple sources of activated proteins contribute to NMO lesion formation. By examining contributions from the classical, alternative, and lectin pathways, I will propose a model describing how various pathway sources may influence the total level of activated complement protein and consequently impact the amount of CNS damage incited.

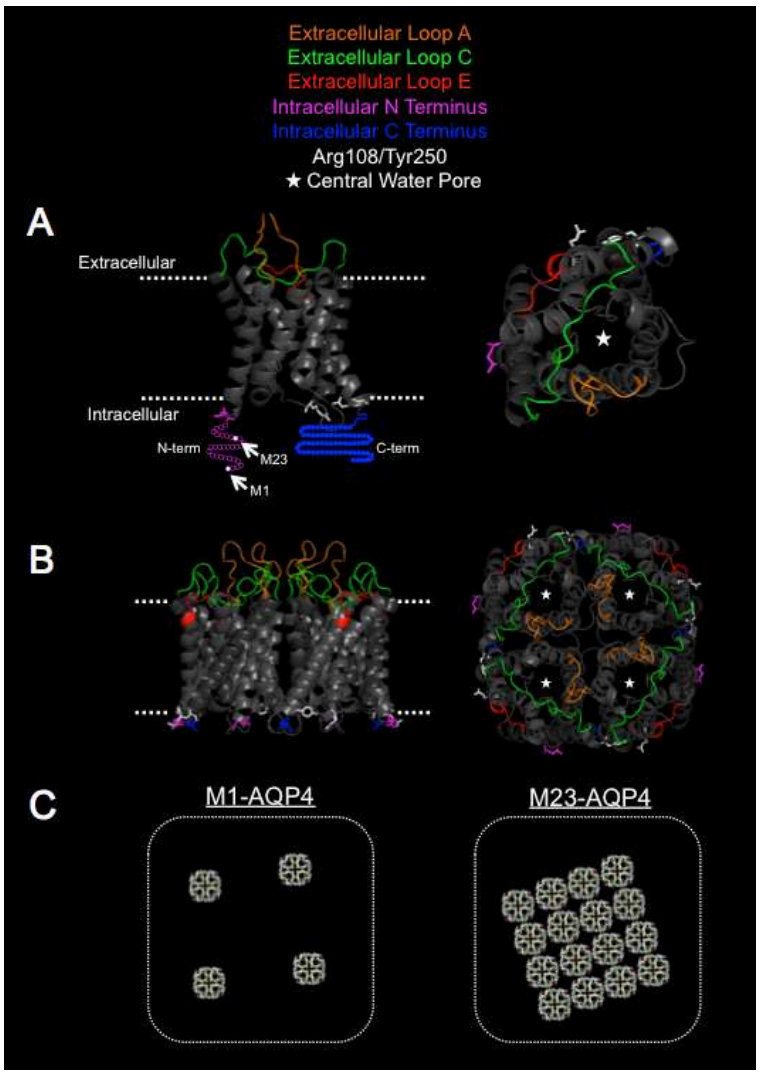

Figure 1.1: Aquaporin-4
(A): Side view (left) and aerial view (right) of an AQP4 monomer (PDB: 3GD8). Transmembrane domains are depicted as black ribbons, and extracellular loops A/C/E are linearly modeled and are colored orange, green, and red respectively. The intracellular N and C-terminal domain amino acids were not crystalized and are represented by an individual circles. The intracellular domains are attacked to the schematic at the appropriate locations. The central water pore is indicated with a white star (right). Dotted lines on the side view represent an artificial membrane to clarify structural locations. Met1 and Met23 are indicated by white arrow, representing the translation start sites for M1-AQP4 and M23-AQP4 respectively. (B): In a cell membrane, AQP4 is not expressed as a monomer as depicted in (A) but as a tetramer. A side view (left) and aerial view (right) of as AQP4 tetramer is shown. (C): Aerial views depicting the membrane organization of M1-AQP4 tetramers (left) and M23-AQP4 tetramers (right). M23-AQP4 tetramers organize into larger sheets made of pure AQP4 protein. The amino acids Arg108 and Tyr250 are proposed AQP4 contacts in the larger membrane arrays, and are depicted as white stick models in A/B. The figure was generated using MacPyMol software.

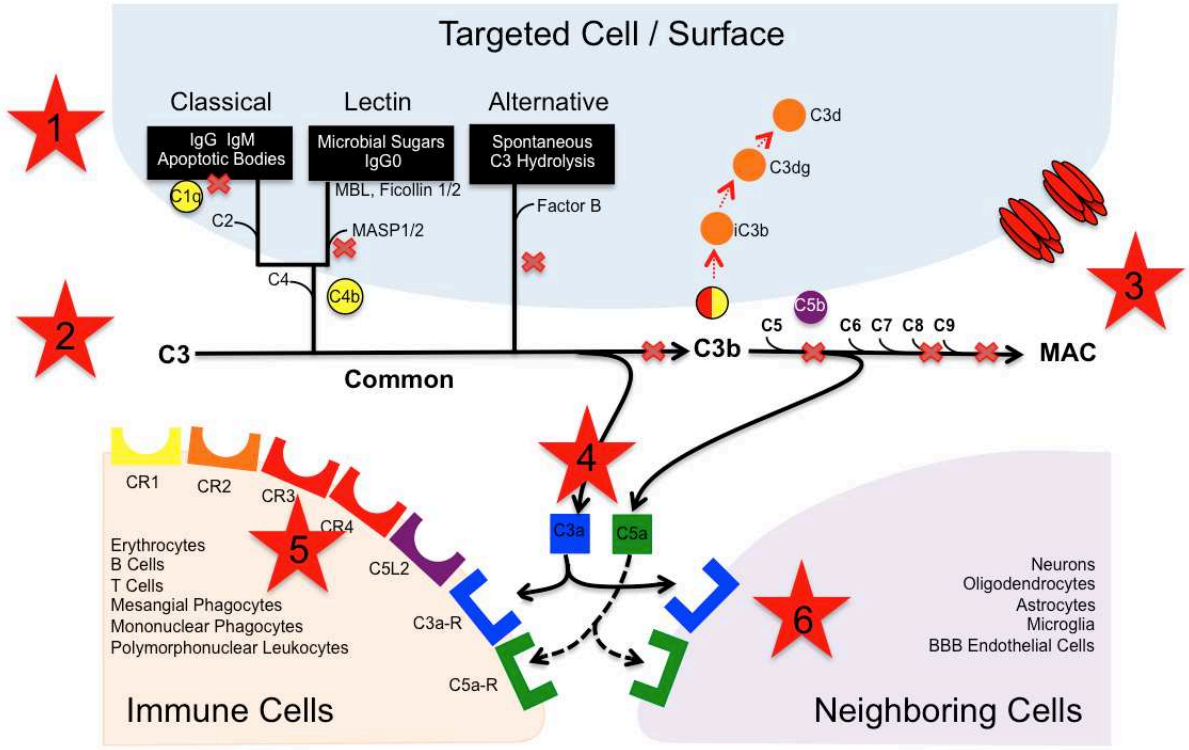

Figure 1.2: The complement system
The complement system is activated on a targeted surface by 3 distinct pathways (Star 1). The black box represents example molecules that can activate the indicated pathway. Each pathway converges to activate the common pathway (Star 2). The common pathway generates activated fragments that are deposited on the targeted surface to ultimately form a membrane attack complex (Star 3), or are soluble (Star 4). Soluble fragments bind respective receptors on immune cells to recruit them into the local environment. Additional complement protein receptors (Star 5) interact with deposited complement proteins; interacting proteins and receptors are indicated by the same color. Some examples of immune cells expressing complement receptors are indicated in the example immune cell. Activated fragments can also interact with neighboring cells in the tissue environment (Star 6). Examples of CNS cells expressing complement receptors are listed in the example neighboring cell. Pathway activation is regulated at many steps; a red x indicates general regions of pathway regulation.

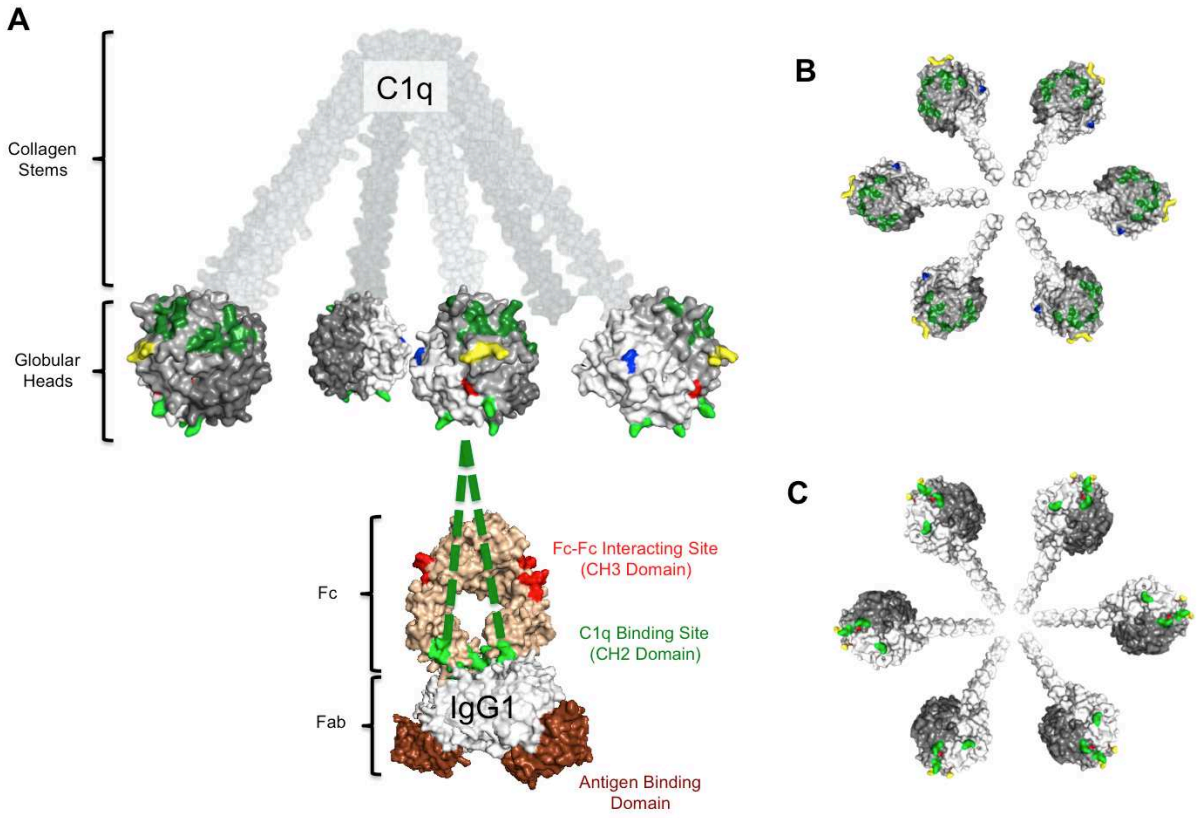

Figure 1.3: IgG and C1q globular head amino acid contacts
(A): Major structural domains of C1q (top) and IgG (bottom) are indicated to the left of the schematics. The stalk of C1q is omitted, and only 4 of 6 globular heads are shown for clarity in depicting highlighted amino acids. Amino acids critical for C1q binding to IgG are indicated in green on the surface representations. On C1q, hypothesized initial amino acid contacts are shown in light green, and final contacts are shown in dark green. Red amino acids are a calcium binding site and yellow amino acids are proposed pivot points that drive globular head rotation. On IgG, the Fc fragment is colored in light brown and the Fab fragment white. Red amino acids represent CH3 domain contacts at an IgG hexamer interface, green are C1q binding site contacts, and dark brown represents the CDR region. Additional top-down (B) and bottom-up (C) models of C1q provide alternate views of the C1q globular head contacts. The schematics were generated using MacPyMol software (PDB entries 1PK6, 1HZH, 2D3H).

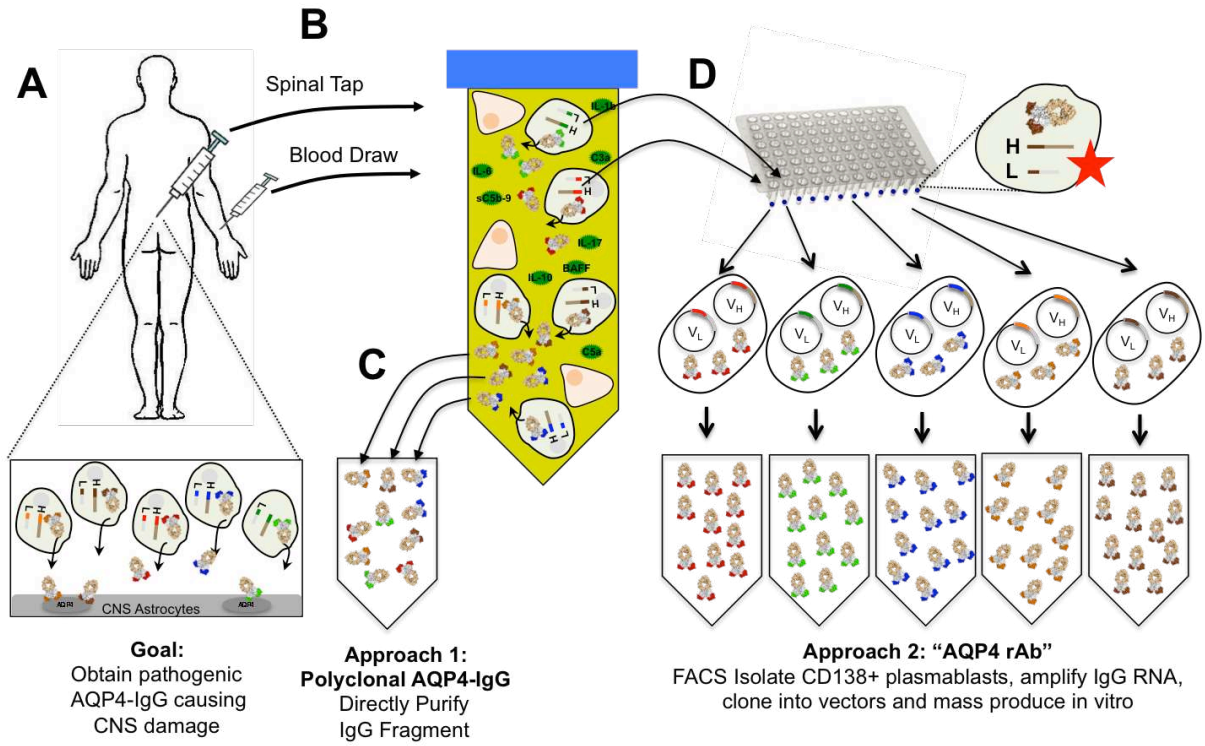

Figure 1.4: Methods to acquire AQP4-IgG for experimental study
(A): In human patients, AQP4-IgG is produced by CD138+ plasmablasts, and binds to CNS astrocytes to cause tissue damage. The cells show the paired RNA heavy and light chain encoding for the respective Ig protein. Multiple CDR colors indicate different sequence composition. Note the potential for differing pathogenic subpopulations; all AQP4 autoantibodies do not necessarily equally engage AQP4 (B): Patient CSF or blood containing CD138+ plasmablasts, additional cells (nucleated blobs) and non-IgG protein (green fragments; example cytokines/proteins elevated in NMO patients are indicated) can be acquired via peripheral blood draw or spinal tap. (C): One method to purify AQP4-IgG is as polyclonal AQP4-IgG via protein A purification. Note that the method captures all Ig in addition to AQP4-IgG. (D): A second method is to generate recombinant, monoclonal AQP4-reactive antibodies (termed AQP4 rAb). CD138+ cells are isolated via FACS into individual PCR well, paired antibody heavy and light chain sequences are amplified (red star) and cloned into IgG1 constant region vectors, and the vectors are transfected into cells in culture. The cells mass-produce the respective rAb which is then purified from the cell culture supernatant.

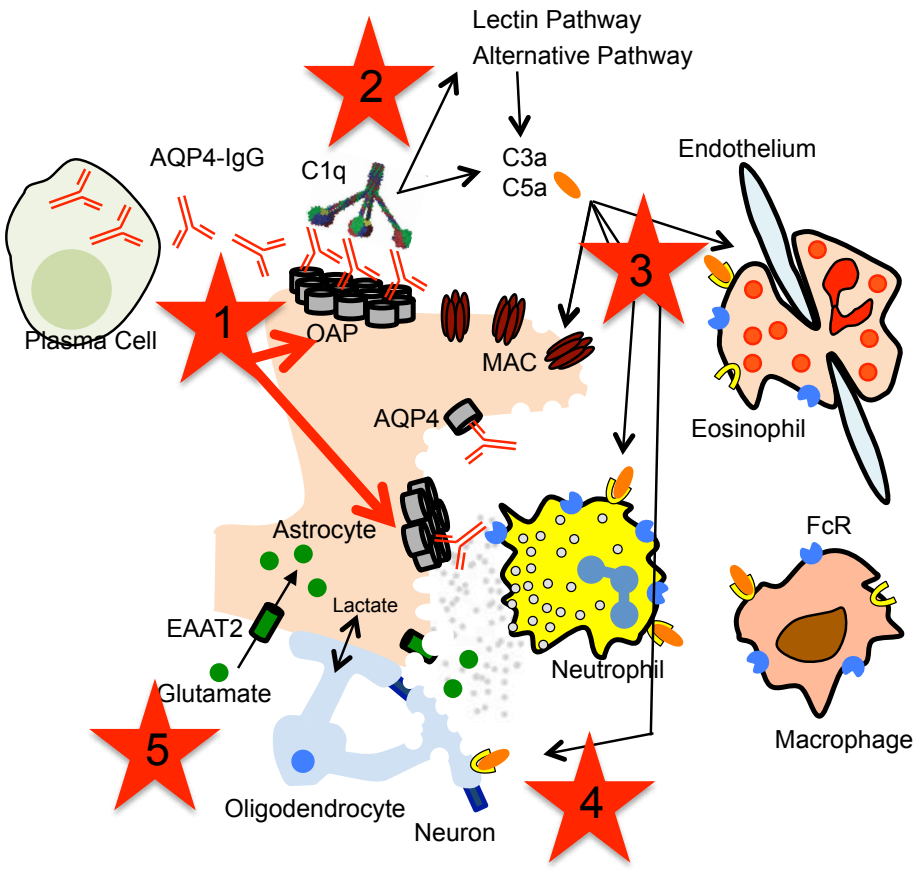

Figure 1.5: NMO lesion pathogenesis
AQP4-IgG binds to CNS astrocytes and activates immune effector mechanisms to initiate astrocyte damage (Star 1). Classical pathway activation by AQP4-IgG (Star 2) plays a coordinating role in lesion formation, initiating a cascade of complement activation that allows for the fullest potential of immune cell recruitment and co-stimulation (Star 3). Complement proteins and immune cell degranulation/activation may directly incite CNS damage (Star 4) or indirectly promote damage via disrupted CNS cellular homeostasis (Star 5). Figure is modified from Kowarik et al (2014).

CHAPTER II

DETERMINING THE SPATIAL RELATIONSHIP OF MEMBRANE BOUND ANTI-AQUAPORIN-4 AUTOANTIBODIES BY STED NANOSCOPY

Abstract

Determining the spatial relationship of individual proteins in dense assemblies remains a challenge for super-resolution nanoscopy. The organization of aquaporin-4 (AQP4) into large plasma membrane assemblies provides an opportunity to image membrane-bound AQP4 antibodies (AQP4-IgG) and evaluate changes in their spatial distribution due to alterations in AQP4 isoform expression and AQP4-IgG epitope specificity. Using stimulated emission depletion (STED) nanoscopy, we imaged secondary antibody labeling of monoclonal AQP4-IgGs with differing epitope specificity bound to tetramers (M1-AQP4) and large orthogonal arrays of AQP4 (M23-AQP4). Imaging secondary antibodies bound to M1-AQP4 achieved lateral resolution of ~20 nm, allowing us to infer the size of individual AQP4-IgG binding events. This information was used to model the assembly of larger AQP4-IgG complexes on M23-AQP4 arrays. A scoring algorithm was generated from these models to characterize the spatial arrangement of bound AQP4-IgG antibodies, yielding multiple epitope-specific patterns of bound antibodies on M23-AQP4 arrays. Our results delineate a novel approach to infer spatial relationships within protein arrays using STED nanoscopy, offering insight into how information on single antibody fluorescence events can be used to extract information from dense protein assemblies under a biologic context.

Introduction

Protein spatial distribution within larger assemblies is often intimately linked to protein function. Historical approaches to visualize protein distribution at high spatial resolution have been largely limited to electron microscopy, as conventional light microscopy is restricted to low spatial resolution (~200-300 nm laterally) [318]. In STED nanoscopy, optical super-resolution is obtained by depletion of the fluorescence emission peripheral to the excitation beam target. Depletion is elicited by a red-shifted STimulated Emission Depletion beam that is shaped into a donut-like intensity distribution for 2D resolution enhancement [319, 320], with the zero intensity centered over the excitation beam. The STED beam effectively switches "off" fluorescent molecules in the periphery of the excitation spot, but not in the zero-intensity center. As a result, STED nanoscopy increases resolution down to tens of nanometers, allowing for novel studies of protein spatial distribution and function. For example, STED localization of surface protein assemblies has provided novel insight into both vesicular membrane protein recycling and HIV-1 host cell infectivity [321, 322].

It remains a challenge to identify the geometric arrangement and stoichiometry of individual proteins within larger assemblies *in vivo*. The light emitted by a single fluorophore forms a Gaussian intensity distribution - a finite-sized spot - that will blend with light emitted by other fluorophores when packed at high densities. Recognizing individual proteins within dense assemblies often requires restrictive experimental conditions that perturb the model system away from the *in vivo* environment to reorganize protein assemblies into resolvable components or to observe real-time protein dynamics [323]. In addition, the lack of information on target spatial orientation, uncertainty on access to primary and secondary

antibody epitopes, and variable labeling efficiency pose considerable imaging challenges [324]. Lastly, fluorophore tags or secondary fluorescent antibodies may interfere with normal structural arrangement or biologic function. A better understanding of how individual fluorophores can be resolved at higher densities in a non-disruptive biologic context would allow for the development of more rigorous methods to correlate spatial protein distributions with functional outcomes.

We have generated a large repertoire of aquaporin-4-(AQP4)-specific monoclonal recombinant antibodies (rAbs) from neuromyelitis optica (NMO) patient cerebrospinal fluid plasmablasts [267]. These autoantibodies cause extensive CNS damage upon binding to AQP4 on astrocyte membranes through a variety of immune mechanisms [86, 254, 268]. The unique organization of AQP4 in the plasma membrane provides an opportunity to understand how antibodies may be localized at high density in a biologically relevant, *in vivo* context [108, 118, 325]: the M1-AQP4 isoform maintains a tetrameric structure (~8-9 nm) in plasma cell membranes, whereas the M23-AQP4 isoform forms large orthogonal arrays of particles (OAPs) that are able to bind multiple antibodies at high density. On OAPs, the spatial distribution of bound AQP4 rAb is likely dependent on the geometrical arrangement and density of the target epitope [299], offering the opportunity to visualize the impact of epitope specificity on fluorescence patterns detected by STED nanoscopy. As the spatial organization of bound surface IgG may impact complement activation [306], fluorescence patterns may also provide unique information on the molecular events driving tissue injury. Here, we use STED imaging to analyze fluorescence patterns of AQP4 rAb binding events on M1-AQP4 tetramers and M23-AQP4 OAPs to develop a framework for evaluating dynamic changes in

protein distribution in a biologic context. The result is a novel algorithm to evaluate the spatial relationship of individual proteins in larger assemblies without direct resolution.

Materials and Methods

Antibodies

Recombinant monoclonal anti-AQP4 antibodies were produced from plasmablasts isolated from the cerebrospinal fluid of neuromyelitis optica patients [267]. Antigen and epitope specificities were identified as described [267, 299]. Four monoclonal recombinant antibodies (AQP4 rAbs #53, #58, #186, and #153) with unique epitope specificities [2] were selected for this study. For rAbs #53, #58, and #186, the E345R point mutation was introduced into the Fc region by site-directed mutagenesis (Life Technologies) and confirmed by DNA sequencing. The E345R mutation promotes the ordered assembly of antibodies on surface targets [163].

Crystal Schematics

Crystal structures of IgG1 (PDB ID: 1HZH) [171], AQP4 (PDB ID: 3GD8) [107], C1q globular head (PDB ID: 1PK6) [194], and collagen (PDB ID: 2D3H) [326] were used to generate schematics. C1q was assembled by approximating globular head/collagen assemblies based on known structures [194, 327]. For simplicity, the collagen stalk is removed from all C1q structures.

Sample Preparation and Immunohistochemistry

M1- and M23-AQP4 expressing CHO cells were cultured as described [299] and plated on #1.5 laminin-coated glass coverslips (neuVitro). The following day, media was washed twice, and AQP4 rAbs (2ug/mL and 10ug/mL) were bound to living cells for 30 minutes. Cells were then fixed in 4% PFA containing 0.1% gluteraldehyde for 15 minutes at 4C. Biotinylated Fab anti-human Fc domain (Novus Biologics) was used to detect bound AQP4 rAb and rabbit polyclonal antibody against the intracellular C-terminal domain of AQP4 (Santa Cruz) was used to label AQP4 tetramers and arrays. Primary antibodies were detected using streptavidin-conjugated Atto647N (Atto-tec) and goat anti-rabbit STAR 590 (Rockland Inc.). Coverslips were mounted using ProLong Gold (LifeTech) supplemented with 2.5% DABCO, and rested 24 hours prior to imaging.

Imaging with STED Nanoscope

Coverslips were imaged using a home-built two-color STED nanoscope (Meyer SA, Gibson E, Restrepo D, unpublished data) at the Anschutz Medical Campus Light Microscopy Core. All images were generated with a pixel size of 19.52x19.52 nm. The color channels are designed for Atto 590 and Atto 647N dyes. A Fianium Advanced Laser Platform pulsed at 20 MHz provides white light output that is optically filtered for the excitation sources (570 nm and 647 nm) and two high power outputs for the STED light (711 nm and 745 nm). The delayed and interleaved laser pulses arrive at the sample every 25 ns, alternating between colors. The two STED beams are combined into one polarization-maintaining fiber; the two excitation beams are combined into another. They are collimated, the STED light is sent through a vortex phase mask and then a polarizing beam splitter combines them. A quarter

waveplate imparts circular polarization on the STED beams, which form a donut PSF at the focus of the objective lens in the center of the excitation spot. We use an Olympus IX-71 microscope platform with brightfield, widefield, epifluorescence, and DIC imaging to find the part of the sample for STED imaging with the 30x30x10 micrometer range piezo stage for imaging. A custom dichroic filter passes the STED and excitation colors and reflects the fluorescence colors, which are split by another dichroic and focused into multimode fiber confocal pinholes to send to two avalanche photodiodes. A custom digital circuit performs gated detection on each avalanche photodiode (APD) signal, which is then sent to the data acquisition (DAQ) card on the computer that controls the scanning with analog output with the program Inspector, generously provided from the research laboratory of Dr. Stefan Hell.

Analysis and Statistics

All image analyses and simulations were performed with MATLab_R2015a software (The MathWorks, Inc) using scripts coded in-house. Script integrity was confirmed by comparing script data output for all image quantifications (as described below) with known distributions on artificially generated images containing multiple scenarios for pixel intensity organizations. Data was imported into Graphpad Prism 6 software to generate plots and perform statistical tests.

Image Processing

The image processing approach was to first identify where AQP4 is expressed on the target cell using the intracellular AQP4 label (STAR590 channel), generate regions of interest (ROIs) by applying size inclusion (M23-AQP4) or size exclusion (M1-AQP4) filters

to identify or eliminate OAPs respectively, and then analyze the spatial distributions of extracellular AQP4 autoantibodies (647N channel) within all ROIs. To maximize the number of detected autoantibodies (therefore minimizing analysis bias from low frequency spatial distributions of potential biologic significance), the 590 channel was not further processed beyond background noise subtraction with all remaining pixels containing an intensity value considered positive for an AQP4 tetramer. Stricter quantification did not change the data analysis (data not shown), likely attributable to the extensive processing criteria for scoring the Atto647N channel as described below.

AQP4 Tetramer and Array Analysis

On M1-AQP4, AQP4 tetramer clusters, at least 4 pixels in size, were identified and excluded from further analysis as these may represent leaky, low level M23-AQP4 expression and would potentially confound the analysis [108]. On M23-AQP4, OAPs that were at least 8 pixels in size were included to run all analyses. All included pixels were then used to mask the Atto647N channel to perform all analyses. At least n=3 cells per antibody were analyzed.

Determination of Mean Object Size

A non-biased algorithm was applied across the entire Atto647N image to eliminate user-bias, with the goal of identifying the mean resolvable object size based on a maximum likelihood algorithm [328]. The output was a 2-dimensional array, of which a Gaussian distribution was fit in 2 dimensions with the mean object size being calculated as the FWHM of the Gaussian fit. To test the accuracy of our calculation given 19.5nm pixel size, we

calculated the object size for 2-dimensional Gaussian distributions modeled for objects of known-sizes 14-75 nm at 1nm increments. Our algorithm was not accurate for objects sized 14-19 nm, while it accurately calculated object sizes above 20nm.

This analysis requires user input of the estimated mean object size, which was obtained by imaging Atto647N fluorophore alone and randomly immobilized antibodies. However, this size is not necessarily reflective of the size of larger fluorophore densities that may label larger antibody clusters, therefore the analysis was repeated with multiple user estimations of object size. User object size approximations were the pixel dimensions for a 2-dimensional array, containing enough pixels in each dimension to fit a 2 dimensional Gaussian +/- 3 standard deviations from Gaussian peak.

For each experimental group, the calculated object FWHM met the following criteria: 1) the output array for all images had a general Gaussian appearance, i.e., a center peak bordered with lesser values, 2) the calculated object FWHM came from an array meeting the minimum size requirements to fit the respective Gaussian, and 3) the calculated object size was stable with increasing sizes of the user-input size estimate. The calculated object FWHM value of each image was then averaged with the remaining images for each experimental group. For statistical comparisons, a one-way ANOVA was performed with Tukey's test for multiple comparisons (adjusted $p < .05$ considered significant, comparison alpha = .05).

Generation of Simulated Images to Determine the Localization Efficiency of Fluorophores in Non-Resolvable Clusters

To analyze the spatial arrangements of bound autoantibodies in more detail, a scoring system was developed (as described below) whose application is dependent on the accurate

localization of an individual fluorophore(s) to a single pixel. A data simulation was designed comparing known, random distributions of fluorophores (represented as a binary image) to the theoretical STED image obtained by that distribution. Fluorophores were modeled as being 12 nm in size, with random positioning requiring at least a 12 nm spacing between events. A cell was simulated with 100 distinct OAPs, and a random fluorophore distribution was generated over each OAP. To generate the theoretical STED image, each fluorophore was convolved to model the theoretical photon detection pattern based on the object representation obtained for autoantibody #58, and background noise was simulated. The representation of autoantibody #58 was selected because it closely resembles that of Atto647N alone, and the mean object size was consistent for both M1-AQP4 and M23-AQP4. STED pixel dimensions were then super-imposed, with each pixel representing the total sum of all photons in the pixel area.

Threshold Analysis of Simulated Images

After generating the simulated STED images, all pixels for the 647 channel (detecting simulated fluorophore distributions) contained a pixel intensity. We therefore asked if a threshold value could be applied that would accurately resolve fluorophore signal from background noise. Images were first deconvolved using the PSF for rAb #58, using a Lucy-Richardson deconvolution algorithm [329]. A series of simulations was performed in which the threshold intensity was increased at 5% increments starting at 5%, where any pixels with an intensity value below the threshold percent compared to the maximum pixel value on the OAP were reassigned a value of zero to exclude the point from the analysis. All remaining pixels were considered to contain a fluorophore. The resulting data set was compared to the

binary STED image representing the true locations of all pixels containing fluorophores. For each image, the sensitivity (defined as the number of correctly identified fluorophore-containing pixels), false positive percentage (defined as the number of incorrectly identified fluorophore-containing pixels over the total number of identified pixels), and false negative rates (defined as the number of incorrectly missed fluorophore-containing pixels) were calculated.

Generation of the Antibody Spatial Arrangement (ASA) Score

A scoring system was developed to rank each pixel containing a fluorophore (as determined above) based on the potential for that pixel to participate in a multivalent interaction with the immune protein C1q. The ASA scale was devised based on approximate sizes of C1q-antibody complexes as previously reported from crystallization and cryo-EM studies [163, 190], compared with the size of each STED pixel. An ASA score of 1 represents an isolated pixel with no surrounding intensity signal, ASA Score 2: 2/4 pixels containing signal, ASA Score 3: 3/4 pixels containing signal, and ASA Score 4: 4/4 pixels containing signal. Each pixel received a final score based on the maximum possible ASA score it could receive over a 2x2 pixel area, out of the 4 possible scores it could have been assigned.

The accuracy and sensitivity of this scoring system was tested by data simulation. A random distribution of fluorophores was generated and thresholded as described above (n=10 cells). ASA scores were then calculated for both the predicted localizations, and compared with the respective binary image. The initial ASA score demonstrated a systematic bias. A non-linear fit was applied to ASA scores 1 and 4, which were first normalized. Scores of 2

and 3 were normalized based on the final percent scored as a 1 or 4. The final scoring algorithm was tested on a second data simulation (n=10 cells), with results representing the goodness-of-fit for a linear regression of each ASA score.

ASA Scoring of Bound AQP4 Autoantibodies

All 647N images were deconvolved and thresholded as described above, using a 40% threshold. For M23-AQP4, each OAP across the entire image was scored individually with data output representing the mean percentage of ASA scores across all OAPs. M1-AQP4 does not form OAPs, therefore the ASA score was calculated across the entire cell. Data output represents the average ASA score distributions calculated for all images in the dataset. Cumulative ASA score distributions were compared using a Mann-Whitney test.

Results

Characterizing STED Lateral Resolution Using a Biologic Approach

In astrocytes, M1- and M23-AQP4 are co-assembled into tetramers with differential abilities to coalesce into larger orthogonal arrays of particles (OAPs) [17]. M1-AQP4 inhibits OAP assembly and, when solely expressed, assembles into isolated plasma membrane tetramers; M23-AQP4, however, facilitates AQP4 tetramer assembly into larger OAPs. Based on the relative size of AQP4 and IgG, only a single AQP4 rAb molecule is presumed to bind to a M1-AQP4 tetramer; whereas multiple rAbs may bind to the surface of AQP4 OAPs based on epitope organization (Figure 2.1A/B) [289]. In this model, single antibodies bound to plasma membrane M1-tetramers should be readily resolved because the distance between fluorophores is large compared to the resolution of the STED nanoscope (Figure

2.1C). In contrast, on M23-AQP4 OAPs, the short distance between bound AQP4 rAbs may allow fluorophores to cluster at distances smaller than the resolution of the STED nanoscope, thereby interfering with the detection of discrete binding events. As a result, on OAPs, fluorescent signal may represent multiple antibodies binding in close proximity (a cluster), rather than a single antibody molecule (Figure 2.1D). Based on the distribution of plasma membrane M1-AQP4 tetramers, the size of M23-AQP4 OAPs, and the distribution of target epitopes within OAPs, some monoclonal AQP4 rAbs may appear as similar sized objects on both AQP4 isoforms, while others may appear as larger objects on M23-AQP4 OAPs.

To test this hypothesis, several individual monoclonal AQP4 autoantibodies recognizing unique AQP4 extracellular epitopes were bound to live cells expressing either M1-AQP4 or M23-AQP4 and imaged via STED nanoscopy. We quantified the apparent size (full width half maximum intensity, FWHM) of a resolvable object on M1-AQP4 and M23-AQP4 for each monoclonal antibody. Raw images were analyzed without any background correction or additional processing. Apparent size was acquired using an adapted, blinded algorithm that identifies the mean 2-dimensional array representation for a single resolvable object across the entire image, based on a maximum likelihood algorithm [328]. A 2-dimensional Gaussian was then fit to calculate the FWHM of the signal distribution (Figure 2.1C/D). Given the relative size of a single antibody compared to the STED pixel dimensions (12-15 nm vs. 19.52 nm, respectively), differences in apparent object size on M1- vs. M23-AQP4 for an identical monoclonal antibody indicate distinct spatial distributions of bound fluorophores.

The computed FWHM for all AQP4 rAb bound to M1-AQP4 was ~ 20 nm, residing at the size of a single pixel (Figure 2.2A/E). These object sizes did not differ statistically

from individual fluorophores or fluorescently-labeled antibodies randomly immobilized on glass coverslips (one-way ANOVA, p=.16), supporting our conclusion that the majority of resolvable objects for AQP4 rAb bound to M1-AQP4 tetramers represent isolated antibodies on the cell surface. In contrast, the size of resolvable objects bound to M23-AQP4 OAPs increased significantly for multiple AQP4 rAb antibodies. At 10 ug/mL, the mean object size for rAb #58 was similar between M1-AQP4 tetramers and M23-AQP4 OAPs; however, the mean object size for rAbs #53 and #186 were significantly larger (Figure 2.v2E), suggesting an epitope-dependent clustering of antibody on M23-AQP4 OAPs (Figure 2.2B/C/E). To test this conclusion, we introduced a point mutation (E345R) into the Fc domain of several AQP4 rAbs to promote the assembly of individual antibodies into larger surface clusters [163]. AQP4 antibodies containing the E345R Fc mutation were detected as larger objects compared to their wildtype counterparts (Figure 2.2B/D/E). Increasing antibody concentrations did not significantly shift the distribution of the average object size for rAb #58, #186, and #153, demonstrating that the increase in object size represented an antibody-intrinsic, epitope driven phenomenon rather than random juxtaposition of multiple independent binding events on AQP4 OAPs (Figure 2.2E). Interestingly, the mean object size for rAb #53 trended towards a significant increase at higher concentrations on M23-AQP4 OAPs (21 nm at 2 ug/mL vs. 33 nm at 10 ug/mL; Tukey's adjusted p=.055), suggesting that increased occupancy of rAb #53 epitopes facilitated surface clustering over this concentration range. In summary, manipulation of AQP4 assembly (M1-AQP4 tetramers vs. M23-AQP4 OAPs) and rAb interaction (E345R Fc mutation) allowed us to detect shifting spatial arrangements of AQP4 rAbs on the cell surface.

Generation of Score of Antibody Spatial Arrangement

The spatial arrangement of antibody molecules bound over surface epitopes may have a profound impact on Fc-domain mediated effector function activation [19]. Activation of the classical complement pathway begins after the multivalent protein C1q binds to antibodies on a target surface, triggering a proteolytic cascade to lyse targeted cells (Figure 2.3A). The inability of AQP4 autoantibodies to activate the classical complement pathway on M1-AQP4 suggests that the spatial organization of bound antibodies contributes to complement activation [306]. We therefore formulated a metric to quantify the C1q multivalent binding potential for antibody spatial arrangements.

C1q has a "stem and tulips" structure, with each of 6 stems containing a globular head that is able to bind to an antibody Fc domain. While there are multiple spatial distributions of AQP4 rAb that can support multivalent C1q binding, a hexamer pattern potentially represents a best-fit solution that can engage each of the globular heads [163]. When superimposed over STED image pixel dimensions, multivalent C1q binding has the potential to occur across 4 pixels in a 2x2 pixel area (Figure 2.3B, top). We developed a 4-point scoring system to quantify the probability of multivalent C1q binding termed the Antibody Spatial Arrangement (ASA) score. Each pixel from a processed image receives a ranked integer score (1-4) based on the maximum number of neighboring pixels with signal intensity across a 2x2 area (Figure 2.3B, bottom). ASA score 1 represents an isolated binding event with low probability for multivalent binding, while ASA score 4 represents a dense cluster with the highest probability for multivalent C1q binding. The effective application of this scoring system across an entire cell (Figure 2.3C) is dependent on the ability to localize a fluorophore to each pixel. Since individual fluorophores cannot theoretically be resolved on neighboring

pixels (see Figure 2.1C/D), a series of data simulations were performed to reconstruct single binding events (as observed on M1-AQP4) within denser clusters (as observed on M23-AQP4) to test the possibility of developing an image processing algorithm that can assign fluorophores to any given pixel in an otherwise non-resolvable object.

Data Simulations Validate the ASA Algorithm

Random fluorophore distributions were generated to model antibody spatial distributions over 100 AQP4 arrays on a simulated cell (Figure 2.4A, left top). Two simulated images were generated for each random distribution. In one image, STED image pixel dimensions were immediately super-imposed to create a binary image where each pixel with an intensity value represents a pixel containing at least one Gaussian fluorophore peak (Figure 2.4A, left middle). In a second image, each fluorophore was convolved using the hypothesized point spread function (PSF) as calculated for individual antibodies binding to M1-AQP4. STED image pixel dimensions were then super-imposed over the second image to generate a simulated image representing a STED image for that particular fluorophore distribution (Figure 2.4A, right top).

We then asked if a threshold could be reliably applied to identify pixels containing a fluorophore. A threshold effectively eliminates pixels with a low probability of containing a fluorophore, as any detected photon events from these pixels would have a low probability of falling within the FWHM of a single fluorophore event. After application of a threshold, each remaining pixel has a high probability of having a Gaussian peak of intensity falling somewhere within that pixel. Too low of a threshold would produce a high number of false positives (low specificity), while too high of a threshold would only detect the brightest

events (low sensitivity). All simulated images were stepped through a series of thresholds at 5% increments to identify an endpoint with high sensitivity and specificity across a range of fluorophore densities (2.7-74.9% of array area, ~100 OAPs quantified per density). The threshold accuracy was determined by comparing all pixels containing detected events (defined as all non-zero pixels post-threshold, Figure 2.4B right middle) to the binary image to calculate the number of true and false positive events (Figure 2.4B). With a threshold value of 40%, 88.2% of all fluorophores were accurately localized with a 12.6% false positive rate. Although a 35% threshold yielded similar sensitivity, this threshold produced a higher number of false positives at denser concentrations (data not shown).

We subsequently used the 40% threshold to compare the calculated ASA score distribution for all positive pixels with the actual ASA score distribution on binary control images (Fig 2.4A, bottom). A linear relationship between calculated and actual ASA scores was not observed (data not shown), however, each calculated score was readily normalized, as score distributions followed clear polynomial relationships. The final algorithm was then tested with a second simulation series of random fluorophore distributions. Calculated ASA scores were highly correlated with actual ASA score distributions for ASA scores of 1, 2, and 4 (r^2 = .98, .99, .98 respectfully). ASA score 3 showed a slightly weaker correlation (r^2 = .83) as the algorithm was not as accurate at higher fluorophore densities (Figure 2.4C). The blinded best fit linear regression of each score was not significantly different from y = x (f=.62, p=.65). When averaged across the entire data set, the total calculated distribution represented the theoretical distribution with 98% accuracy. We conclude that information about single fluorophore spatial distributions can be extracted from an otherwise non-

resolvable object, given prior knowledge of how individual fluorophores are represented in an image.

Monoclonal Antibodies Display Different Potentials for Multivalent C1q Binding

We evaluated STED images of AQP4 rAbs on M1- and M23-AQP4 to evaluate the multivalent binding potential of resolvable objects using the ASA scoring system. Consistent with the lack of C1q-mediated complement activation on M1-AQP4 tetramers, the ASA scores for images of AQP4 rAbs on M1-AQP4 differed significantly from images on M23-AQP4. On M1-AQP4, the distribution of ASA scores was heavily skewed towards 1. For rAbs #53 and 58, ASA probability scores on M23-AQP4 were skewed towards 2 or higher despite, either no detectable increase, or only a small increase in apparent object size relative to M1-AQP4 (Figure 2.5A, Figure 2.2E). An even larger skewing was observed for rAbs #186 and #153 binding to M23-AQP4 OAPs. The larger object sizes generated by these two antibodies (Figure 2.2) were reflected in significantly higher median ASA scores. An identical shift in the ASA scoring distribution was produced when the clustering mutation E345R was introduced into rAbs #53, #58, and #186. Interestingly, some pixels with larger ASA scores (3 and 4) were detected at significant frequencies in images of rAbs that otherwise averaged smaller resolvable objects by FWHM calculations (e.g., rAbs #53 and #58). This may represent close juxtaposition of individual binding events. In summary, by applying a functional analysis constraint, we were able to identify different spatial arrangements amongst fluorescence patterns produced by densely packed rAbs within a confined surface area.

Discussion

We quantified multiple spatial arrangements for membrane-bound AQP4 autoantibodies with STED nanoscopy using two distinct biologic contexts. Using relatively dispersed M1-AQP4 tetramers, we were able to calculate the PSF of secondary labels in our STED images and subsequently use that information to develop methods to recognize differences in the spatial organization of antibodies in close proximity on M23-AQP4 arrays. The recognition of an individual binding event on M1-AQP4 also allowed us to more rigorously understand how fluorophores could be localized to individual pixels, without the direct ability to absolutely resolve events between neighboring pixels. Distinct spatial organizations were observed for some, but not all, monoclonal rAbs when comparing images on M1- and M23-AQP4. These differences correlated with changes in spatial distribution induced by a Fc-mutation that facilitates antibody clustering, suggesting that target epitopes may be spaced and oriented on M23-AQP4 OAPs to facilitate AQP4 rAb interaction, and subsequent C1q binding *in vivo*.

The advent of super-resolution imaging has introduced many new challenges in resolving individual proteins *in vivo*. Ideally, images would be obtained in a manner that allows for the resolution of individual molecular targets without compromising specificity or function. The relative size of many proteins compared to the size of the detecting fluorophore has the potential to confound precise localization and disrupt the local cellular environment. For example, our attempts to produce AQP4 rAb fusion proteins containing autofluorescent proteins resulted in disruption of both antibody binding and complement-activation (unpublished data). Labeling efficiency may also impact accuracy in quantifying protein assemblies. In our model, the C-terminal intracellular AQP4-specific commercial antibody

labels entire arrays, whereas extracellular-targeted rAbs label only portions of arrays. Therefore, the two antibodies would produce different results when used to calculate the size and number of AQP4 OAPs. The impact of such 'labeling' artifacts on image resolution was recently investigated in detail by Lau and colleagues [324].

Alternative super-resolution imaging approaches may offer novel solutions. For example, innovative single-molecule fluorophore labeling approaches and STORM imaging have been used to investigate both the mobility of M1- vs. M23-AQP4 tetramers on plasma membranes and the organization of M1- vs. M23-AQP4 tetramers within OAPs [112, 122, 330]. Atomic force microscopy has been used to demonstrate the potential for IgG antibodies to form hexameric assemblies [331] and for antibodies to move along repetitive surfaces and form transient antibody clusters [332]. In the future, atomic force microscopy could be adapted to examine antibody hexameric assemblies on AQP4 OAPs.

STED nanoscopy resolution depends not only on the physical properties of the nanoscope, but also on the efficiency of depletion of the specific fluorophore. STED resolution is generally ~40 nm, although other studies have reported resolution near 20 nm [333, 334]. In our study, we achieved a resolution of ~20 nm. However, the true resolving capabilities in our experiment remain unknown, as our pixel size (19.5 nm by 19.5 nm) limits calculation accuracy. Despite this limitation, our ASA analysis is consistent with localization of secondary antibody fluorophores to individual 19.5 nm pixels. Data simulations performed at lower lateral resolutions (generally >30nm) were not able to accurately localize fluorophores or produce images with features similar to our STED images (data not shown), further indicating that true 20 nm resolution is driving the successful application of our threshold analysis approach. Imaging at a smaller pixel sampling size could improve

resolution; however, increased pixel density comes at the expense of image acquisition time. Depending on the goals of the imaging experiment, this tradeoff may be self-defeating. For example, although a multivalent IgG platform is a known requirement for C1q binding, inadequate understanding of C1q binding site geometries, combined with uncertainty regarding the position of the secondary fluorophores, significantly limits the impact of resolution on multivalent binding potential calculations. Indeed, our processing algorithm represents a novel approach to overcome resolution limitations and infers protein spatial relationships without necessitating direct resolution of single molecules. Testing how this algorithm performs under alternate experimental environments may assist in understanding how generalizable our approach may be for other imaging paradigms. Lastly, as resolving capabilities are dependent on detecting changes in pixel intensity, analysis of mean pixel intensity deviations between adjacent pixels may represent an alternate method for future algorithms. Such approaches were not pursued in this study given our well-defined imaging environment and our initial success with the ASA scoring system.

In conclusion, we were able to image two unique plasma membrane structures at high resolution using STED nanoscopy and model variable patterns of antibody clustering in relation to epitope specificity and AQP4 array assembly. Future investigations that correlate these spatial arrangements with additional functional studies of C1q activation may provide a framework to understand how AQP4-IgG promotes tissue destruction in neuromyelitis optica. Expanding this approach to additional model systems may facilitate the development of novel algorithms to dissect larger protein assemblies at lower lateral resolutions and advance our understanding of the organization and function of protein clusters.

Endnotes

This study was funded by the Guthy-Jackson Charitable Foundation, a National Multiple Sclerosis Society Collaborative grant, the National Institutes of Health (NEI EY022936, NIDCD NS048154) and the National Science Foundation (MRI 1337573). This content of this chapter is currently under peer review.

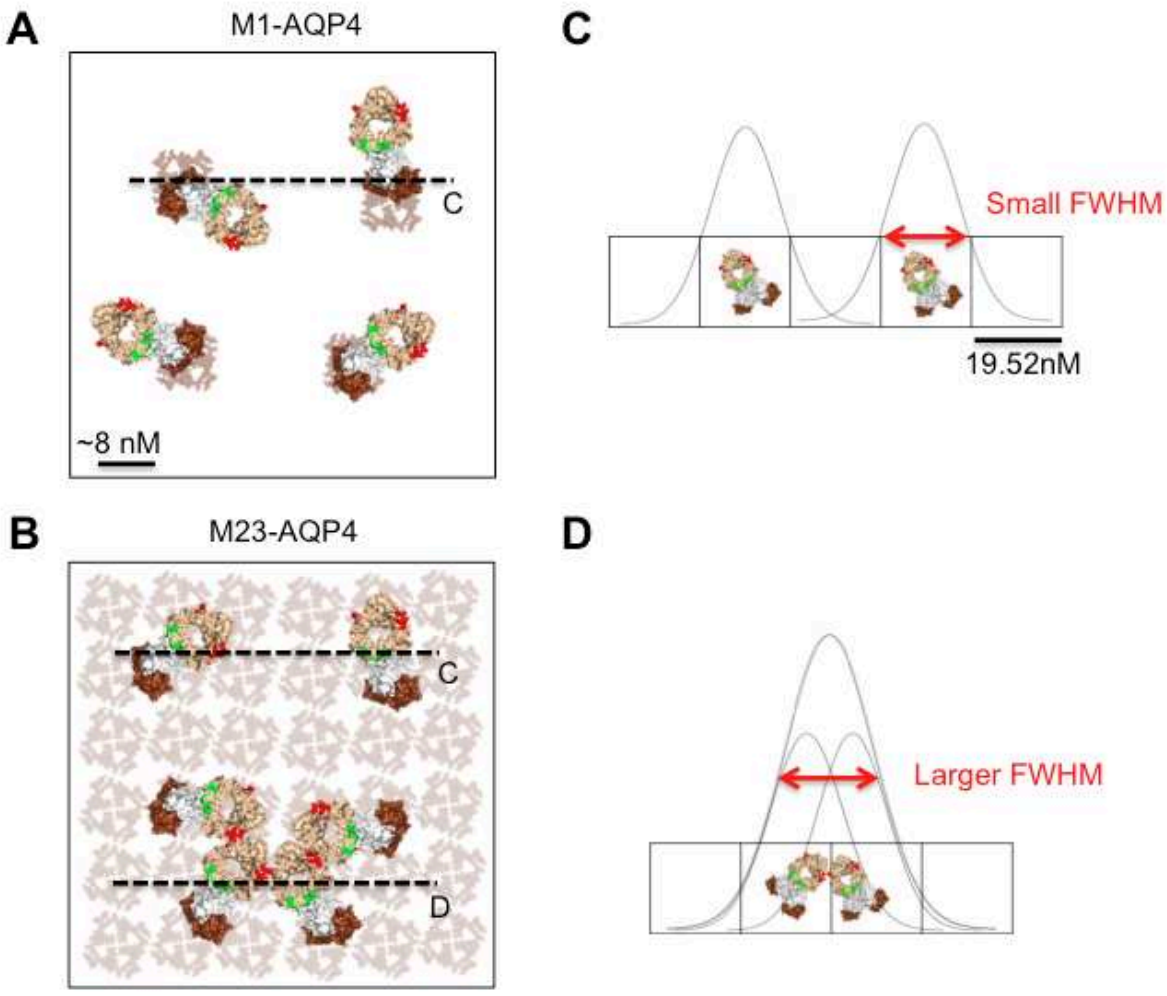

Figure 2.1: AQP4 autoantibodies have the potential to bind in multiple spatial distributions to M1-AQP4 and M23-AQP4
(A,B) Surface schematics of AQP4 rAbs bound to cell surface AQP4. (A) M1-AQP4 tetramers repel each other on the cell membrane, resulting in isolated, bound AQP4 autoantibodies. (B) M23-AQP4 organizes into large arrays on a cell membrane, offering the potential for multiple spatial distributions of bound autoantibodies depending on epitope geometry and organization. (C,D) Because the size of the AQP4 scaffold is of a similar size as the STED resolution, the size of a resolvable object, defined as the full width half maximum intensity (FWHM) of a Gaussian fit, is proportional to the size of antibody clusters. The antibody distributions in (C) and (D) represent the distributions indicated by dashed lines in (A) and (B), with STED pixel coordinates and a theoretical Gaussian fit superimposed.

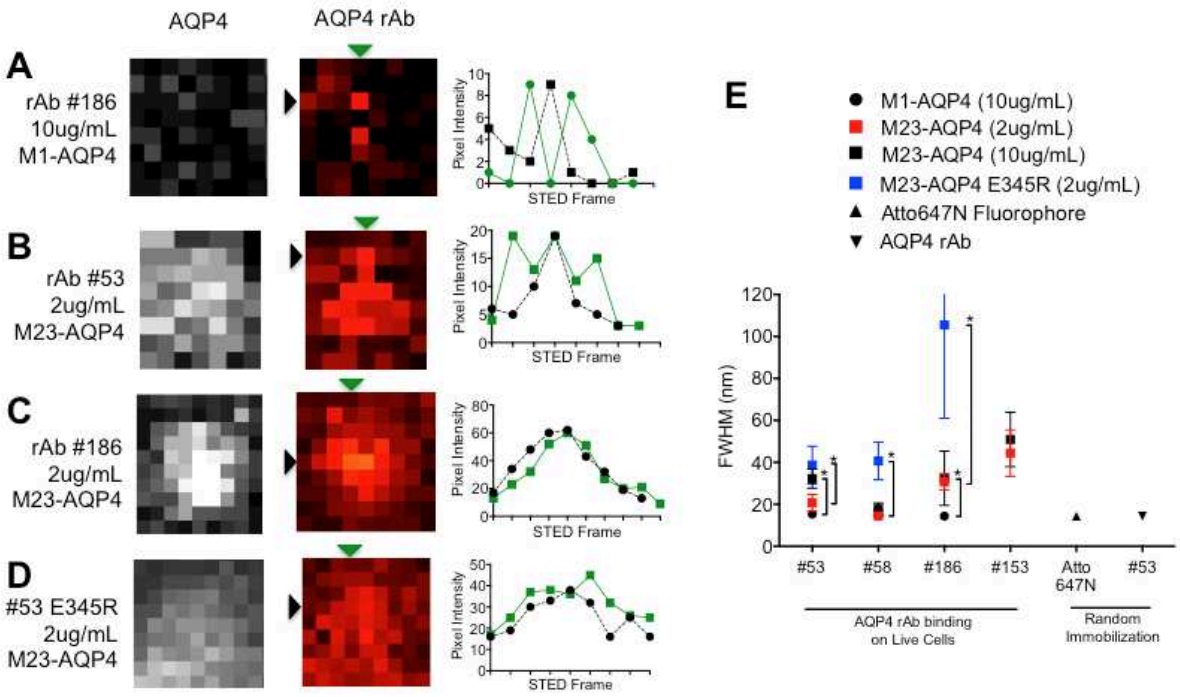

Figure 2.2: Quantification of mean object size on STED images
(A-D): Representative antibody images are shown for several AQP4 autoantibodies binding to M1-AQP4 (A) and M23-AQP4 (B-D). An intracellular antibody (left) detects all AQP4, extracellular autoantibody binding (middle) is shown with pixel intensity histograms (right) for all rows/columns labeled with an arrow. (E): Calculated mean FWHM of each resolvable object averaged across an entire image. Data was compared using one-way ANOVA with Tukey's test for multiple comparisons (*, adjusted $p < .05$). STED image scale: 19.5x19.5nm/pixel

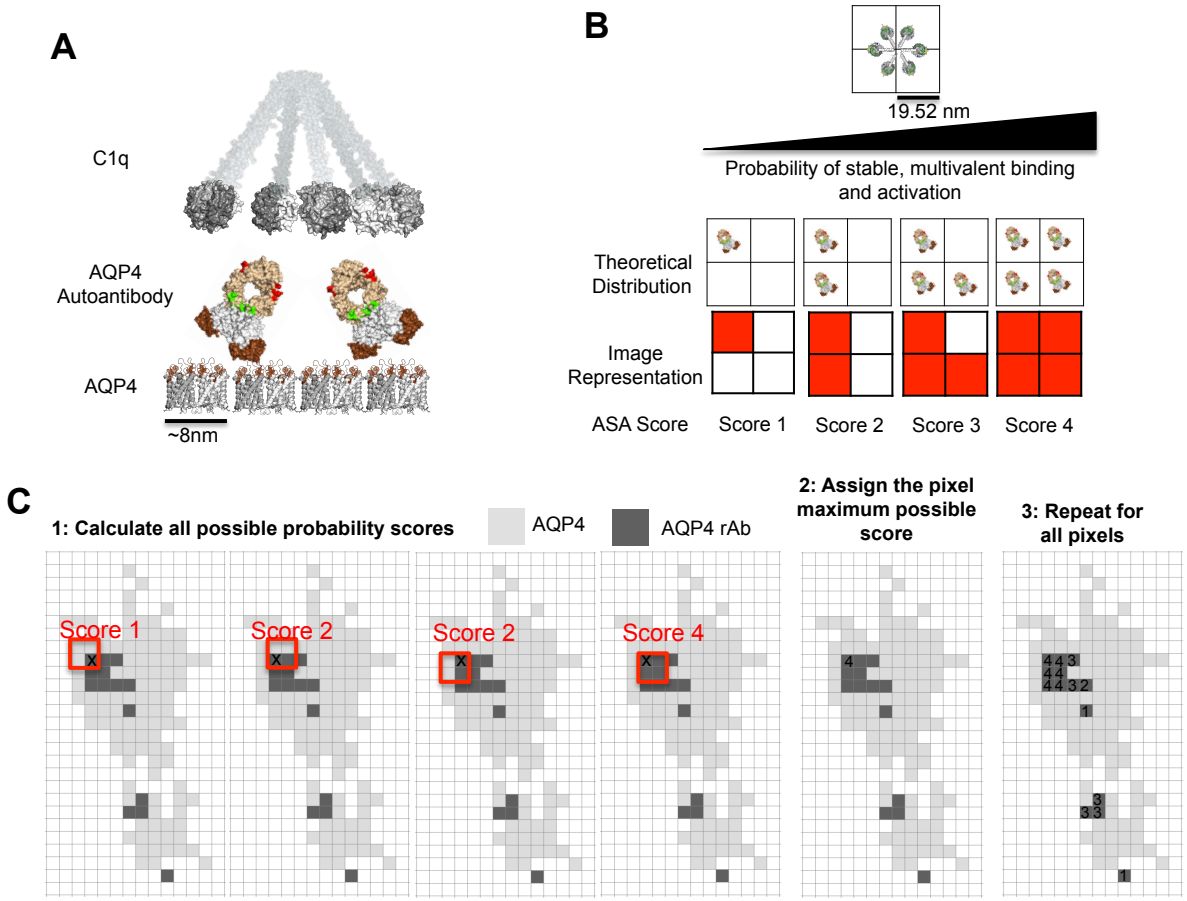

Figure 2.3: A method to score rAb antibody scaffolds that interact with C1q
(A): A schematic of C1q interacting with membrane-bound AQP4 autoantibodies demonstrating the potential assembly of multivalent autoantibodies on AQP4 OAPs. (B): (Top) Top-down depiction of a C1q molecule super-imposed over STED pixel coordinates. (Bottom) Schematic paradigm for scoring distributions of AQP4 antibodies that support multivalent C1q binding. (C): Sample application of the ASA scoring system to a theoretical STED image. The ASA score is determined in an iterative fashion using MATLab code. All pixels with a fluorescence signal are scored for each of the 4 possible ASA score arrangements (1), then the pixel is assigned the maximum possible ASA score (2), and the process is repeated for all pixels across the image (3).

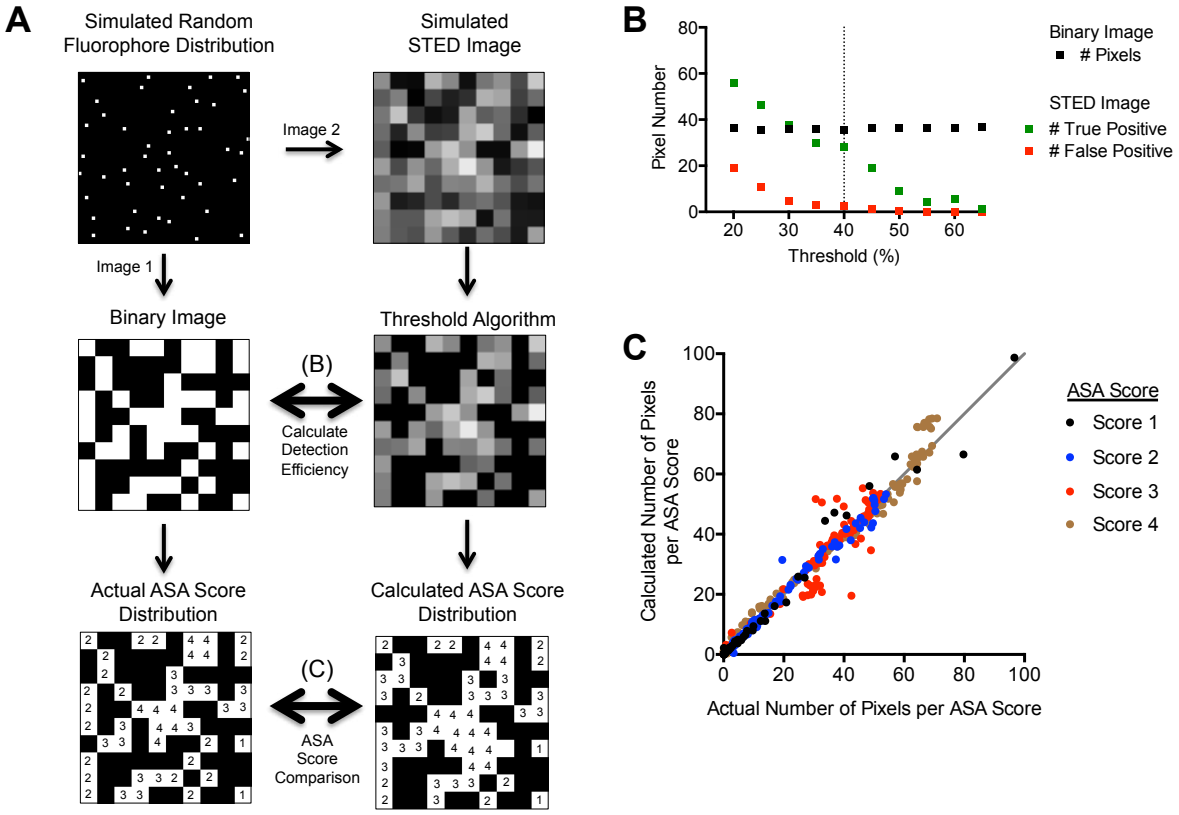

Figure 2.4: Data simulations validate the ASA scoring system on large protein assemblies

(A) Application of the ASA scoring system to a simulated OAP distribution. A random fluorophore distribution is created (top left) and converted into both a binary image demonstrating pixels containing a fluorophore (left middle) and a simulated STED image (top right). The simulated STED image was placed through a series of experimental thresholds to test how well a threshold may identify fluorophore-containing pixels, compared to the known distribution of fluorophores (middle row). The ASA score for both known and calculated distributions was tallied (bottom row) and compared. (B) Sample AQP4 array data demonstrating the accuracy of various detection thresholds. (C) Quantification of the performance of the final ASA scoring algorithm using a 40% threshold on independent simulated data set.

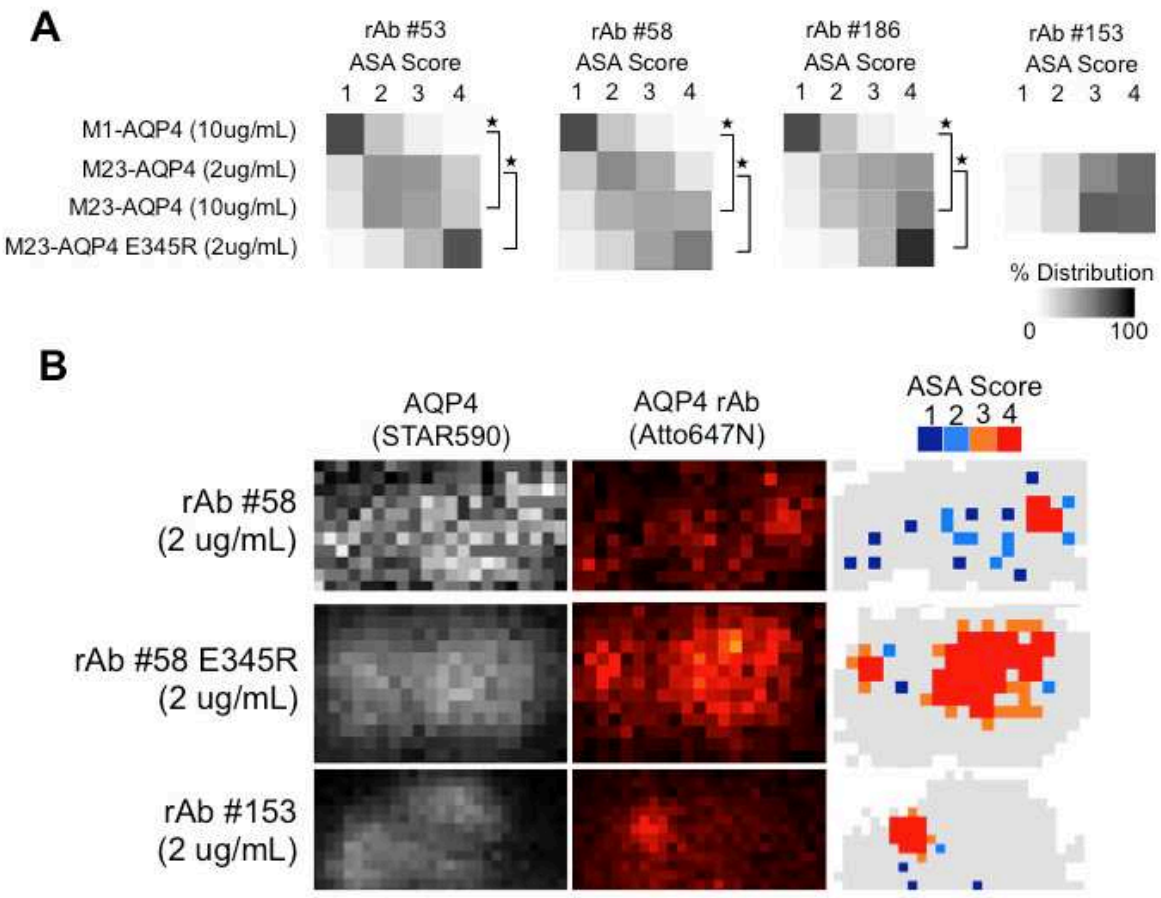

Figure 2.5: ASA scores of membrane-bound AQP4 rAbs
(A): The ASA score distributions for multiple AQP4 rAb are presented as a heat map representing the relative frequency of each ASA score across all OAPs (M23-AQP4) or across an entire cell (M1-AQP4). The median ASA score was significantly increased for all AQP4 rAbs on M23-AQP4 compared to M1-AQP4 and for E345R-mutated AQP4 rAbs on M23-AQP4 (*p<.001, Mann-Whitney). (B) Sample STED images of AQP4 (left) and AQP4 rAb (middle) for three AQP4 rAbs. The corresponding ASA score (right) is shown for the AQP4 rAb image (middle). Grey represents an AQP4 array, and each ASA score is represented by a colored pixel (1: Dark blue, 2: light blue, 3: orange, 4: red).

CHAPTER III

CELL SURFACE ASSEMBLY OF AQUAPORIN-4 AUTOANTIBODIES REGULATES CLASSICAL COMPLEMENT ACTIVAITON IN NEUROMYELITIS OPTICA

Abstract

Neuromyelitis optica (NMO) is a severe, inflammatory CNS disorder associated with autoantibodies that bind the aquaporin-4 water channel (termed AQP4-IgG). AQP4-IgG mediated complement activation plays a central role in NMO lesion formation. We investigated the molecular determinants driving C1q activation by AQP4-IgG using recombinant AQP4-specific autoantibodies (AQP4 rAb) derived from individual NMO patient cerebrospinal fluid plasmablasts. We identified a unique group of AQP4 rAbs that activate complement at an enhanced level despite lower AQP4 binding affinity. These rAbs recognize a unique AQP4 extracellular epitope that promotes an IgG Fc domain interaction that accentuates C1q activation without directly enhancing antibody Fc-C1q binding. Using M1- and M23-AQP4 isoforms, we demonstrate that individual AQP4 rAb do not efficiently engage the multivalent complement protein C1q to activate CDC. Instead, an optimal C1q activation site is formed via the formation of stable, multivalent IgG platforms whose assembly is driven by Fc domain interactions between neighboring antibodies upon surface binding. This model provides a framework for understanding IgG-mediated classical complement pathway activation in human autoantibody-mediated disorders.

Introduction

Neuromyelitis optica (NMO) spectrum disorders are a family of demyelinating disorders of the central nervous system historically defined by inflammatory attacks of optic neuritis and transverse myelitis. Approximately 80% of patients test seropositive for autoantibodies targeting aquaporin-4 (termed AQP4-IgG), the predominant homeostatic water channel of the central nervous system (CNS) [19, 236, 301]. The recognition of AQP4-IgG as a disease-specific biomarker has since led to an appreciation of more global CNS involvement [65]. The histopathology of CNS lesions and substantial experimental data support a direct pathogenic role of AQP4-IgG in tissue injury [86, 301, 335].

AQP4-IgG likely mediates CNS destruction through multiple mechanisms [47, 86]. Both clinical and experimental data, however, support AQP4-IgG mediated classical complement activation as the primary mechanism initiating and driving CNS injury. Classical pathway activation is initiated when IgG or IgM engages the multimeric complement protein C1q to trigger a proteolytic cascade that ultimately produces an array of biologically active proteins implicated in lesion formation: opsonins, anaphylatoxins, chemotactic agents, and the membrane attack complex (MAC) [336, 337]. To reproduce AQP4-IgG, monoclonal human AQP4 recombinant autoantibodies (termed AQP4 rAb) were generated using AQP4-IgG sequences obtained from individual cerebrospinal fluid plasmablasts of clinically relapsing NMO patients [267]. Indeed, *in vivo* and *ex vivo* experimental NMO lesion formation is dependent on AQP4 rAb activation of the classical complement pathway [306, 338]. Interestingly, complement-mediated cross-activation of additional effector processes is also required for full NMO lesion development, collectively attributing multiple direct and indirect injury pathways emanating from C1q activation by

AQP4-IgG [253, 254]. In support of these models, NMO patients demonstrate serologic [36, 38, 339] and histologic [47, 340] evidence of complement activation, and complement inhibitors have shown early promise in acute and prophylactic clinical trials [102, 103].

Experimental and clinical data indicate that C1q activation by AQP4-IgG is influenced by AQP4 structure and antibody-intrinsic features. Two AQP4 isoforms are expressed within plasma membrane AQP4 tetramers: a full length M1 protein and a shorter M23 protein [124]. Each isoform has identical extracellular domains and differs only in the N-terminal amino acid sequence. M23-AQP4 promotes and M1-AQP4 limits the organization of AQP4 into large arrays on the cell surface termed orthogonal array of particles (OAPs). OAP formation is essential for classical complement activation by AQP4-IgG, attributed to efficient multivalent C1q binding by clustered AQP4-IgG on larger arrays [306]. In NMO patients, however, disparities between AQP4-IgG titers and complement-mediated injury severity suggest that not all AQP4 autoantibodies have similar potentials to activate C1q [283]. This difference may arise from the epitope specificity of individual AQP4-specific autoantibodies as almost all are IgG1 [51]. Indeed, while most AQP4-IgG target epitopes are broadly defined by a conformational requirement for two or three extracellular loops, there exists significant microheterogeneity in the specific loop amino acids that are critical for optimal binding of individual autoantibodies [299]. As individual AQP4-specific autoantibodies also have distinct affinities for AQP4 OAPs [289, 300], it is likely that multiple molecular interactions may simultaneously promote AQP4-IgG-mediated C1 activation *in vivo*.

To date, an *in vivo* model of C1q activation by IgG1 does not exist [159, 192]. A recent model proposed that the ordered assembly of IgG hexamers upon membrane binding

yielded a best-fit model for C1q binding and activation [163]. We tested this model in the context of pathologic human autoimmunity using AQP4 rAbs, as AQP4 rAb are generated directly from NMO patients at the time of clinical activity. Using multiple AQP4 rAbs with differing epitope specificities, engineered Fc domain mutations to modulate C1q binding, pharmacologic manipulation, and super-resolution microscopy, we evaluated the impact of rAb epitope specificity and multimeric IgG complex formation on AQP4-IgG-mediated classical complement activation. The results demonstrate how intrinsic antibody binding properties may organize multimeric IgG assemblies upon surface binding to facilitate complement C1q activation, establishing a framework for understanding and treating antibody-mediated autoimmunity.

Results

AQP4 membrane organization and AQP4 Loop C epitopes promote or limit CDC activation by AQP4 rAb

Complement activation by individual AQP4 rAb was investigated by quantifying complement-dependent cytotoxicity (CDC) on CHO cells expressing pure M1- or M23-AQP4 via LDH release. In this assay, CDC was dependent on classical pathway activation as demonstrated by the absence of lysis using C1q-depleted serum (rescued with recombinant C1q supplementation), no significant change with alternative or mannose-binding lectin pathway depletion, and no CDC when only mannose-binding lectin pathway is able to activate through depletion of both alternative pathway protein Factor D and classical pathway protein C1q (Figure 3.1A for example using rAb #58).

AQP4 rAbs activated complement on M23-AQP4 with variable efficiency (Figure 3.1B). C1q activation did not correlate with either levels of bound AQP4 rAb or C1q, indicating that C1q binding and subsequent activation are distinct processes (Figure 3.1 C/D). Interestingly, one group of rAbs activated CDC efficiently at low levels of bound C1q or rAb (Figures 3.1C/D, dashed boxes). We observed that these rAbs shared an unique sensitivity to the extracellular loop C amino acids His151 and/or Leu154 (Figure 3.1E/G) [299]. Indeed, alanine substitutions at these positions abolished binding (Figure 3.1G) but did not affect rAbs requiring significantly higher levels of bound rAb to activate complement (Figure 3.1F).

His151/Leu154 binding facilitates Fc domain interactions on OAPs

The IgG1 Fc fragment includes a CH2 domain that directly interacts with C1q and a CH3 domain that contains a large hydrophobic patch critical for non-covalent interactions between neighboring IgG Fc domains. In a model of C1q engagement to OAP-bound AQP4 autoantibody (Figure 3.2A), binding of C1q to antibody Fc CH2 domains may act in concert with the interaction of neighboring CH3 domains to stabilize a tripartite complex capable of initiating the classical complement pathway. Therefore, the assembly of AQP4 into OAPs may geometrically organize repetitive targets for Fab binding, the spacing of which may differentially promote the surface assembly of stable antibody complexes optimal for C1q activation.

Using His151/Leu154 dependent- and independent-AQP4 rAbs, we tested the relative contributions of CH2-C1q affinity and CH3 Fc-Fc interactions on C1 activation *in vitro*. Fc domain point mutations were introduced to increase or decrease CH2-C1q affinity (AEFTE

G236A/S267E/H268F/S324T/I332E increases, K322A decreases) [162] and promote or limit CH3 domain Fc-Fc interaction (E345R promotes, I253D limits) [163] (Figure 3.2B). These mutations did not impact antibody binding (data not shown). We first examined two AQP4 rAbs, #53 (His151/Leu154 independent) and #186 (His151/Leu154 dependent), that differentially activated CDC (Figure 3.1B) despite similar binding affinity for M23-AQP4 (K_D: 15.2 +/- 2.4 nM for rAb #186 and 14.8 +/- 2.4 for rAb #53). Enhancing C1q-CH2 affinity had little to no effect on CDC by either rAb (Figures 3.2D/G). An E345R mutation that enhanced CH3 Fc-Fc interaction, however, significantly accentuated rAb #53-mediated CDC (Figures 3.2 D/G) to levels similar to rAb #186. Both rAbs required Fc-Fc interaction to activate CDC, as the Fc-Fc disrupting mutation I253D inhibited all complement activity. The effect of the I253D mutation could not be overcome by concurrently enhancing C1q-CH2 affinity (I253D/AEFTE mutations, Figures 3.2 D/G). In addition, CDC activation was not further enhanced when the E345R and AEFTE mutations were introduced in parallel in either rAb. Together, these findings demonstrate that CH3 domain interactions formed between AQP4 autoantibodies upon OAP binding are key for efficient complement activation.

We next examined how complement activation correlated with maximum levels of bound C1q (C1q B_{MAX}). For native rAb #53 IgG1, the half-maximal effective concentration for CDC ($EC50_{CDC}$) was achieved when levels of bound C1q were close to the C1q B_{MAX}, whereas the EC50 for rAb #186 fell well below its C1q B_{MAX} (Figures 3.2D/G). In general, rAb #186 bound C1q at higher levels than rAb #53 (Figure 3.2D/G); however, further increases in C1q binding (mutations AEFTE and E345R, Figure 3.2G) did not further enhance CDC. Although the AEFTE mutation provided the most notable enhancement of

rAb #53 C1q binding, the E345R mutation provided a far greater improvement in CDC. Indeed, rAb #53 containing the AEFTE mutation demonstrated C1q binding that surpassed that of native rAb #186, although did not completely bolster activation.

The data obtained from rAbs #53 and #186 indicate that C1q activation requires CH3 domain-driven assembly of AQP4 autoantibodies upon OAP binding to achieve some minimal threshold of C1q binding sufficient for activation. We examined these criteria further using additional His151/Leu154-dependent and -independent rAbs with a broad range of epitope specificities and binding affinities. The $EC50_{CDC}$ of His151/Leu154$^-$independent rAbs was proportional to antibody binding affinity (K_{M23}) to M23-AQP4 (rAb #53 > rAb #58 > rAb #121; Figure 3.2D/E/F). Since these AQP4 rAbs have similar maximal binding (B_{MAX}) and bind similar levels of C1q, the data suggests that activation of multivalent C1q is likely driven by the organization of CH2 domain binding sites facilitated by rAb saturation of the target AQP4 array. Indeed, disruption of CH3 domain interactions with Fc mutation I253D abrogated CDC activity in all His151/Leu154$^-$independent rAbs, and facilitation of CH3 Fc-Fc interactions with the Fc mutation E345R substantially increased CDC activity to levels similar to the His151/Leu154$^-$dependent rAb #186 (Figure 3.2D-F).

For His151/Leu154-dependent rAbs (Figure 3.2G-J), increasing C1q-CH2 affinity or CH3-CH3 interactions had mixed effects on CDC: there was no significant effect on rAbs #186 and #93, but rAbs #153 and #33 showed some moderate increase. Nevertheless, CDC by rAbs #153 and #33 significantly exceeded the His151/Leu154-independent rAbs #53, #58, and #121 despite identical or lower levels of both IgG and C1q binding. Interestingly, rAbs #153 and #33 showed extremely low C1q binding (Figures 3.2I and 3.2J) compared to other His151/Leu154-dependent rAbs. Perhaps microheterogeneity amongst His151/Leu154-

dependent epitopes [299] promotes structural variations on multimeric tripartite assemblies. Each satisfies the molecular requirements for high-level C1q activation despite the potential for the total number of C1q binding sites being constrained by the level and orientation of bound rAb, particularly among rAbs with very low levels of C1q binding. Not surprisingly then, and as observed, modulating tripartate interactions would be expected to have mixed effects dependent on the relative strength of the initial assembly. Indeed, the I253D Fc mutation inhibited complement activation by His151/Leu154-dependent rAbs although complement activation by rAb #93 was not completely inhibited (Figure 3.2H). The I253D mutation, however, may not have completely inhibited CH3-CH3 interactions between bound rAbs #93, as C1q binding was still measurable on M23-AQP4 expressing cells (Figure 3.2I).

CH3-CH3 interaction amongst AQP4-IgG Fc is critical for CDC

Prior studies had demonstrated that an Fc-binding peptide (DCAWHLGELVWCT) could interact tightly with the Ig Fc-binding site [341]and partially inhibit monoclonal Ab targeted CDC [163, 341]. We examined the effect of this peptide on His151/Leu154-dependent and -independent rAbs. Fc-binding peptide, but not control peptide, significantly inhibited CDC by both rAb classes (Figures 3.3A and 3.3B). Introduction of the AEFTE mutation to improve CH2-C1q affinity did not rescue complement activation.

Fc-binding peptide also reduced CDC by native polyclonal AQP4-IgG from NMO patient serum. CDC occurred at a range of levels as anticipated [283], with variable levels of peptide inhibition (Figure 3.3C). While this variation is potentially attributed to differing effective peptide concentrations between serum samples given competitive binding to unknown titers of total serum IgG and other serum protein, the ability for targeted CH3

domain peptide binding to disrupt C1q activation across all patients nevertheless demonstrates that the formation of IgG assemblies upon surface binding is key for efficient complement activation.

Poor CDC on M1-AQP4 is Ab Independent

Previous work has demonstrated that AQP4 rAbs are unable to initiate CDC on M1-AQP4 [306]. We investigated whether epitope specificity, enhanced CH2-C1q binding, or facilitation of CH3-CH3 interactions would allow complement activation on M1-AQP4. Despite expressing similar levels of AQP4 [306], M1-AQP4 expressing cells were resistant to CDC by His151/Leu154-independent (Figure 3.4 B-D) and -dependent (Figure 3.4E-H) rAbs. Enhancing Fc-Fc interactions (E345R) or CH2-C1q binding (AEFTE) did not rescue CDC (Figure 3.4B-H). The combination mutation (E345R/AEFTE) was also unable to restore CDC on M1-AQP4 (rAbs #53 and #186). The results suggest that the intrinsic resistance of M1-AQP4 to OAP assembly sterically inhibits CH3-CH3 interaction by preventing the close association of bound AQP4 rAbs.

AQP4 rAb Clustering and CDC on M23-AQP4 Arrays

The accumulated data support a critical role for antibody clustering on M23-AQP4 OAPs for classical pathway activation. We next used STED nanoscopy of membrane-bound AQP4 rAb to test whether differences in AQP4 rAb clustering on M23-AQP4 could be directly associated with enhanced complement activation. We have previously shown that super-resolution STED nanoscopy may be used to image AQP4 OAPs and tetramers (see 5A for example images) (Chapter 2), and developed and validated a STED image processing

algorithm to quantify the average size of AQP4 rAb clusters bound over AQP4 at ~20nM resolution. Although fluorescence nanooscopy is unable to directly image Fc-Fc interactions, we hypothesized that larger average antibody cluster sizes would increase the potential for multiple IgG contacts with the globular heads of C1q. As a result, the spatial arrangement of antibody clusters could be used to generate a hypothetical score for multivalent C1q binding that could be correlated with data on epitope specificity, Fc-Fc interaction, and accentuated complement activation. Our analysis is limited to STED imaging of rAb binding to M23-AQP4, as antibody clusters were not observed on M1-AQP4 (Chapter 2).

We first asked if His151/Leu154 -dependent rAbs generally bind in larger clusters by grouping the average resolvable antibody cluster size for multiple rAbs by epitope specificity. Indeed, His151/Leu154-dependent rAbs generally appear as larger clusters when comparing rAbs with similar (#53 vs #186) or distinct (#58 with #153; Figure 3.5B) binding affinities. As anticipated, the E345R mutation increased the general size of His151/Leu154-independent rAb clusters towards an average size that was similar to the His151/Leu154-dependent rAbs. These findings suggest that rAbs dependent on His151/Leu154 are oriented upon array binding in a manner that optimizes organization into multimeric clusters capable of facilitating complement activation.

The multivalent C1q binding potential for any given antibody spatial arrangement was scored on a 1-4 scale (termed ASA score) (Chapter 2). ASA score of 1 represented a low probability for multivalent C1q binding, while a score of 4 represented a high probability (Figure 3.5C). Each rAb was observed to have a unique distribution of scores over M23-AQP4 arrays with some rAb favoring multivalent C1q contacts while others were more isolated. We asked if epitope-dependency correlated with the observed differences in

multivalent binding potential. A non-biased hierarchal clustering analysis demonstrated that ASA score distributions for His151/Leu154-dependent AQP4 rAbs were skewed toward higher probability scores than His151/Leu154-independent rAbs (Figure 3.5D). Similarly, rAbs containing the E345R Fc mutation demonstrated a similar skewing of their ASA score. In contrast, His151/Leu154-independent rAbs demonstrated lower ASA score distributions that resembled those produced by rAb binding on M1-AQP4. ASA scores was largely independent of rAb concentration indicating that AQP4 antibody clustering on M23-AQP4 OAPs is driven predominantly by antibody intrinsic properties.

Consistent with the importance of antibody clustering for complement activation, we observed a relationship between the ASA score, the concentration of bound C1q and C1q activation (Table 3.1). At concentrations of rAb where 100% cell lysis occurred, AQP4 rAb with lower ASA scores required higher levels of bound C1q. The rAbs with low ASA distributions were His151/Leu154-independent and activated C1q only after sufficient saturation of M23-AQP4 OAPs. In contrast, His151/Leu154 -dependent rAbs had higher ASA scores and required roughly half the level of bound antibody to activate C1q. Although our limited sample size prevented a meaningful statistical analysis, a clustering model of complement activation by AQP4 autoantibodies explains how epitope specificity organizes IgG platform assemblies via CH3 domain interactions into stable complexes that support multivalent C1q binding and efficient complement activation.

Discussion

A Unified Model of Classical Complement Pathway Activation

This study outlines the first model of the molecular interactions driving classical complement activation in pathologic human autoimmunity. Using human, pathogenic recombinant monoclonal anti-AQP4 antibodies derived from clinically relapsing NMO patients, we demonstrate that the assembly of multimeric arrays of autoantibodies upon binding to sheets of membrane AQP4 protein is critical for C1q activation, as anticipated by the work of Diebolder et al. (2014). The membrane organization of AQP4, driven by AQP4 isoform, and the epitope specificity of AQP4-IgG combine to orient bound Fc domains into spatial configurations that augment CH3 domain interactions and the construction of multimeric assemblies that optimize C1q binding and activation (Figure 3.6A). M1-AQP4 predominant tetramers are mobile in the plasma membrane and resist array assembly, consequently limiting the formation of Fc-Fc interactions amongst bound autoantibodies to prevent C1q engagement and activation (Figure 3.6A, left panels). In contrast, large M23-AQP4 OAPs allow for efficient target binding without rapid internalization [122, 307] (Figure 3.6A, middle and right panels). The binding affinity, epitope specificity, autoantibody titer, and OAP size combine to determine the distribution and orientation of autoantibodies on the AQP4 plasma membrane arrays. High or low affinity AQP4 autoantibody with His151/Leu154 epitope specificity will orient and self-assemble into clusters that are stabilized by adjacent CH3-CH3 binding (Figure 3.6A, top middle and right panels), permitting efficient C1q binding and activation despite relatively low levels of bound IgG. His151/Leu154-independent autoantibodies, however, require higher levels of array binding to assemble IgG platforms sufficient for C1q binding and activation (Figure

3.6A, bottom middle and right panels). As a result, multiple antibody intrinsic and extrinsic factors likely combine to influence the distribution, severity, and timing of CNS lesions in NMO: AQP4 array size, number, and accessibility at the tissue level, interplaying with AQP4-IgG titer, binding affinities, epitope specificity, and post-translational modifications. The level of C1q activation that this platform activates needs to sufficiently overcome the local expression of complement inhibitors (Figure 3.6B).

The molecular mechanisms regulating C1 activation have been the subject of considerable investigation [159, 160]. C1 activation requires a mechanical stress upon IgG binding to disrupt the C1r2:C1s2 complex housed within the C1 collagenous stems [161, 192]. Our observed relationship between levels of bound C1q and EC50 indicate that C1q binding is not sufficient for C1 activation (Figure 3.1B). Indeed, variable augmentation of complement activation despite significant enhancements in C1q binding (Figure 3.2D-J) suggests that certain IgG platforms (Figure 3.6A) may facilitate C1r2:C1s2 dissociation. An IgG hexamer may represent a best-fit platform to incite mechanical stress, most notably demonstrated by fluid-phase complement activation in the absence of target antigen [163]. Since only 4 C1q globular heads were noted to be in contact with the fluid-phase platform, it is possible that alternative platforms with equal activating capabilities may drive C1 activation on AQP4 OAPs. This is supported by our observation of distinct levels of maximal C1q binding despite similar levels of antibody saturation for unique AQP4 rAb epitopes. A hexameric organization may represent the predominant structural backbone driving IgG assembly, with variations in assembly conformations arising from the unique epitope geometries patterned across an AQP4 array. It also remains unclear if lower size clusters represented by ASA scores of 1 and 2 have the potential to activate C1q. It is possible that

His151/Leu154-independent rAbs require higher levels of bound antibody to increase the frequency of ASA score 3 and 4 clusters, or that a larger number of smaller clusters can cause sufficient mechanical stress, although with lower probability. It is likely that an IgG platform interweaves both CH2-C1q and CH3-CH3 interactions to optimize C1q binding and minimize activation energy. While our data preliminarily favors the importance of CH3-CH3 interactions, more detailed investigations are required to better understand how hexamerization facilitates the mechanical stress needed for C1q activation including the minimal sufficient assembly.

The Regulation of Local Classical Complement Activation in Health and Disease

The predilection for NMO pathology targeting optic nerve and spinal cord generally aligns to sites where AQP4 is expressed and assembled into OAPs at higher levels within the CNS [125, 342]. Pathologic complement activation may only occur if the interplay of AQP4 OAP assembly with IgG titers combine to allow the threshold level of complement activation necessary to overcome local tissue complement inhibition (Figure 3.6B). In NMO, pathology is also notably absent in peripheral organs despite significant AQP4 expression [343], AQP4-IgG binding [260], and tissue susceptibility to complement activation. For example, the kidney is particularly susceptible to an array of complement-mediated disorders but is spared in NMO despite expressing high levels of AQP4 [147, 344]. While the local expression of complement inhibitors likely plays a critical role in setting the threshold level for C1q activation required for cell lysis [256], modulating AQP4 OAP array formation may offer a novel therapeutic strategy for disease prophylaxis by limiting the formation of stable AQP4-IgG assemblies [306].

The importance of IgG assembly formation upon target binding for complement activation may have clinical implications for other nervous system autoimmune disorders. For example, in anti-N-methyl-D-aspartate receptor (NMDAR) encephalitis, anti-NMDAR IgG1 antibodies produce prominent memory and behavior deficits in the absence of tissue destruction. Complement activation is not observed in human histology studies, despite a predominance of IgG1 autoantibodies [345]. Anti-NMDAR antibodies cause disease pathology by inducing receptor internalization (antigenic modulation) [346]. Rapid internalization following bivalent receptor binding likely prevents CH3 domain Fc-Fc interactions between plasma membrane bound anti-NMDAR IgG1. Conversely, in myasthenia gravis, autoantibodies against the nicotinic acetyl choline receptor (nAChR) bind monovalently and bivalently to dense, highly ordered hexagonal lattices at the neuromuscular junction [347]. Although modulation of nAChR signaling may occur [348], complement activation is commonly observed in regions of anti-nAChR IgG deposition and destruction of neuromuscular junctions appears to be the primary pathogenic mechanism [349]. Indeed, large immobile arrays of target antigen may be the ideal target for complement-mediated antibody defense or destructive autoimmunity by allowing the formation of CH3-CH3 interactions for stable antibody assemblies.

Complement Activation and NMO: Implications for Prognosis and Treatment

The requirement of ordered Fc domain organizations for complement activation by AQP4-IgG introduces several challenges to patient care. First, as evidenced by His151/Leu154-independent and –dependent AQP4 rAbs, individual AQP4 autoantibodies may differ profoundly in their ability to activate complement. As a result, NMO patient

serum may activate complement with quite different efficiencies despite similar autoantibody titers. Quantifying the specific titers of AQP4 autoantibody sub-populations may better predict disease activity and outcome measures. Complement activation may be further impacted by antibody glycosylation [285, 291, 350] resulting in dynamic fluctuations in antibody effector function despite stability in AQP4-autoantibody populations. Diagnostic assays and therapeutic interventions designed to measure and modulate these variables may significantly impact treatment strategies.

A second challenge arises measuring the impact of circulating AQP4-IgG on CNS pathology. First, it remains unclear if the readily assayed serum AQP4-IgG titers are reflective of AQP4-IgG populations in the CNS [270]. In addition, the binding affinity of AQP4-IgG may have limited influence on disease severity as AQP4-IgG binding and complement activation may be facilitated by the cross-stabilization of IgG multimeric assemblies on AQP4 OAPs and the rapid activation of C1q. Novel approaches to image complement activation in CNS tissue may represent a more useful approach to measure tissue injury and relate serum AQP4-IgG composition to prognosis [147, 351]. Since the classical complement pathway cross-activates the alternative pathway to drive tissue injury in a variety of disorders [158], the potential role of alternative pathway activation may need to be studied *in vivo* to fully gauge potential complement-mediated CNS injury.

The importance of CH3 domain Fc-Fc interactions for classical complement activation may provide an alternative approach to specifically inhibit complement activation in NMO. Current complement therapeutics target complement proteins C5 or C1q [86], with adverse risks including meningococcal infections [352] or kidney aggregation [353]. More targeted inhibition of IgG CH3 Fc-Fc interactions may prevent AQP4-IgG complement-

mediated astrocyte destruction yet leave alternative pathway, mannose-binding lectin pathway, and IgM-mediated classical pathway activation intact. Experimental investigations are required to identify candidate small molecule therapeutics, including optimal dosing and efficacy studies (Figure 3C). Alternatively, engineered mutations that limit Fc-Fc interactions may enhance the efficacy of competitive AQP4 monoclonal blocking antibodies [300]. Finally, AQP4 rAbs with Fc-Fc enhancing mutations may facilitate the development of next-generation NMO experimental models [254].

In conclusion, we developed a molecular model for classical complement activation in NMO. The model explains the influence of AQP4-IgG epitope specificity and AQP4 OAP array assembly on autoantibody-mediated CDC and offers new avenues for improved patient care and therapeutic development. This model advances our understanding of the pathogenesis of antibody-mediated autoimmune disorders, and highlights a novel approach for complement therapeutics.

Methods

AQP4 Recombinant Antibodies

To reproduce disease-relevant AQP4 autoantibodies found in NMO patients, CSF plasmablasts were isolated from clinically relapsing NMO patients to generate individual recombinant monoclonal AQP4 autoantibodies as described [267]. Briefly, single cell reverse transcriptase PCR was performed on isolated CD138+CD19- CSF plasmablasts to amplify heavy- and light-chain variable regions, and the resulting cDNA subsequently cloned and co-transfected into HEK293 EBNA cells. Recombinant antibodies (rAbs) were purified from culture supernatant using protein A columns, with structural and functional integrity

confirmed by non-denaturing gel electrophoresis and immunohistochemistry. AQP4 rAb used in this study were generated from 3 AQP4-seropositive patients: patient 07-05 rAb clones #10, #43, #53, #58, #93, #186; patient 09-03 rAb clones #26, #33; patient 10-01 rAb clones #121, #153. The extracellular loop amino acid epitope specificities of AQP4 rAb are described in Owens et al, 2015.

Isotype control antibodies were generated from a measles patient (rAb 2B4), a patient with idiopathic CNS inflammation (ICO 5-2-2), and a non-AQP4 autoantibody clone generated from an AQP4 seropositive patient (rAb #132).

Fc-domain point mutations to manipulate either the Fc-C1q interface (G236A/S267E/H268F/S324T/I332E increases C1q affinity, K322A decreases C1q affinity) [162] or the Fc-Fc interface (E345R promotes, I253D limits) [163] were introduced into AQP4 rAbs by site-directed mutagenesis (Life Tech) and confirmed by DNA sequencing. Amino acid numbering follows Eu nomenclature.

NMO Patient Serum

Patient serum was obtained from AQP4-IgG seropositive and seronegative NMO patients. Complement-dependent cytotoxicity (CDC) assays were performed using 5% heat-inactivated serum as described below.

Complement Source

Normal human serum was used as a source of human complement, with Factor B-, C1q-, and C4-depleted, and Factor D and C1q-codepleted normal human serum used for depletion studies (all purchased from Complement Technologies, Inc.). MBL protein was

depleted from normal human serum over a Sepharose 4B column, with depletion confirmed via western blot.

Small Molecule Peptides

The peptides DCAWHLGELVWCT [163, 341] and WHTPDSLRLSNSGGGC [354] were synthesized by GenScript and Sigma, respectively.

Cell Culture and Reagents

CHO and U87 cells expressing M1- or M23-AQP4 were generously provided by Dr. Alan Verkman and cultured with G418 supplementation to maintain AQP4 expression [299]. A permanent U87 cell line expressing M23-AQP4$^{H151A/L154A}$ was generated for epitope mapping studies. AQP4 expression on each cell line was confirmed via immunohistochemistry. All cells were incubated at 37°C in 5% CO2. All cell lines, including HEL cells for rAb production, were authenticated at the CU Cancer Center Monoclonal and Tissue Culture Core with mycoplasma contamination testing performed via PCR.

CDC Assays

CHO cells (for AQP4 rAb) and U87 cells (for patient serum) were plated at 37,500 and 52,500 cells/well respectively and incubated O/N. Cells were washed twice with F12 media (Gibco) and incubated at 37°C for 60 minutes with serial dilutions of rAb or 5% patient serum in F12 media containing 5% pooled human serum (Complement Technology, Inc.) as a source of complement. LDH release was quantified using an LDH Cellular Cytotoxicity Kit (ClonTech) by adding 50uL of culture supernatant into 100uL of reaction

mixture. Absorbance at 490nM was measured after 20 minutes of reaction development at room temperature using an absorbance plate reader (Molecular Devices). Complete (100%) LDH release was measured by lysing cells in a 1% triton solution, and background (no lysis) was determined by adding human serum to wells without AQP4 rAb. Cell death is presented as % Lysis for all rAb, calculated as (LDH Experimental Well - LDH Background)/(LDH 100% Lysis - LDH Background) x 100%. Data was fit to sigmoidal 4 point binding curve to calculate EC50 values. For CDC assays using patient serum, LDH release was normalized to heat-inactivated patient serum alone in the absence of supplemental human serum as a source of complement and is presented as LDH absorbance. Each treatment has n=4 wells/experiment. For experiments with peptide inhibitors, the final concentration of peptide was 40 μM.

AQP4 rAb Binding Measurements

Cells were washed twice in basal F12 media, and incubated in live cell blocking buffer (minimal essential media containing 2% NGS, 1% BSA, 1mM NaPyr, 1mM NEAA) for 30 minutes at 37°C. Serial dilutions of rAb in live cell block were added for an additional 30 minutes at 37°C. Cells were washed once in basal MEM, fixed in chilled 4% PFA for 15 minutes, and washed 3 times in 1x PBS. Cells were blocked and permeabilized (10% NGS / 1% BSA / .1% Triton in 1x PBS) for 30 minutes, washed once in 1x PBS, and a commercial intra-cellular AQP4 antibody (Santa Cruz) was added for 30 minutes at room temperature in 5% NGS / 1% BSA / 1x PBS. Cells were washed 3 times in 1x PBS, and secondary antibodies (anti-human AlexaFluor594, 1:400; anti-rabbit AlexaFluor488, 1:400; Life Technologies) were added for 30 minutes at room temperature in 2% NGS / 1% BSA / 1x

PBS, followed by 3 washes in 1x PBS. Binding affinity was calculated by non-linear regression of background subtracted red/green fluorescence intensity ratios. When EC50 values are super-imposed over IgG binding curves, the data points used to generate the curves are removed for clarity. Each experimental condition had n=3 wells/treatment with at least N≥3 biologic replicates. AQP4 rAb #075-53 or #075-186 was tested in each experiment to confirm assay consistency. To quantify AQP4 expression without AQP4 rAb treatments, cells were fixed immediately after washing in basal F12 media and IHC was performed as above.

C1q Binding

Cells were washed twice in basal MEM media, and AQP4-specific or control rAb was added in the presence of 5% C4-depleted serum (Complement Technologies, Inc.). After 30 minutes, cells were washed 3 times in basal MEM and a FITC-conjugated anti-C1q antibody (LifeTech, 1:40) was added in live cell block solution for 30 minutes. Cells were washed once with basal MEM and fixed in chilled 4% PFA for 15 minutes. 3 washes with 1x PBS were performed, and FITC fluorescence intensity was immediately quantified. Staining for AQP4 was then performed as above. Data is represented as the fluorescence intensity ratio of C1q/AQP4 after background subtraction. When EC50 values are super-imposed over C1q binding curves, the data points used to generate the curves are removed for clarity. C1q binding to AQP4 rAb #186 was tested in each experiment to confirm assay consistency.

Modeling

Structural models were created using MacPyMOL v1.7.4.4 (Schrodinger LLC) and the crystal structures of AQP4 (PDB ID: 3GD8) [107], IgG1 (PDB ID: 1HZH) [171], IgG1 Fc Domain (PDB ID: 1DN2) [341], C1q globular head (PDB ID: 1PK6) [194], and collagen (PDB ID: 2D3H) [326]. C1q globular heads were joined to collagen assemblies based on predicted structures [194, 327]. For simplicity, the collagen stalk is removed from all C1q models.

STED Super-Resolution Imaging and Analysis

AQP4 rAb were previously imaged via stimulated emission depletion (STED) nanoscopy at ~20nm lateral resolution, with image acquisition, processing, and analysis approaches as described in Chapter 2 Briefly, bound AQP4 rAb are labeled with Atto647N, and AQP4 tetramers are detected with anti-rabbit STAR590 (Rockland). STED nanoscopy was performed (minimum 3 images per AQP4 rAb) using a non-commercial STED nanoscope at the Anschutz Light Microscopy Core. A series of MATLab (R2015a software) programs were coded in-house to quantify the average size of all membrane-bound AQP4 rAb clusters across the entire STED image. Cluster size was calculated as the full width half max (FWHM) of a resolvable object. The potential for multivalent C1q contacts (termed ASA score) was quantified on a 1-4 scale for all antibody spatial arrangements. This scale was derived using probable geometric constraints of a multivalent IgG-C1q interaction based on the size of C1q and IgG hexamers [163, 190]. The ASA score scoring system is capable of quantifying all bound rAb in a non-biased manner so that all frequency distributions are included in the analysis (Chapter 2). A non-biased hierarchal clustering analysis was

performed using the Statistics and Machine Learning Toolbox™ in MATLab to group AQP4 rAb ASA scores based on similarity and dissimilarity.

ASA scores were converted into a single 1-4 score representing the cumulative score distribution as a means to correlate membrane spatial distributions to relative antibody binding affinity. The single score was generated using the following formula:

Cumulative ASA = 1 x (% distribution ASA Score 1) + 2 x (% distribution ASA Score 2) + 3 x (% distribution ASA Score 3) + 4 x (% distribution ASA Score 4)

A low cumulative ASA score is therefore indicative of an AQP4 rAb with ASA score distributions that favor lower ASA scores of 1 and 2, while a high cumulative ASA score is indicative of an AQP4 rAb whole distribution favors higher ASA scores of 3 and 4. The relationship between average antibody cluster size and rAb epitope specificity was tested by ANOVA.

Statistics

Statistical analyses were performed in GraphPad Prism 6 software. For all analyses, $p<.05$ is considered significant.

Study Approval

Written informed consent was received from participants prior to inclusion in the study. This study was approved by the institutional review board at the University of Colorado Anschutz Medical Campus.

Endnotes

This work was funded by NIH R01EY022936 awarded to Dr. Jeffrey Bennett, a National Multiple Sclerosis Society Collaborative Grant, and the Guthy Jackson Charitable Foundation. The work compiled in this chapter is in the process of being prepared for peer review.

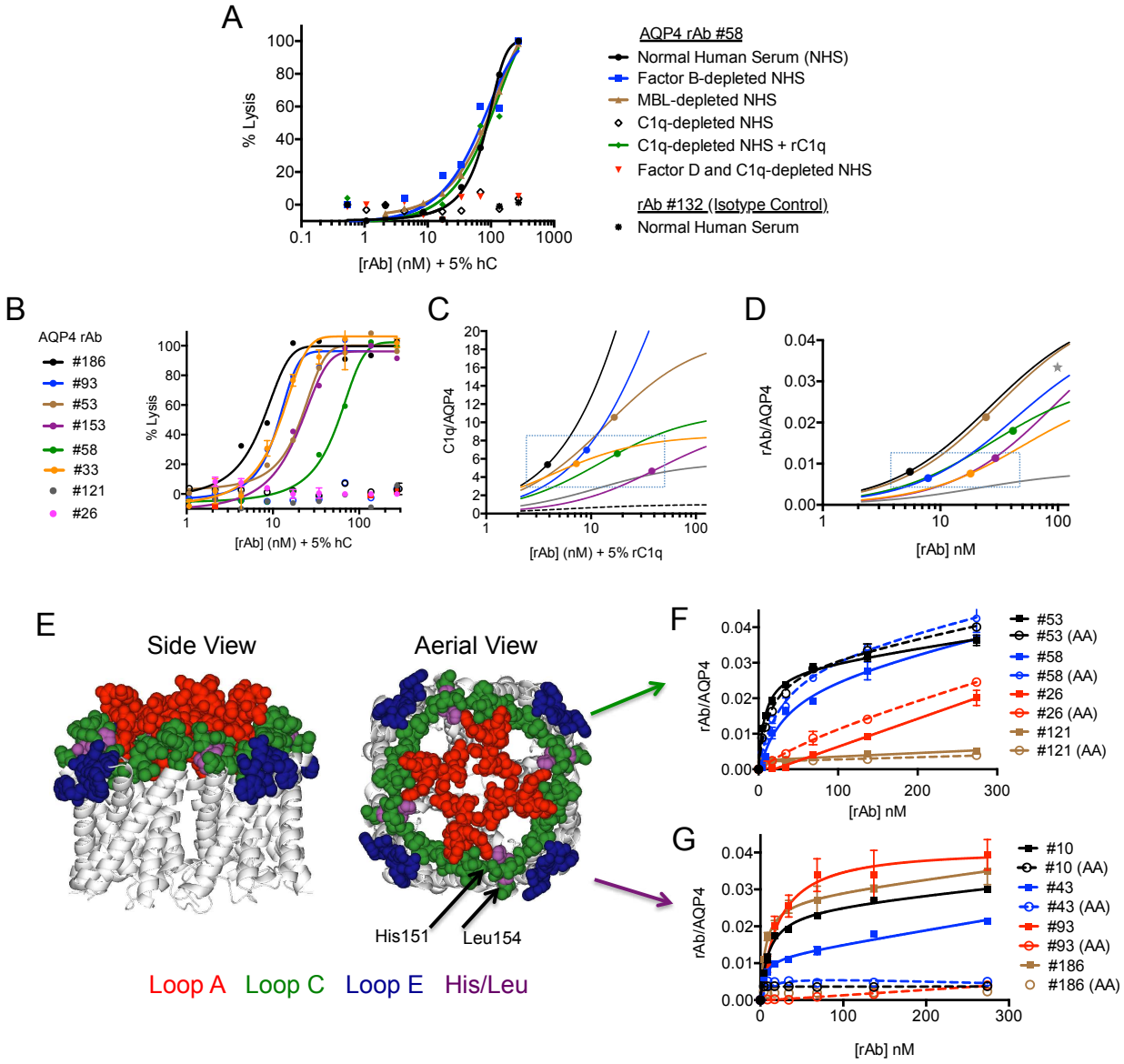

Figure 3.1: AQP4 recombinant antibody (rAb) binding and classical complement activation on M23-AQP4

Figure 3.1: AQP4 recombinant antibody (rAb) binding and classical complement activation on M23-AQP4

(A) LDH release assay quantifies classical pathway-driven CDC by AQP4 rAb. Data is presented for AQP4 rAb #58 or isotype control rAb #132 with each treatment representing a different human serum preparation with no protein depletion (normal human serum) or depletion of indicated complement protein(s). (B) CDC by monoclonal AQP4 rAb with differing epitope specificities (C) The ratio of bound C1q to AQP4 is plotted against AQP4 rAb concentration. (D) The ratio of bound rAb to AQP4 is plotted against AQP4 concentration. For (C) and (D), the individual points denote the half maximal effective concentration (EC50) for complement activation of each respective AQP4 rAb, with star indicating a data point limiting by x axis range. The boxes indicate rAb with accentuated complement activation capabilities. (E) Side (left) and aerial (right) views of an AQP4 tetramer. Extracellular loops A, C, and E are colored red, green, and blue respectively. Loop C amino acids His151 and Leu154 are colored purple. Membrane-spanning and intracellar amino acids are colored grey. (F/G): AQP4 rAb binding curves to wildtype M23-AQP4 (solid line) and M23-AQP4$^{H151A/L154A}$ (abbreviated AA, dashed line) demonstrate rAbs whose binding is independent (F) or dependent (G) on loop C amino acids His151/Leu154. CDC assays are performed on n=4 wells/treatment and n ≥3 biologic replicates; rAb and C1q assays are performed on n=3 wells/treatment and n ≥3 biologic replicates. Representative data from one experiment are shown.

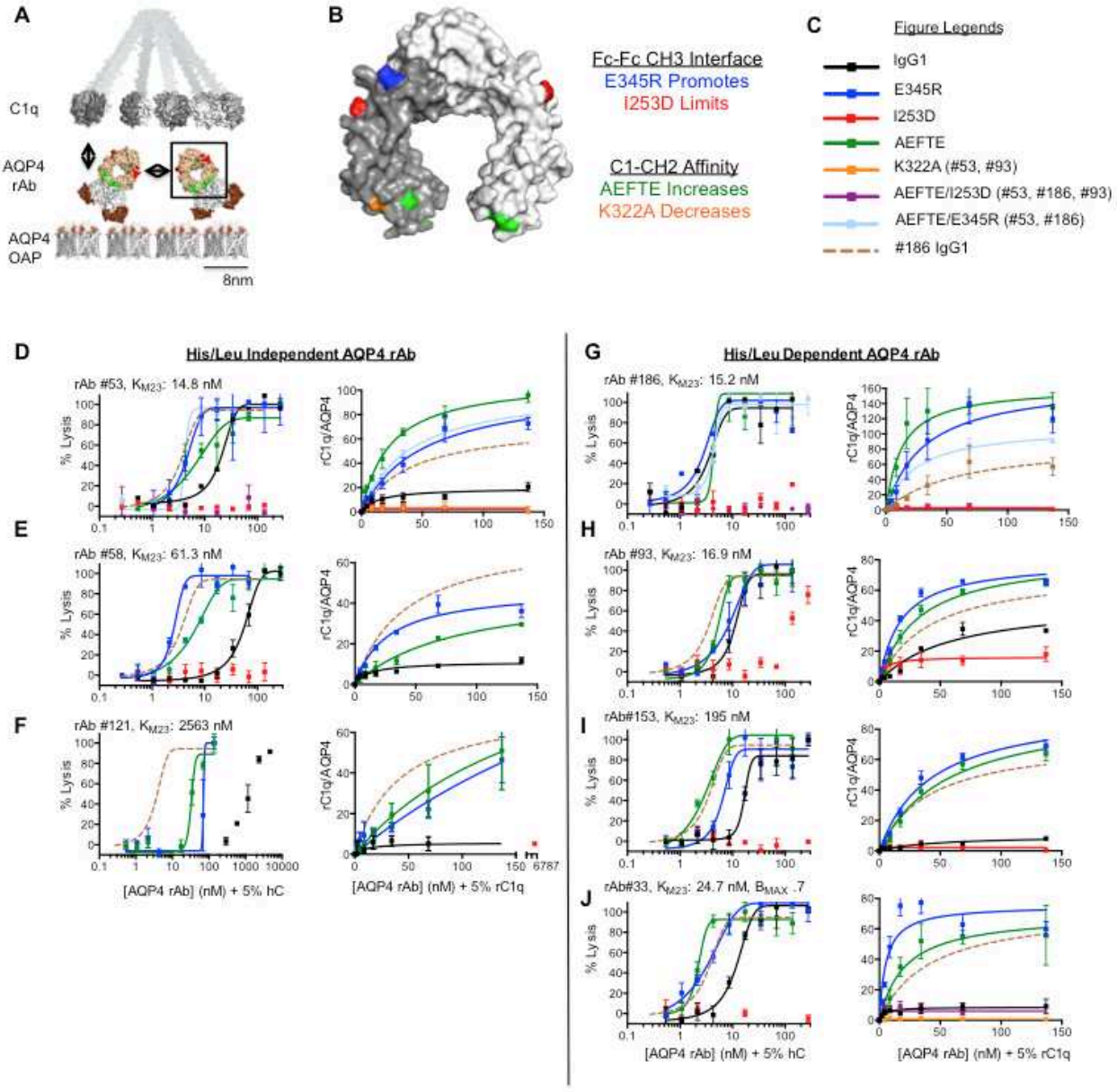

Figure 3.2: CH3 Fc-Fc interaction is critical for AQP4-IgG mediated complement dependent cytotoxicity (CDC)

Figure 3.2: CH3 Fc-Fc interaction is critical for AQP4-IgG mediated complement dependent cytotoxicity (CDC)
(A) Space filling and ribbon models of C1q, AQP4 rAb, and M23-AQP4 OAPs illustrating key interactions potentially driving C1q- AQP4 rAb – AQP4 multivalent complex assembly. C1q globular heads bind to the CH2 domain of AQP4 rAb (green), while neighboring AQP4 rAbs interact via CH3 hydrophobic patches (red). Fab variable regions are colored brown. (B) Space filling model of the Fc region of a divalent AQP4 rAb (box, A) denoting residues with engineered mutations to promote (green, blue) or limit (orange, red) C1q-CH2 or CH3-CH3 binding. (C) Figure legend for CDC (left) and C1q binding (right) plots for His151/Leu154-independent (D-F) and His151/Leu154-dependent (G-I) AQP4 rAbs. The rAb and binding affinity on M23-AQP4 (K_{M23}) are displayed in the top left corner of each CDC graph. The CDC plot and C1q binding curves for rAb #186 (dotted brown line) is displayed in each graph for comparison. CDC assays are performed on n=4 wells/treatment and n ≥3 biologic replicates; rAb and C1q assays are performed on n=3 wells/treatment and n ≥3 biologic replicates. Representative data from one experiment are shown.

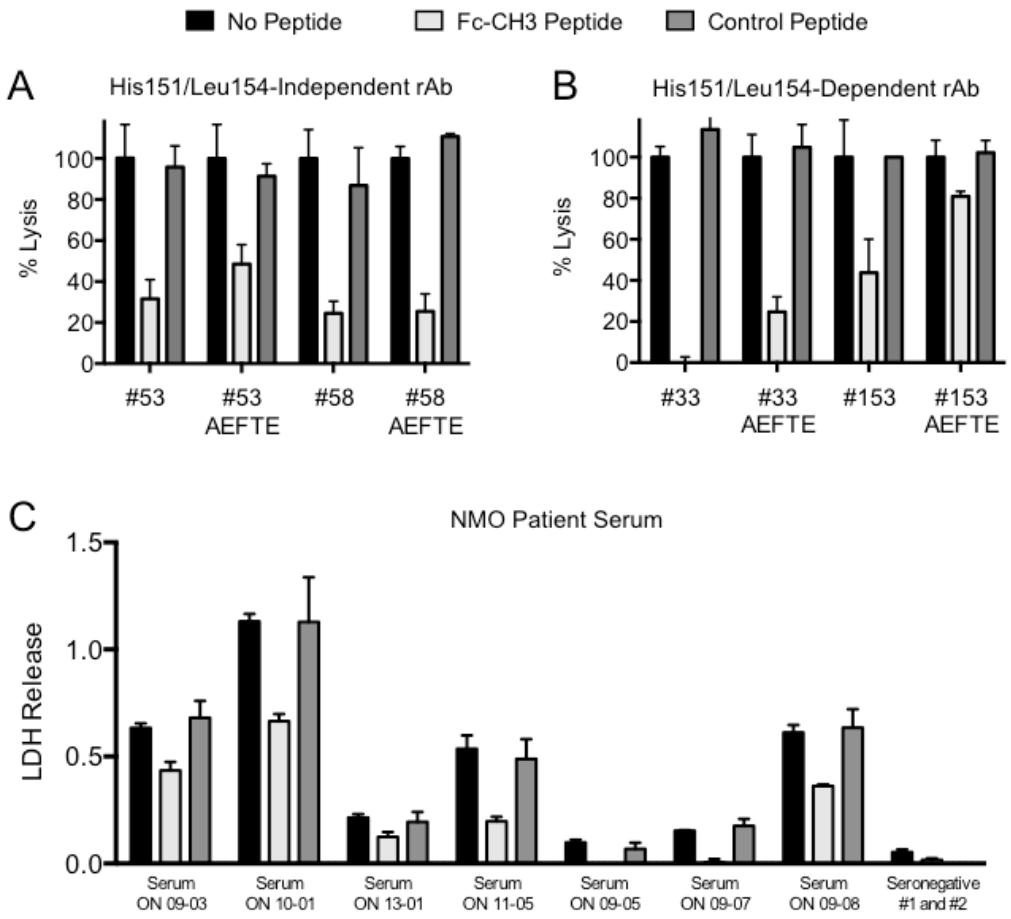

Figure 3.3: A peptide inhibitor of CH3-CH3 interaction impairs AQP4 rAb CDC
The Fc-CH3 peptide designed to bind to the CH3 domain of human IgG1 inhibits His151/Leu154-independent (A) and His151/Leu154-dependent (B) AQP4 rAb CDC when compared to a control peptide. (C) Fc-CH3 peptide inhibits serum CDC mediated by AQP4-IgG in NMO patient serum. For all groups, one-sided ANOVA with Tukey test for multiple comparisons demonstrated significant ($p<.05$) differences between Fc-CH3 peptide with all groups, and no other significant differences for all other possible comparisons.

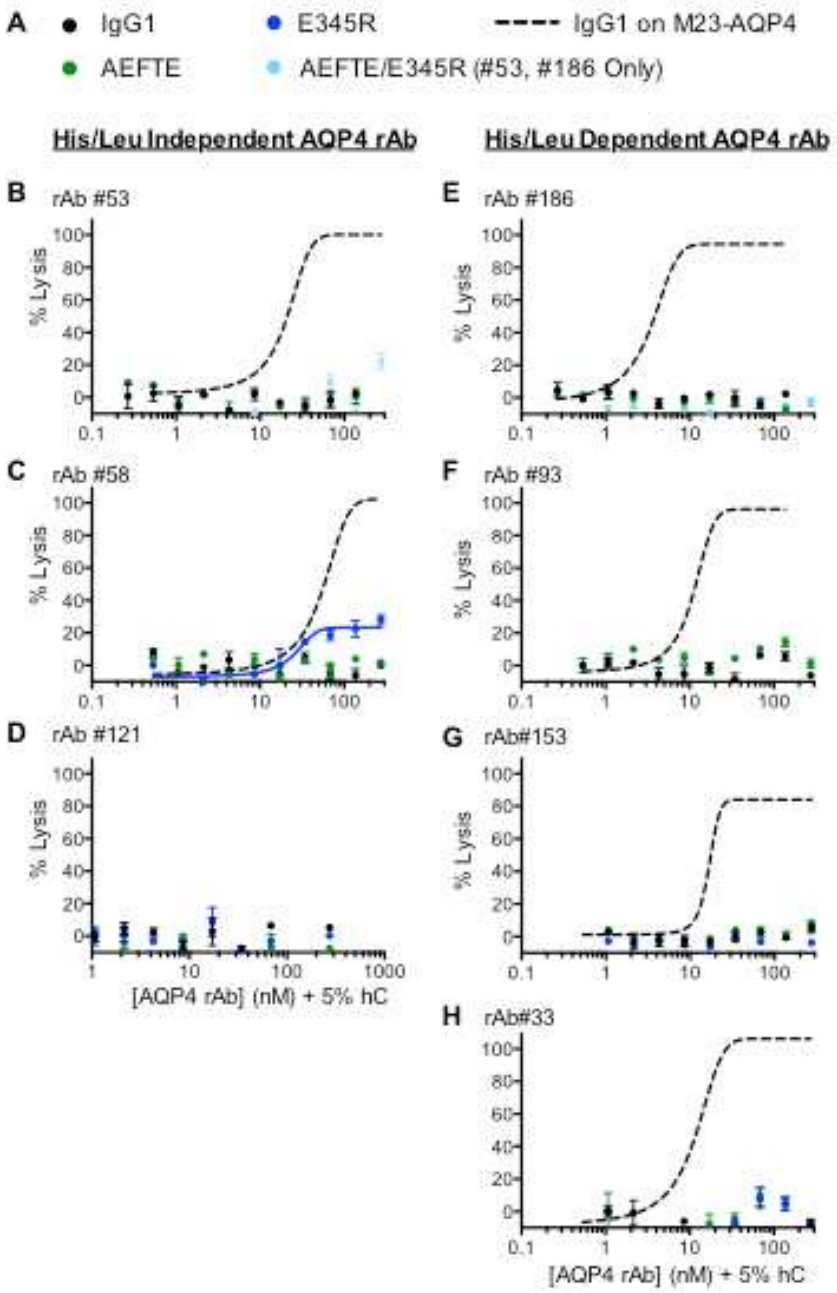

Figure 3.4: Enhanced CH2-C1q and CH3-CH3 interactions do not rescue AQP4 rAb complement-mediated cytotoxicity (CDC) on M1-AQP4

(A) Figure legend for His151/Leu154-independent (D-F) and His151/Leu154-dependent (G-J) AQP4 rAb CDC on M1-AQP4 CHO cells. The CDC curve for the native IgG1AQP4 rAb on M23-AQP4 is noted by the dashed black line. Data is representative data from one biologic replicate (n=4 wells; n=3 biologic replicates performed).

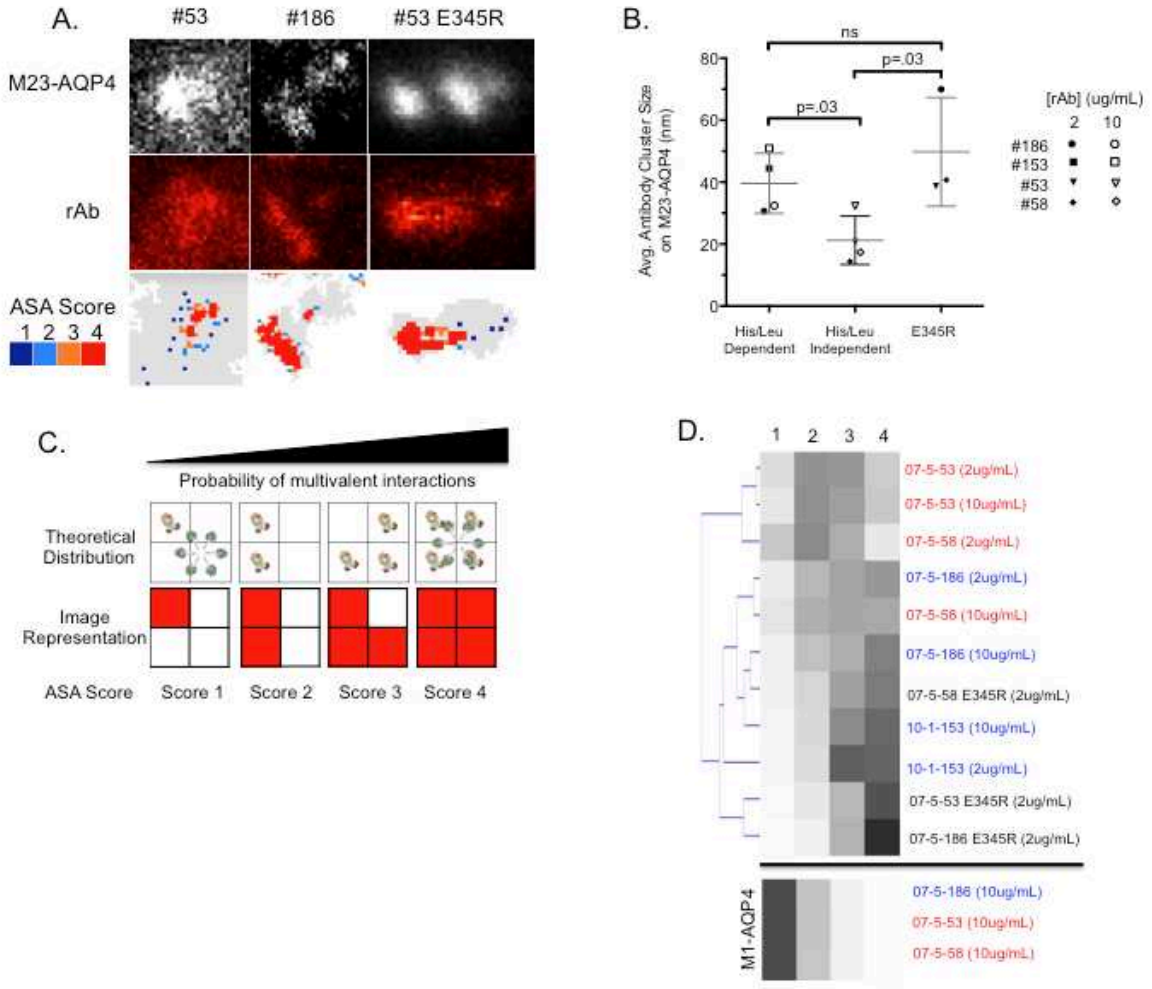

Figure 3.5: Super-resolution STED nanoscopy of membrane-bound AQP4 rAb clustering on M23-AQP4 OAPs.
(A) Representative STED images showing AQP4 (top), AQP4 rAb (middle) and antibody spatial arrangement (ASA) scores depicted with false colors. (B) The average resolvable rAb cluster size was grouped by epitope binding dependence and compared using ANOVA with Tukey's test for multiple comparisons. (C) A theoretical depiction of the ASA scoring scale. A hypothetical antibody distribution is displayed schematically to illustrate the relative size of AQP4 rAb, C1q, and the image pixel. Pixels containing a higher concentration of rAb signal (bottom) are considered to have a higher probability of clustering and forming multivalent contacts with C1q. (D) A hierarchal clustering analysis of ASA scores was performed for His151/Leu 154-independent rAbs (red), His151/Leu 154-dependent rAbs (blue), and engineered E345R-mutated rAbs (black) on CHO cells expressing M23-AQP4 (top) and M1-AQP4 (bottom).

rAb	H/L Dependence	Cumulative ASA Score	C1q at EC50	% AQP4 Saturation at EC50
#53	No	2.44	10.5	0.44
#58	No	2.7	6.5	0.38
#186	Yes	2.93	5.2	0.17
#153	Yes	3.28	4.62	0.16

Table 3.1: AQP4 rAbs with higher ASA scores show lower concentrations of bound C1q and percent saturation of rAb (% AQP4 saturation) at the half maximal rAb concentration for CDC (EC50).
A table summarizing epitope binding dependence to His151/Leu154 (from Figure 1), cumulative ASA score (from Figure 5), the level of bound C1q at CDC EC50 (from Figure 1), and the percent AQP4 saturated at CDC EC50 (from Figure 1) for AQP4 rAbs imaged with STED nanoscopy.

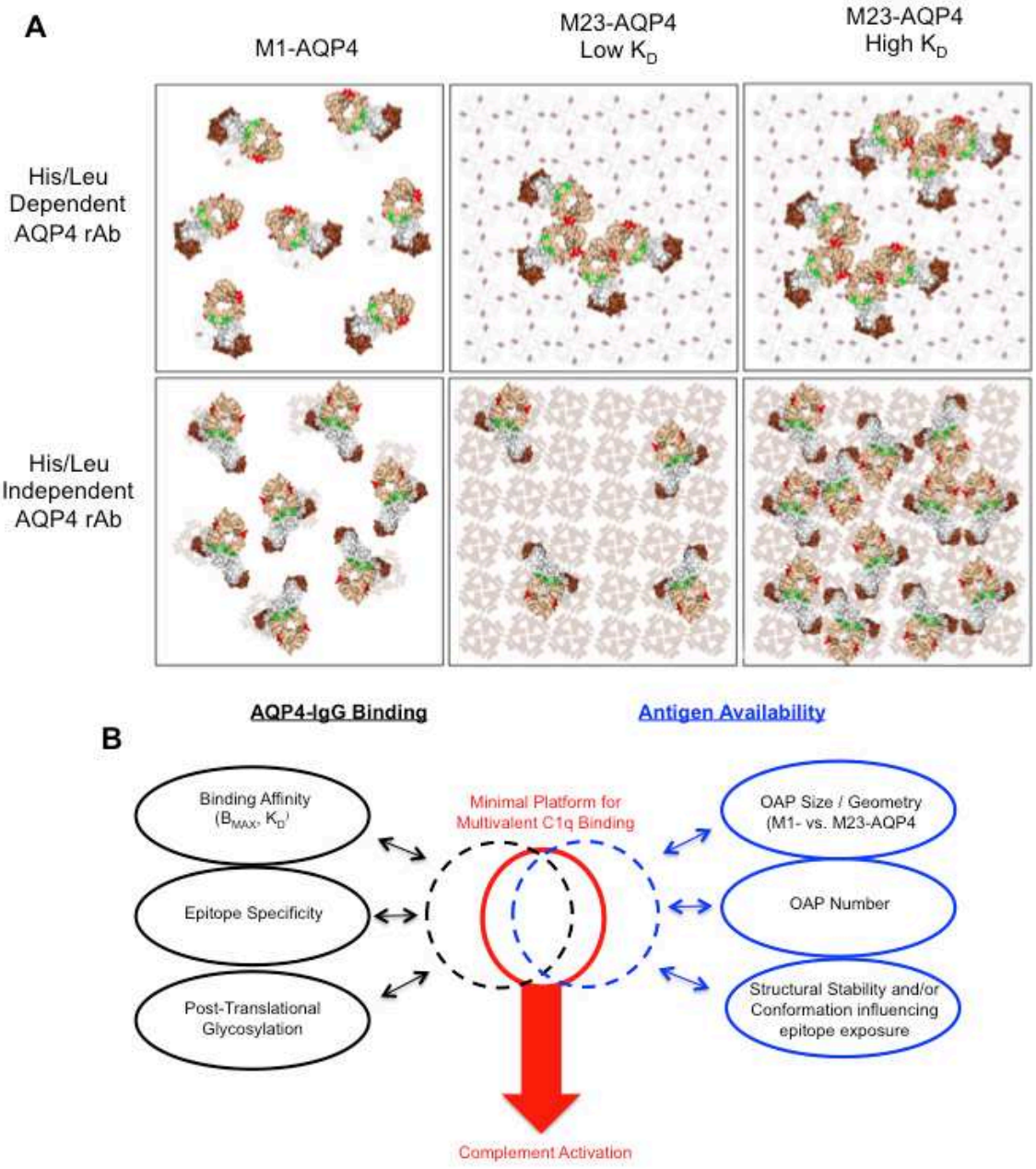

Figure 3.6: Proposed model of classical pathway activation
(A) Space filling models depicting the effect of His151/Leu154 epitope dependence for rAb clustering on M1-AQP4 (left) and M23-AQP4 (middle, right). Due to binding constraints, the Fc domain of His151/Leu154-dependent rAb is oriented in a geometry that optimizes the formation of CH3 domain interactions between neighboring rAbs (top). His151/Leu154-independent AQP4 rAbs that are not constrained by the same epitope-imposed geometry need higher levels of rAb binding to CH3-CH3 domain driven IgG assemblies (bottom). (B) Multiple variables may impact the assembly of IgG hexamers on AQP4 orthogonal arrays of particles (OAPs). These include factors that influence AQP4 IgG binding (left), and OAP assembly (right).

CHAPTER IV

THE SOURCES OF CYTOTOXIC COMPLEMENT PROTEINS DURING NMO LESION FORMATION

Abstract

Here, I test the hypothesis that multiple sources of complement pathway proteins contribute to CNS injury in NMO. Initial studies performed *ex vivo* supported that cross-activation of the alternative pathway may contribute to CNS injury during NMO lesion propagation, although an *in vivo* experimental test provided conflicting results. Multiple experiments were pursued to better understand the disparity. A large limitation is that these latter experiments are largely descriptive in nature. The insight provided, however, could ultimately impact the interpretation of all experimental data and proposes a refined model that describes the cytotoxic sources of complement protein in NMO. Experimental tests of the model are needed and would direct more rigorous quantifications of all data. Thus, the experiments herein provide the cornerstones needed to build an experimental model of complement pathway-specific contributions to CNS injury in NMO.

Introduction

Neuromyelitis optica (NMO) spectrum disorders are a family of demyelinating disorders of the central nervous system (CNS) characterized by recurrent inflammatory attacks of optic neuritis and transverse myelitis, with possible brainstem involvement [32]. Serum autoantibodies targeting aquaporin-4 (AQP4-IgG) are readily detected in the serum of approximately 80% of all patients [237, 301, 355]. AQP4-IgG is pathogenic, binding to and killing astrocytes with secondary demyelination [86, 356]. Establishing molecular models of

lesion pathogenesis is of considerable clinical significance for recognizing and combating early clinical activity.

Complement activation by AQP4-IgG plays a critical role in driving CNS tissue destruction. IgG and terminal complement deposition are hallmark features of human lesions [42] [44-47, 357], patients display evidence of activated complement proteins during relapse [36, 38, 339], and complement therapeutics have demonstrated early promise in clinical trials [102, 103]. Indeed, experimental models have demonstrated the potential for AQP4-IgG to activate complement *in vitro*, *ex vivo*, and *in vivo* [51, 252, 254, 267, 268, 306, 358]. Importantly, full *in vivo* experimental lesion formation is dependent on an interaction between AQP4-IgG and the complement protein C1q to activate the classical complement pathway [253, 254, 257, 258]. The cross-activation of a variety of additional cytotoxic immune and cellular mechanisms emanates from this inciting complement effector event [85, 86].

Despite the coordinating cytotoxic role that complement activation plays in damaging the CNS, the full extent of complement activation and the complete array of direct and indirect cytotoxic mechanisms are not known. Complement may be activated along 3 distinct pathways: the classical pathway via an interaction of C1q with IgG, IgM, or other self proteins, the alternative pathway via spontaneous hydrolysis of the complement protein C3, and the lectin pathway by interaction of MBL or ficolin with equatorial plane-OH sugar moieties [147, 204]. Each pathway converges to activate the common pathway, which produces an array of cytotoxic proteins that may both directly and indirectly incite cellular cytotoxicity. A better understanding of when the system is activated, and the pathway sources of injurious protein, is of considerable therapeutic interest to combat CNS injury.

Here, the timing of complement activation and the cytotoxic contributions of each activation pathway are examined.

Methods

Generation of AQP4 rAb

Monoclonal recombinant AQP4 autoantibody #53 (rAb #53) was generated using paired antibody heavy and light chain sequences obtained from a relapsing NMO patient as described [267]. Control rAb #2B4 was generated from a measles patient. Briefly, a plasmablast was isolated from patient cerebrospinal fluid. Antibody heavy and light chain variable regions were PCR amplified, cloned into vectors, and transfected into cultured HEK cells. rAb was purified from culture supernatant using Protein A columns, with protein concentration and integrity confirmed by absorbance at A280 and denaturing gel.

Complement Source

Normal human serum was used as a source of human complement (Complement Technologies, Inc.). For pathway protein-specific depletion, C1q-depleted serum, Factor D- and C1q-depleted serum, and Factor B-depleted serum were used (Complement Technologies, Inc.). Normal human serum was run over a mannose column to generate MBL-depleted serum in house. Depletion was confirmed via western blot.

Mice

C57/B6 mice, C1q-alpha knockout mice, and MBL knock out mice were purchased from Jax Laboratories. Factor B deficient mice were provided by Dr. Joshua Thurman. PLP-

EGFP mice were provided by Dr. Wendy Macklin; the mice express the enhanced green fluorescent protein (EGFP) under the control of the myelin proteolipid protein promotor [359].

Cell Culture

M23-AQP4 stably expressing CHO cells were provided by Dr. Alan Verkman and cultured at 5% CO2/37°C as described (Chapter 3), using F12 media containing 10% FBS and 1% anti-biotic/anti-mycotic (both Gibco). AQP4 expression was confirmed via immunostaining.

Complement-Dependent Cytotoxicity (CDC) Assay

M23-AQP4 expressing cells were washed twice in F12 media, and treated with rAb #53 (40ug/mL) and 75% human serum as a source of complement. After incubation for 1 hour at 37C, cells were washed twice in F12 media and incubated with calcein-acetoxymethyl (CaAM) and propidium iodide (PI; both at 1uM; Life Technologies) for 15 minutes at room temperature. Cells were washed twice in F12 media, and normal growth media was added to each well. Cells were immediately imaged using a Leica DM IRB inverted fluorescence microscope. Images were acquired for n=4 experimental wells per group. The number of CaAM-positive (indicating live cells) and PI-positive (indicating dead cells) were scored using a MATLab (The Mathworks, Inc) cell counting program coded in-house. Data is presented as the number of living cells ($CaAM^+$) over the total number of cells ($CaAM^+ + PI^+$) x 100%. Groups were statistically compared using a one-way ANOVA test with Tukey's test for multiple comparisons.

Ex Vivo NMO Lesion Model

An *ex vivo* spinal cord explant culture was generated as described [268, 360]. Briefly, spinal cords were dissected from a P7 PLP-EGFP mouse and sliced into 300uM transverse sections using a McIlwain Tissue Chopper. A dissecting microscope was used to confirm slice structural integrity and remove sacral and lumbar slices. Thoracic and cervical slices were evenly distributed across .4uM 30mm Millipore-TM culture membranes and grown for 7-10 days in the following media: 50% minimal essential media, 25% Hanks balanced salt solution (HBSS), 25% horse serum, 1% Pen-Strep, .65% glucose, and 25mM HEPES pH 7.2. Slices were then washed twice in 1x HBSS, and treated in horse-serum-deprived media. 1mL of treatment was applied above and below the culture membrane. 10% human serum was added as a source of complement protein, 15 ug/mL rAb #53 was added to initiate lesions, and some wells were also treated with a monoclonal antibody targeting factor B (mAb^{fB}) [361]. After 24 hours, slices were washed twice in 1x HBSS, fixed in chilled 4% paraformaldehyde for 15 minutes, and washed three times in 1x phosphate buffered saline (PBS). Immunostaining was performed against GFAP as described below.

Astrocyte loss was scored by GFAP immunoreactivity on the following 0-4 scale: 0 = intact slice with normal GFAP expression, 1 = intact slice with some astrocyte swelling, 2 = at least one lesion with loss of GFAP, 3 = multiple lesions with loss of GFAP; and 4 = GFAP loss over >75% of the slice area. Oligodendrocyte loss was scored using the following 0-4 scale: 0 = no EGFP loss compared to culture media controls, 1 = ~1-25% EGFP loss, 2 = ~26-50% EGFP loss, 3 = ~51-75% EGFP loss, 4 = ~76-100% EGFP loss. A non-parametric Kruskal-Wallis test with Dunn's post-test was performed to assess significance.

Intracerebral Injection

Mice were anesthetized with ketamine/xylazine and mounted onto a stereotactic frame. A midline scalp incision was made, and a 1mm diameter burrhole was drilled in the skull 2mm to the right of bregma. A pulled glass pipette was attached to a 50uL gas-tight glass syringe (Hamilton) and inserted 3mm deep to inject experimental treatments. Most mice received 3ug of AQP4 or control rAb and 3uL human serum in a total volume of 5uL, injected at 2uL/minute. Human serum was either normal human serum, C1q-depleted, factor B-depleted, or MBL-depleted. For alternative pathway inhibition, mAb^{fB} (1uL) was included in the 5uL injection. An optimized injection protocol was developed that injected 1ug rAb and .05 uL of human serum in a total volume of 1uL at .5uL/minute. All injections included 4% monastrol blue to mark the injection site. At 48 hours post-lesion initiation, mice were anesthetized and perfused with 4% PFA via cardiac puncture. Brains were post-fixed in 4% PFA for 24 hours and processed for paraffin embedding.

Lesion Staining and Scoring

12 um sections were deparaffinized and rehydrated in a standard ethanol series. Sections were blocked in 10% normal goat serum (NGS)/1 % bovine serum albumin (BSA) in 1x PBS containing .3% triton x-100 for 1 hour. The following primary antibodies were then incubated overnight at room temperature in 5% NGS/1% BSA in 1x PBS: rabbit anti-AQP4 (1:100; Santa Cruz), mouse anti-GFAP (1:200, Millipore), mouse anti-MBP (1:1500; DAKO), mouse anti-C3d (1:100; gift from Dr. Joshua Thurman) [351], and biotinylated goat anti-human IgG Fc domain (1:200, Novus Biologics). Antibodies were washed 3 times in 1x PBS, and the following antibodes/fluorophores were then added for 2 hours at room

temperature in 2% NGS/1%BSA in 1x PBS: goat anti-rabbit Cy3 (1:500, Jackson), goat anti-mouse AlexaFluor488 (Life Technologies, 1:200), goat anti-mouse AlexaFluor594 (Life Technologies, 1:200), and streptavidin-conjugated AlexaFluor594 (Life Technologies).

For luxol fast blue, sections were deparaffinized to 95% EtOH. Sections were then incubated overnight in luxol fast blue solution at 58C, and developed using a standard lithium carbonate/70% ethanol series.

All sections were imaged using a Nikon Fluoresence/Bright Field microscope. 4x and/or 10x magnifications were tiled in FIJI software to score lesion size by hand, with a lesion defined as a loss or abnormal staining pattern as compared to the non-injected hemisphere.

Statistics

Statistical analyses were performed in GraphPad Prism 5 software. Specific tests are described for each test, with $p<.05$ considered significant.

Results

Complement Activation Occurs During Astrocyte Loss and Secondary Demyelination

An intracerebral co-injection of AQP4 rAb with human serum initiates an *in vivo* experimental NMO lesion. Astrocyte loss occurs within 1 hour, oligodendrocyte cell body death at ~3 hours post-initiation, and secondary demyelination occurring over a 72 hour period coinciding with peripheral immune cell infiltration [309]. To understand how activated complement proteins may contribute to CNS injury throughout this temporal progression, we first characterized C3d deposition at 3, 24, 48, and 72 hours post-lesion

initiation. C3d is a breakdown activation product of the early common complement pathway protein C3 (Figure 4.1A). C3d covalently attaches to the targeted cell and has a short half-life; deposition therefore indicates local complement activation. C3d deposition was observed at 3 hours post-lesion initiation, with increased deposition at 24 hours (Figure 4.1B). Expression levels were similar or decreasing at 48 hours, and deposits were largely cleared at 72 hours. C3d deposition was not observed when isotype control rAb was injected (data not shown). These findings indicate that complement activation coincides with both the initial astrocyte attack and secondary oligodendrocyte demise.

Alternative Pathway Activation Damages the CNS ex vivo

AQP4 rAb activate the classical pathway to initiate complement-mediated astrocyte destruction [254, 338, 362, 363]. However, it is possible that cross-activation of the alternative pathway (via activated C3) or lectin pathway (via modified sugar moieties) may contribute to CNS damage. We first tested the potential for alternative pathway cross-activation using an *ex vivo* model of NMO lesion formation [268]. Alternative pathway activity was inhibited by pre-treating slices with an anti-Factor B monoclonal antibody (mAb^{fB}) and by using human serum depleted of factor B as a source of complement protein, in addition to maintaining mAb^{fB} treatment. The addition of AQP4 rAb #53 and normal human serum readily damaged both astrocytes and oligodendrocytes (Figure 4.2A-C). Alternative pathway inhibition rescued oligodendrocyte destruction (Figure 4.2A/C) and partially rescued astrocyte loss. Although the area of overall astrocyte pathology was similar between the two groups (Figure 4.2A/B), higher magnification images demonstrated differences in the structure of the astrocyte network (Figure 4.2D). In control slices,

astrocytes displayed fine GFAP+ processes that resembled a dense network (4.2D left, green arrow). The network was destroyed on slices treated with rAb #53 and an intact complement pathway (4.2D middle, white arrow). In distinction, although astrocyte loss was still evident with alternative pathway inhibition (4.2D right, white arrow), many astrocytes remained and processes could be identified (4.2D right, green arrow). More rigorous analysis quantifying astrocyte cell number, astrocyte process number and morphology are needed to understand the significance of the observation in relation to lesion morphologic progression. Nevertheless, the findings indicate that cross-activation of the alternative pathway may contribute to CNS damage during NMO lesion formation.

Classical Pathway Activation is Sufficient for in vivo Demyelination.

An intra-cerebral injection model was performed to test if cross-activation of the alternative pathway contributes to tissue injury *in vivo*. A control lesion was initiated by co-injecting rAb with normal human serum into a C57 mouse, while alternative pathway inhibition was achieved by co-injection of factor B-depleted serum with mAb^{fB} into a factor B -/- mouse. AQP4 rAb #53 and an isotype control rAb were co-injected into distinct groups for each experiment.

Surprisingly, the injection procedure caused significant astrocyte pathology regardless of experimental group, indicated by a loss of GFAP and AQP4 expression (Figure 4.3A,C-L). The finding limited meaningful astrocyte analyses; however, myelin damage was dependent on AQP4 rAb-mediated complement activation. The area of myelin damage was quantified by luxol fast blue staining; MBP expression confirmed myelin loss in regions of AQP4 loss (Figure 4.3 A/B). Overt myelin loss was observed in control lesions only when

AQP4 rAb #53, but not the isotype control antibody, was co-injected with human serum (Figure 4.3B, C vs D). Furthermore, injection of an AQP4 rAb that could not bind C1q (K322A mutation) rescued myelin pathology (Figure 4.3 C vs L). In distinction to the *ex vivo* model, alternative pathway inhibition did not significantly impact myelin loss *in vivo* (Figure 4.3 C vs F). Lectin pathway inhibition (MBL-depleted human serum co-injected into an MBL -/- mouse) also did not impact demyelination (Figure 4.3 C vs H). Collectively, the findings support that classical pathway activation by AQP4 rAb is sufficient to cause myelin destruction *in vivo*.

Model Optimization

Given the well-established requirement of classical pathway activation to initiate lesion formation in murine models [254, 338], the development of a CNS lesion when the classical pathway was inhibited was surprising (Figure 4.3 J/K). The finding of variable but prominent astrocyte pathology independent of experimental injection was also unexpected (Figure 4.3C-L). A series of experiments was performed to better understand how the composition of the experimental injection, pathway inhibition approaches, and/or experimental injection approach contributed to CNS damage. As multiple mechanisms may contribute, the goal of the experiments was not to conclusively prove specific mechanisms but rather to identify major considerations to design a better injection experiment.

We first asked what the source of complement activation was in the C1q -/- mouse co-injected with C1q-depleted serum and rAb #53. Assuming the complete absence of C1q, IgG-mediated activation may occur via the lectin pathway or via a C1q-like molecule. Lectin activation seemed less likely, as MBL-IgG interactions have only been reported with

aglycosylated IgG (IgG-G0) [200, 201, 364], and a prior *in vivo* NMO model that injected a monoclonal antibody targeting C1q globular heads inhibited lesion formation [338]. Furthermore, *in vitro* CDC studies by AQP4 rAb have not detected lectin pathway activation when using a low percentage (5%) of human serum as a source of complement (Chapter 3, Figure 3.1). An interaction between AQP4 rAb and MBL may nevertheless occur *in vivo* to activate the lectin pathway; prior experimental conditions have favored high levels of classical pathway activation, which may have masked any lectin pathway contributions. To test this possibility, CDC activation was initiated using a higher percentage (75%) of human serum depleted of the key classical and alternative pathway complement proteins C1q and Factor D respectively, leaving only lectin activation as the source of common pathway activation (Figure 4.1A). Cell death was not observed using serum that only maintained lectin pathway activity, while cell death was observed using serum capable of classical pathway activation (one-way ANOVA with Tukey's test, alpha<.05) (Figure 4.4). At the concentration of rAb used (40ug/mL), AQP4 arrays were saturated with rAb #53 [365, 366]. Given the high percentage of human complement used, the findings do not support that AQP4 rAb is an MBL activator.

An alternate explanation is that the inhibition approach largely, but not fully, inhibited C1q activation by the human serum. If even low levels of C1q were present in C1q-depleted serum and initiated the lesion, a lesion could potentially develop if the same C1q-depleted serum was injected into a wildtype mouse. Indeed, a lesion developed upon co-injection of rAb #53 with C1q-depleted serum into a wild type mouse (Figure 4.3E). However, the lesion trended towards a smaller lesions size (Figure 4.3 C vs. E) and displayed a unique pathologic heterogeneity not previously observed (Figure 4.5 A-C). Prior lesions

displayed homogeneous pathology with AQP4 and GFAP loss largely overlapping at the injection core and injection periphery (Figure 4.5A, compare lesion outlines). However, the new experimental lesion was heterogeneous at sites distal to the injection core (Figure 4.5B/C). Here, a central core was defined by complete GFAP and AQP4 loss (4.5B/C Arrow 1), with a surrounding peripheral region defined by complete AQP4 loss but diffuse GFAP immunoreactivity (4.5B/C Arrow 2). The lesion core also demonstrated a high cell density, indicated by DAPI (Figure 4.5C bottom right).

The experimental findings raised an additional possibility: pathology in the *in vivo* model may at least partially reflect the levels of injected C1q and/or additional complement pathway proteins. A group of mice was therefore injected with a much lower volume of complement in a smaller total volume (prior groups: 3uL of 100% human serum in 5uL total, new approach: .05 uL of 100% human serum in 1uL total). AQP4 rAb, but not isotype control rAb, caused astrocyte loss as indicated by a loss of GFAP and AQP4 immunoreactivity (Figure 4.6). Although AQP4 and GFAP loss largely overlapped, regions of AQP4 loss but GFAP immunoreactivity were present, and vice-versa (4.6, Arrow 1 and 2 respectively). Furthermore, prominent demyelination was observed via total MBP loss at the lesion core that was surrounded by significantly altered MBP expression (4.6 A3/B3, arrowheads 1 and 2 respectively). The core also demonstrated a large density of cells, indicated by DAPI staining (4.6 A4/B4, arrowhead). Control rAb caused no apparent loss of AQP4, GFAP, and MBP expression (4.6 C/D) despite targeting the same CNS anatomic site. The white stars in A3 and C3 are added to assist in anatomic orientation. However, more subtle changes in overall MBP expression patterns in regions of astrocyte reactivity (GFAP expression) but no/little AQP4 loss may indicate subtle CNS morphologic changes (Figure

4.6D, white arrow) atypical for NMO [367]. Collectively, the series of experiments supports that osmotic trauma and/or the levels of initially injected complement protein likely influenced lesion phenotype in the *in vivo* injection complement pathway inhibition experiments (Figure 3).

Discussion

Cytotoxic Complement Sources in NMO

Complement activation is a key pathogenic mechanism inciting CNS tissue destruction in NMO. Here, we establish that complement activation is temporally activated for approximately 48 hours during experimental NMO lesion formation, with the clearance of the complement degradation product C3d largely cleared at 72 hours. *In vitro* and *ex vivo* models support that CDC is initiated by classical pathway activation, and that cross-activation of the alternative pathway has the potential to contribute to tissue destruction. Despite this cytotoxic potential, alternative pathway activation is not required for astrocyte loss and demyelination *in vivo*. Rather, activation of the classical pathway appears to be sufficient to cause demyelination.

In NMO, proposed cytotoxic complement proteins (C3a, C5a, MAC) are all activated through the common complement pathway [85, 86, 335]. A sufficient level of common pathway activation will kill the targeted cell(s), even if higher concentrations of activated complement proteins are present (Figure 4.7A). Additional *in vivo* injection experiments suggested that the conclusion that classical activation is sufficient for *in vivo* lesion formation may potentially be confounded by the experimental injection composition. Rather, the *ex vivo* and *in vivo* experiments may instead collectively support a model where any combination of

classical or alternative activation may sufficiently fuel common pathway activation to damage CNS tissue (Figure 4.7A/B). Under conditions of lower classical activation, alternative activation is required to cause full CNS injury (Figure 4.7B, left). However, alternative activation is not necessarily required if sufficient classical activation fuels common pathway activation (Figure 4.7B, middle). Indeed, a human serum titration experiment performed on primary glial cells by other laboratory members supported a similar conclusion (Figure 4.7C). Higher levels of supplied serum did not require alternative activation to achieve maximum levels of astrocyte lysis, whereas alternative activation was required for maximum astrocyte lysis when lower levels of human serum were supplied.

The proposed model requires testing via a combination of *in vitro*, *ex vivo*, and *in vivo* experiments. A key experiment is to test the *in vivo* potential for lesion formation when lower levels of complement are injected using the optimized protocol (Figure 4.7B, right). The experiments would also provide significant insight into approaching more rigorous data quantifications for the presented descriptive data. For example, experiments that titrate human serum levels in the *ex vivo* model may guide a scoring system of the astrocyte cellular network (Figure 4.2D) to quantify the number of healthy astrocytes with intact processes as well as determine the morphologic progression of astrocyte cell death in order to quantify the extent of astrocyte damage within the network. Although astrocyte processes appear In vivo experiments would guide insight into meaningful C3d expression quantifications (for example, total levels and/or correlations with specific astrocyte morphology patterns within heterogeneous lesions; Figure 4.1B). An expanded analysis to include neuronal markers may also characterize cytotoxic contributions not detected in assays that only analyze astrocytes and oligodendrocytes.

In vivo Model Optimization

Indeed, the findings of significant astrocyte pathology independent of experimental injection and the change from homogenous to more heterogeneous lesion phenotypes after modulating injected complement protein levels led us to reconsider the levels and sources of activated complement proteins in the injection model, as well as how the injection protocol may cause astrocyte damage. Key questions included what represented pathology incited by AQP4 rAb, and what represented pathology incited by the injection procedure. Candidate cytotoxic mechanisms incited by the injection procedure included osmotic trauma due to the injection volume and/or infusion rate, toxicity incited by the human serum, and the potential for alternate complement activation sources including lectin and/or unappreciated murine sources.

A first challenge was dissecting AQP4 rAb effector-mediated pathology. Significant astrocyte pathology was observed independent of experimental injection (Figure 4.3), suggesting that the injection procedure was significantly disturbing CNS homeostasis. Although the pathology was similar to AQP4 rAb-mediated pathology in that AQP4 and GFAP expression was lost, the findings that neither C3d nor MAC deposition was present, and that immune infiltrate may differ (data not shown) is suggestive of an alternate pathogenic mechanism. We injected 3uL of human serum and 3ug of rAb in a total volume of 5uL at a flow rate of 1uL/minute. Other intracerebral injection models did not report similar pathology and injected 1-38uL total volume, and up to 8uL of human serum at a similar injection rate [252-254, 310]. Perhaps the flow rate and small diameter pulled glass pipette created a higher hydrostatic pressure that damaged brain tissue, or that an astrocytic stress response occurred due to an immediate and rapid change in local fluid volume. The

human serum itself may incite damage, however when only mAb^{fB} was injected in the absence of human serum similar astrocyte pathology was observed (data not shown).

A second question was understanding how AQP4 rAb-mediated complement activation occurred in the classical pathway depletion experiment (Figure 4.3L). A murine NMO model was chosen for this study given the powerful complement genetic toolkit available, but comes at the expense of having to overcome an unknown complement inhibitor that limits experimental lesion formation [368]. A co-injection of human serum is proposed to stimulate complement activation, however, why the injection now permits complement activation within the CNS to induce an experimental lesion is unclear. It was not readily possible to distinguish a human or mouse CNS complement source in the experiment. On one hand, residual human C1q may be present in the injected serum. Immediate AQP4 rAb binding and subsequent activation may rapidly occur to initiate lesion formation. Alternatively, a serum murine inhibitor may also be present within the CNS and can bind the IgG component of human serum. It is possible that the serum Ig outcompetes inhibitor binding, allowing a mouse C1q-like protein to bind AQP4 rAb and activate the lesion. The possibilities require testing to differentiate. Regardless, the performed experiment (Figure 4.5) introduced 2 critical considerations regarding the levels of complement protein injected. First, is that differences in lesion phenotype compared to a non-depleted serum injection suggested that excessive C1q protein in the human serum could drive complement-mediated pathology. This could mask the natural lesion progression that would otherwise occur. Second, is that pharmacologic inhibition may also be required to fully inactivate pathway activity. If residual C1q was present and drove lesion formation, it is also possible that residual MBL present in the MBL-depleted serum is sufficient to drive any lectin pathway

mediated pathology. As a result the *in vitro* experiment would not necessarily translate *in vivo*. The consideration may not impact alternative pathway findings, as a pharmacologic inhibitor (mAb^{fB}) was included in the *in vivo* injection.

The findings collectively supported an experimental test that injected a smaller percentage of human complement in a smaller total volume at a slower infusion rate. Indeed, an experimental lesion ideal to quantify both astrocyte and oligodendrocyte loss developed when only 1uL total volume, of which human serum was .05 uL, was injected at .5 uL/min. Robust lesion pathology was observed for AQP4 rAb, but not control rAb. Furthermore, the lesion was significantly more heterogeneous than the more homogeneous nature of the previous lesions. The findings supported that the larger amount of human complement protein introduced into the CNS likely contributes at least partially to the lesion phenotype of the initial injection approach. The optimized approach also addressed any potential contribution due to serum protein toxicity and/or osmotic trauma.

The optimized model raises the question as to how lower levels of injected complement may modulate the deposition of C3d (Figure 4.1). One possibility is that C1q binding to CNS tissue at higher levels could more quickly deplete the pool of available C3, thus deposition may be observed across a larger time span in the optimized model. It is also possible that lower levels of deposited protein, or altered deposition patterns, may be observed depending on the relative contributions of murine vs. human C3. Repeating the time course in the optimized model may offer novel insight into these questions and assist in differentiating complement-dependent vs. independent toxicity mechanisms. The experiment may also enhance our understanding of how the *in vivo* detection of activated complement protein fragments could serve as a biomarker for CNS destruction and lesion activity [351].

Aspects of the heterogeneous lesion (Figure 4.6) may more closely resemble the "penumbra" recently characterized in rat NMO lesion models [258]. Here, an NMO lesion developed after peripheral injection of AQP4 rAb and an intra-cerebral needle-prick, but no intra-cerebral injection. The needleprick was proposed to open the blood brain barrier to provide AQP4 rAb CNS access. Regions referred to as a "penumbra" were observed where AQP4 expression was decreased, but GFAP expression remained intact. The proposed interpretation is that the penumbra represents a region of perturbed homeostasis through complement-independent mechanisms. Multiple molecular mechanisms may therefore perturb the CNS and the interplay between the mechanisms needs to be better understood to elucidate lesion pathogenesis. Our injection model is the first murine model to observe significant lesion heterogeneity and potential penumbra-like pathology. The optimized model may offer the ability to better appreciate how complement pathway-specific mechanisms can cross-activate these other processes.

A Counterargument

It is also possible that the *in vitro* and *ex vivo* environments create an artificial environment that does not reflect *in vivo* CNS complement activation potential. Thus, the initial conclusion that classical pathway activation is sufficient for *in vivo* lesion formation may be correct. Perhaps the large culture volumes influence the concentration and activation kinetics of the complement activation pathway proteins. An *in vivo* environment may provide a more continuous assembly line that ensures rapid and complete pathway activation. This, potentially in conjunction with lower CNS expression levels of complement inhibitors [202], may allow for significant tissue injury to emanate from only a small level of classical

pathway activation. Astrocytes do put up a fight against AQP4-IgG [256]; initial runaway pathologic activation as a consequence of low inhibitor levels seems less likely. Nevertheless, the amount of initial activation required may be lower than anticipated if CNS cells unintentionally fuel pathway activation by releasing pathway complement proteins directly onto the activation assembly line [204]. It does seem likely that at some point the level of classical pathway activation will be too low to initiate CNS damage; the question is if other pathways (for example, the alternative pathway) can drive CNS injury at that point or if the system is effectively inhibited. Thus, *in vivo* injection experiments may require titrating levels of introduced complement even further. An injection of .05 uL of C1q-depleted serum, instead of .05uL of normal human serum, may represent an insightful first experiment in this regard.

Therapeutic Implications

The implications of our findings pose several challenges for the clinical delivery of complement therapeutics in NMO. Eculizumab, a C5 inhibitor, has shown promise in early trials and functions by inhibiting the common pathway [103]. This comes at the expense of global complement inhibition, predisposing patients to potentially lethal infections [352]. Targeting specific pathways offers a promising alternative to leave at least part of the activation pathway intact. If classical pathway activity is sufficient for lesion formation, targeted classical pathway inhibitors may be an attractive therapeutic alternative. An early study demonstrated that C1-Inh is safe to administer to NMO patients [102]. However, the approach may have limited clinical utility if alternative activation incites the majority of CNS tissue damage. Testing alternative pathway contributions when lower overall levels of

complement protein are artificially supplied would provide significant insight in this regard and may more broadly impact our understanding of complement-mediated autoimmunity.

A last question is what proteins of the common pathway induce cytotoxicity. C3a, C5a, and MAC have all been proposed to play direct or indirect roles [85, 86, 335]. It would be interesting to expand the studies and inhibit the common pathway at multiple levels (C3, C5, and C9), or to use complement receptor -/- mice to understand the potential for pathway cross talk. The studies may provide insight into the utility of blocking complement receptors as an alternate therapeutic strategy.

In conclusion, the experiments demonstrated that complement activation occurs during both initial astrocyte destruction and secondary demyelination in an *in vivo* model of NMO lesion formation. Classical pathway activity is sufficient to drive CNS tissue destruction *in vivo*, although an ex vivo model demonstrated the potential of alternative cross-activation to contribute to CNS damage. Future studies that reduce the initial cytotoxic insult by classical pathway may delineate both direct and indirect cytotoxic roles for alternative and MBL pathways, and assist in guiding clinical therapeutic approaches with novel pathway-specific complement therapeutics.

Endnotes

This work was supported by a National Multiple Sclerosis Society grant and NIH R01EY022936.

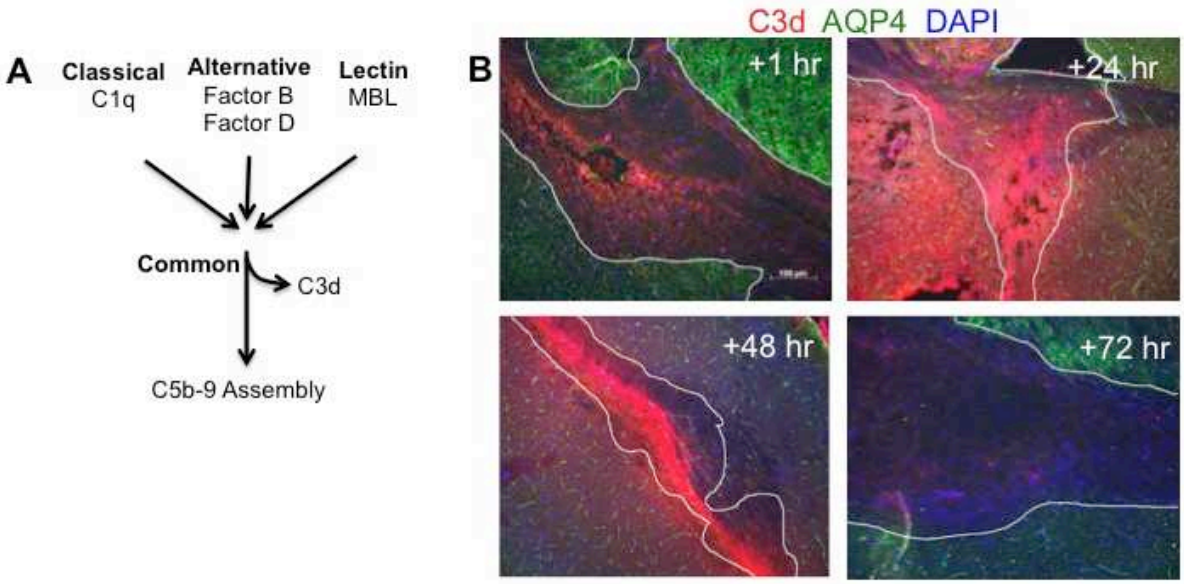

Figure 4.1: C3d deposition during experimental NMO lesion formation
(A): A schematic demonstrating the 3 traditional mechanisms of complement system activation with key proteins participating in each respective pathway. Activation of the common pathway results in C3d deposition on the targeted surface. (B): Images of experimental *in vivo* NMO lesions demonstrating patterns of C3d deposition. Lesions are characterized by a loss of AQP4 expression; lesion area is outlined in white. The time point examined represents the number of hours post-lesion initiation and is indicated in the upper right corner.

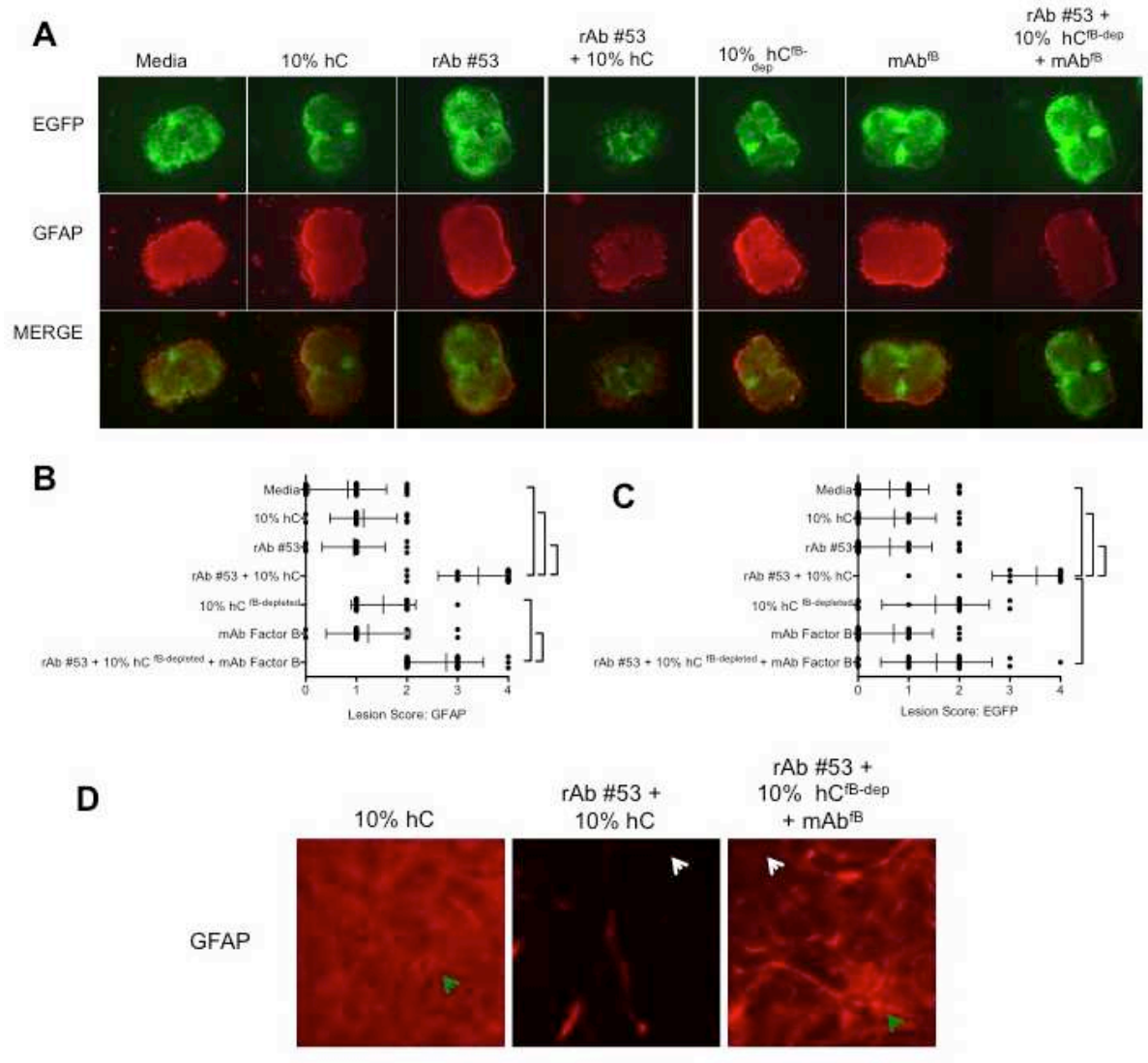

Figure 4.2: Alternative pathway activation contributes to *ex vivo* lesion formation
(A): Representative images of *ex vivo* NMO lesions after 24 hours of treatment. Oligodendrocytes are identified using a PLP-EGFP transgenic mouse (top), and astrocytes are identified via GFAP immunostaining (middle). (B/C): Lesion development is quantified by examining GFAP (B) and EGFP (C) expression/morphology using a 0-4 scale reflecting the area of lesion damage. Data represents cumulative slices from n=3 biologic experiments. Significant comparisons are indicated by the black bars (Kruskal-Wallis with Dunn's post test, alpha<.05). D: Higher magnification GFAP images for the indicated treatment. Green arrow heads indicate examples of more intact astrocyte networks, white arrow heads are examples of regions where the network is destroyed.

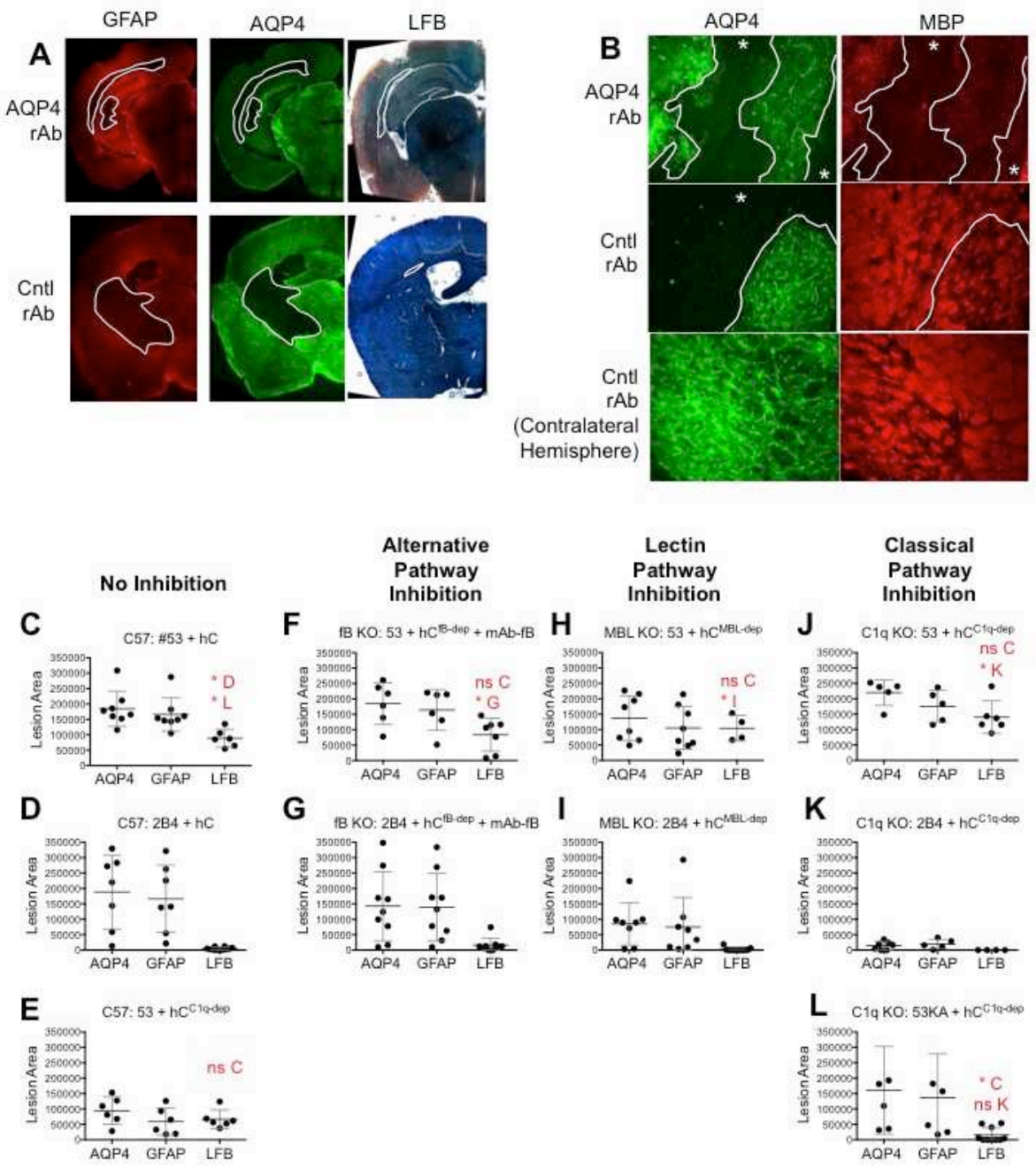

Figure 4.3: Classical pathway activation is sufficient for *in vivo* demyelination.

Figure 4.3: Classical pathway activation is sufficient for *in vivo* demyelination.
(A): Example images showing GFAP, AQP4, and LFB staining after 48 hours of experimental lesion formation *in vivo* for an AQP4 rAb (top) and isotype control rAb (bottom). Lesion area is outlined in white and represents an example data point as scored in C-L. (B): 20x magnification of AQP4 and MBP expression in the same field of view for lesions incited by AQP4 rAb (top) and control rAb (middle/bottom). *=lesion area. (C-L): Quantification of *in vivo* lesion area as demonstrated in (A). Each graph states the mouse strain, rAb injected (AQP4 rAb #53 or isotype control rAb 2B4) and human serum injected. A monoclonal antibody targeting factor B was also injected for F/G. Antibody 53KA (L) is an effector complement-null antibody. Astrocyte lesion area did not significantly differ (one-way ANOVA p=.08 for GFAP). Significant LFB comparisons are indicated in red above each LFB group (one-way ANOVA with Tukey's test for multiple comparisons, *= family alpha <.05 or ns = >.05).

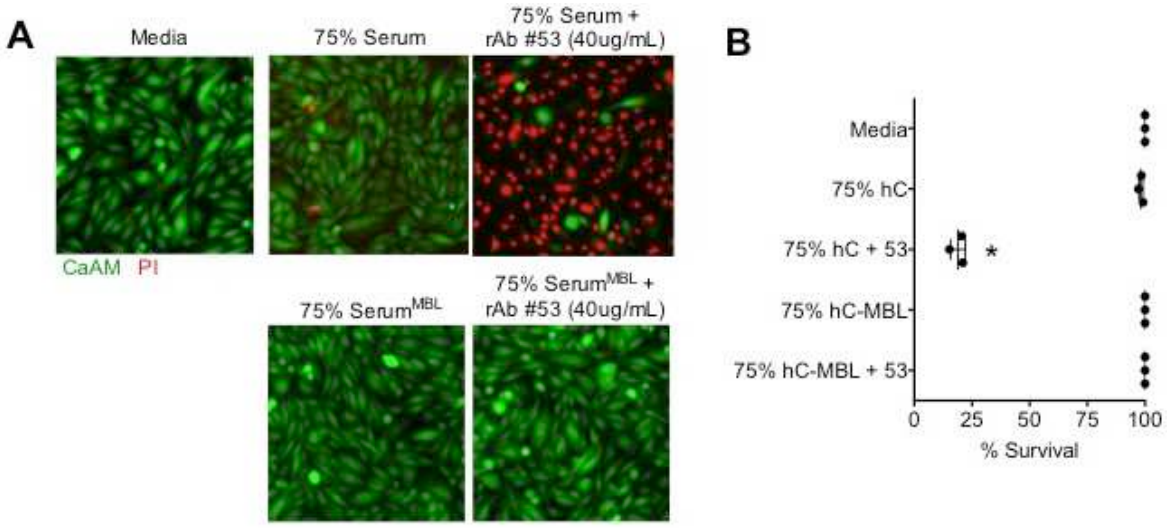

Figure 4.4: AQP4 rAb do not activate the lectin pathway
(A): Representative images showing CaAM (live cells) and PI (dead cells) fluorescence for indicated treatments. Serum^{MBL} is human serum that can only activate the lectin pathway as C1q and Factor D have been depleted. (B): Cell counts expressed as the total percentage of surviving cells. The percentage of surviving cells did not significantly between groups except for the indicated group (one-way ANOVA with Tukey's test for multiple comparisons, * = $p<.05$).

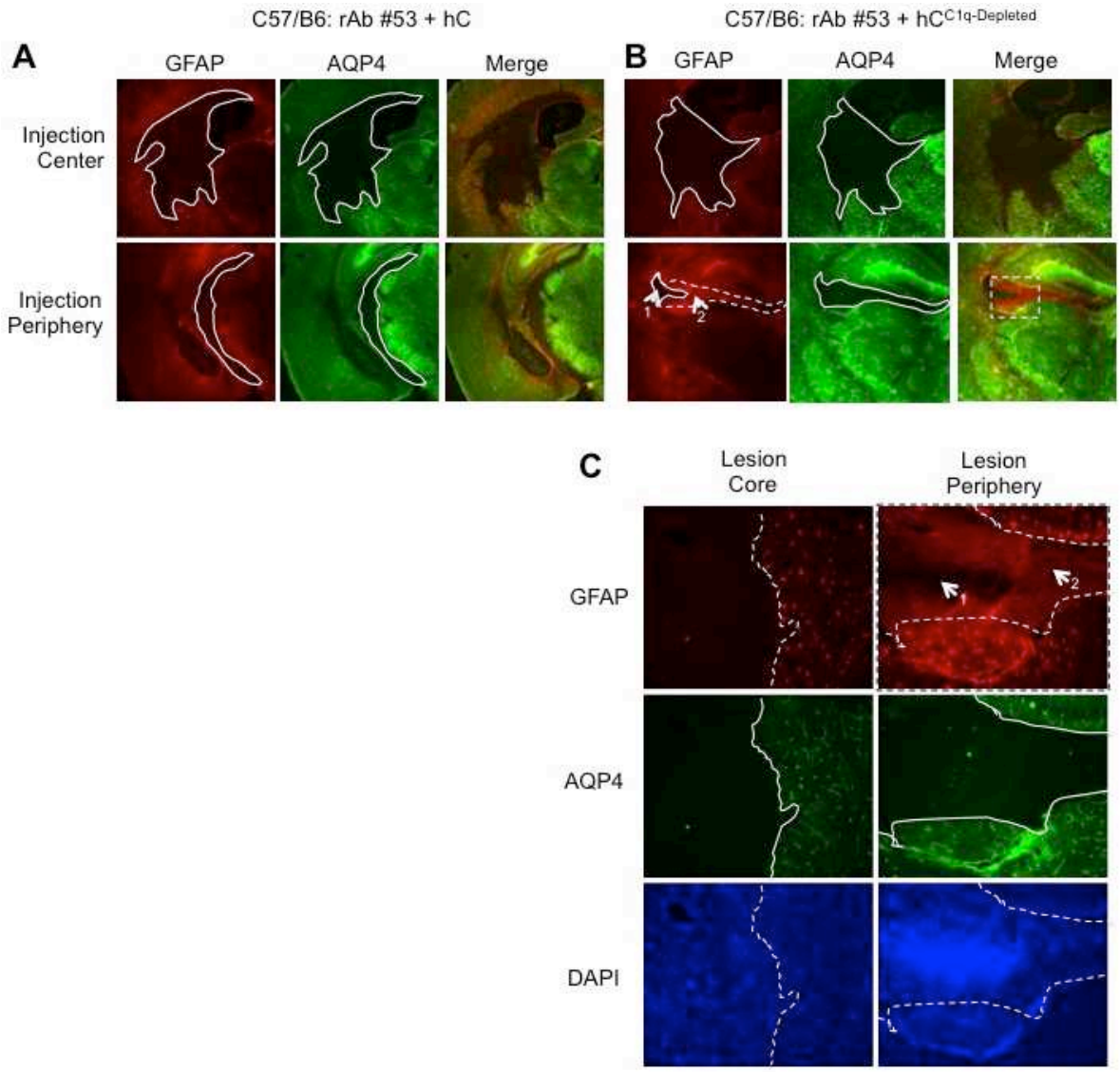

Figure 4.5: Altered lesion phenotype with co-injection of C1q-depleted serum and AQP4 rAb into a C57 mouse.

(A/B): GFAP and AQP4 expression at the injection site center (top) and periphery (bottom). Lesions are shown when 3uL of normal human serum (A) or C1q-depleted human serum (B) are co-injected into a C57 mouse with AQP4 rAb. Lesion area is outlined in solid white white. The lesion area in dashed white (B, lower left) indicates area of AQP4 loss superimposed over GFAP image. Areas of complete GFAP loss at a lesion core (arrow 1) and incomplete GFAP loss (arrow 2) are hihglighted (B, bottom left). The dashed box (B, bottom right) indicates the region magnified in (C). (C): Higher magnification images of GFAP (top), AQP4 (middle), and DAPI (bottom) at the injection center and periphery when C1q-depleted serum is co-injected. Numbered arrows represent same findings as in (B). The lesion area was determined by outlining regions of AQP4 loss (middle); the regions are then super-imposed over GFAP and DAPI images as white dashed lines to highlight multiple staining patterns within the lesion area.

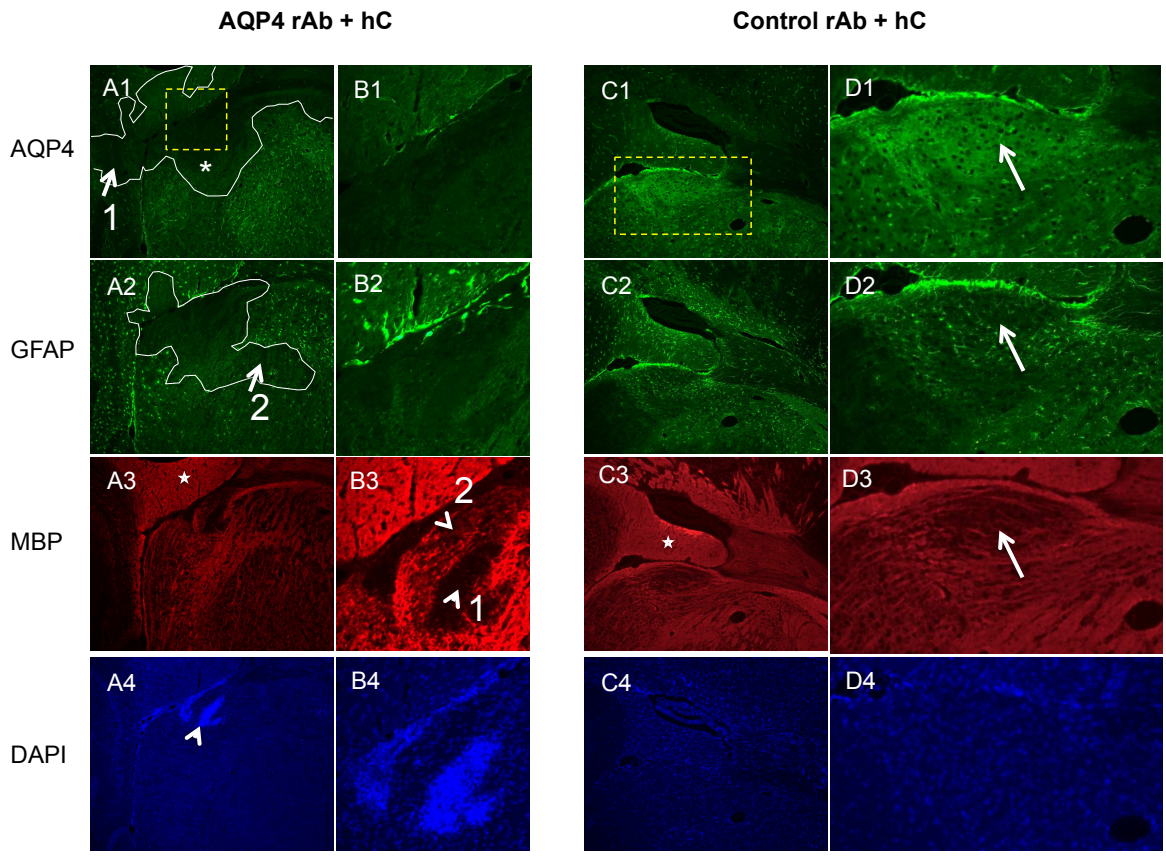

Figure 4.6: An optimized injection model
Low (A/C) and high (B/D) magnification images of a lesion initiated by AQP4 rAb (A/B) or isotype control rAb (C/D). The dashed yellow box (A/C 1) indicates the magnified region in B/D. AQP4 (1), GFAP (2), MBP (3), and DAPI (4) expression were examined. Lesions are defined as a loss of AQP4 or GFAP expression and are outlined in white; lesions were not observed in isotype control injections (A-D 1-2). (A1/A2): White arrow #1 indicates region of AQP4 loss but intact GFAP, white arrow #2 indicates area of GFAP loss but intact AQP4. (A3/C3) White star is provided for anatomic orientation in comparing AQP4 rAb vs. control rAb lesion. (B3): White arrowheads indicate complete (arrow #1) or partial (arrow #2) MBP loss. (A4): Arrowhead indicates increased DAPI expression.

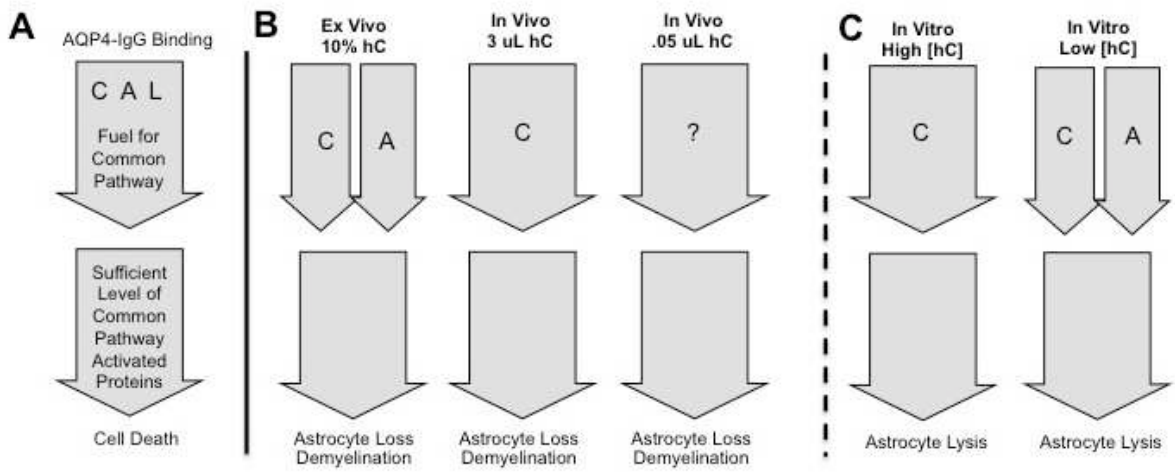

Figure 4.7: A model of complement pathway contributions to CNS injury
(A) To cause CNS injury, some level of common pathway activation is needed. as indicated by the volume of the common pathway arrow. Common activation needs to be fueled by classical (C), alternative (A), or lectin (L) activation. (B): A model is proposed whereby lower C activation requires A activation to fuel common pathway CNS destruction (*ex vivo* experiment, left), whereas higher C activation does not require A activation (*in vivo* experiment, middle). *In vivo* pathway contributions are unknown at lower levels of C activation (right). (C): Laboratory experiments performed on primary glial cultures that titrated the level of supplied serum support the potential for classical activation to individually (left) or in comnination with alternative activation (right) fuel common pathway activation.

CHAPTER V

DISCUSSION

Introduction

The full realization of NMO treatment goals requires a better understanding of the molecular events inciting initial astrocyte damage and propagating lesion formation. As CNS tissue injury emanates from complement effector activation by AQP4-IgG, the goal of this body of research was to better understand how the classical complement pathway is initially activated by AQP4-IgG and if additional complement pathways contribute activated complement proteins during lesion propagation. Two models were constructed that contribute significant insight in the relationship of AQP4-IgG and NMO, the molecular drivers of NMO lesion formation, and novel treatment approaches. The models offer broader insight in the fields of complement and humoral autoimmunity.

A novel approach to infer protein spatial relationships on cell membranes was also developed (Chapter 2). While the direct significance was to assist in building the molecular model of classical pathway activation, additional applications of the algorithm studies are sprinkled throughout the following discussion.

Classical Pathway Activation by AQP4 rAb

A Molecular Model

First, a molecular model of C1q activation by AQP4 rAb was identified (Figure 3.6). C1q binding and activation occurs over AQP4 autoantibody assemblies that are formed upon membrane binding to AQP4 arrays. A critical molecular driver of platform assembly is Fc-Fc interactions between neighboring rAb. The interaction orients a stable, well-exposed C1q

binding site ideal for high level C1 activation. Epitope-imposed structural constraints in Fc domain geometric organization resulted in the formation of a variety of IgG platforms with differing abilities to engage and activate C1q. The model also recognized a key role of large, immobile AQP4 arrays in supporting the formation of antibody membrane assemblies.

AQP4-IgG Membrane Assemblies and NMO

The requirement for the self-assembly of AQP4-IgG molecular platforms for C1q activation introduces multiple considerations in better understanding the relationship between AQP4-IgG and NMO. First, the epitope-imposed regulation of IgG assembly supports that various AQP4-IgG epitope subpopulations are likely of differing pathogenic potential. The effective translational application of AQP4-IgG titers beyond diagnostic utility may therefore require assays with the ability to quantify levels of these specific pathogenic subpopulations. A consideration in this regard is that single amino acid contacts (H151/L154) significantly impacted Ig membrane assembly. While AQP4-IgG epitopes may be broadly characterized into 2 patterns based on binding dependencies to specific extracellular loops (Pattern 1 and Pattern 2) [299], shared individual amino acid contacts may ultimately limit the translational utility of broad epitope characterizations. For example, AQP4 rAb from each pattern were demonstrated to contact H151/L154; each broad pattern may therefore harbor subpopulations of significant pathogenic potential. Broader epitope characterizations may nevertheless offer novel insight into how the general epitope reactivity of AQP4-IgG changes over time.

Although the data establishes a key role for Ig membrane assemblies in activating C1q, the full array of molecular variables impacting Ig assembly and/or subsequent C1q binding and activation are not understood. For example, post-translational modifications may

produce an array of glycosylation patterns on IgG and impact AQP4-IgG effector activation [291]. Sialylated IgG was recently demonstrated to impair CDC activation [285]. Applying a similar experimental approach (Chapter 3) using glyco-engineered AQP4 rAb would offer novel insight into how variations in glycosylation patterns contribute to platform assembly, C1q binding, and/or activation. It is possible that antibody glycosylation, in addition to epitope specificity, imposes structural constraints on the IgG Fc domain to impact how Ig may self assemble upon membrane binding. Alternatively, glycosylation may play little to no role in assembling the platform but significantly influence how C1q interacts with the platform. When examining a glycosylated Fc domain schematic, the sugar moieties extend within and along the inner face of the Fc domain (Figure 5.1, compare A vs. B). The residues, at least as depicted, do not appear to interfere with Fc-Fc domain interactions and may favor the hypothesis that glycosylation patterns impact C1q binding and activation as the residues border the C1q binding site. However, the model does not rule out a potential influence on overall secondary structure that may nevertheless modulate Ig platform assembly. Furthermore, glycosylation could impact the ability of specific epitopes to orient the Fc domain if the epitope places sugar moieties in close proximity to the AQP4 surface, creating a steric clash. The possibility has not been explored in any model to date.

Another potential limitation in recognizing AQP4-IgG pathogenic subpopulations is that the pathogenic significance of Ig membrane assemblies has only been investigated for complement effector activation. A key question is how Ig membrane assemblies influence the activation of additional immune effector mechanisms. For example, ADCC is involved in NMO lesion formation, and IgG-mediated phagocytosis remains unexplored [254]. Adapting the experimental approach to investigate these mechanisms is needed to recognize the full

array of pathogenic subpopulations and their various roles in lesion pathogenesis. ADCC models may require expanding the STED image analyses to include rAb organizational patterns across a larger area to test how FcR clustering may impact activation. It would also be interesting to place the effector mechanisms in competition to better understand the interplay between complement and FcR toxicity mechanisms. For example, C1q binding may limit the number of IgG contacts available for Fc receptors, but it may also co-stimulate cytotoxic activation. Various IgG glycoforms may also favor one effector mechanism over another [364, 369, 370], introducing an additional level of potential regulation.

AQP4-IgG Assemblies: Beyond NMO

Beyond NMO, the model represents the first model of IgG-mediated classical pathway activation in human autoimmune disease and offers significant insight into the translational relevance of IgG hexamerization [163]. The data supports two independent mechanisms of Ig platform assembly that converge on a common mechanism driving C1q activation. Many questions remain regarding how structural variations in IgG platforms influence both C1q binding and activation.

The super-resolution imaging approach, in conjunction with *in vitro* binding and activation data, support that AQP4 rAb assemble into multiple unique Ig platforms with differing abilities to both bind and activate C1q. In our study, C1q binding did not correlate with C1q activation (Figure 3.1). This contrasted with prior studies that generally observed a strong correlation between C1q binding and C1q activation [162, 163]. A caveat, however, is that these studies used single monoclonal Ig with introduced point mutations that modulate only 1 structural interaction (either CH2-C1q interactions, or CH3-CH3 interactions) on the

interwoven IgG platform. Quantifications are therefore made against a single base platform and it is not necessarily surprising that activation correlates with how well a single platform component is strengthened. A strength of our approach is that multiple unique monoclonal rAbs were studied in parallel, with experimental modulation of both CH2 and CH3 domain interactions. The approach allowed for an appreciation of multiple initial Ig platforms with differing relative dependencies on each respective interaction in binding and activating C1q, potentially explaining the apparent discrepancy.

It would be interesting to stratify our C1q binding/activation correlations by epitope binding dependency with a larger number of rAb. Data supports that the Ig platforms formed by H151/L154-dependent rAbs likely significantly vary in structure; the platforms formed by H151/L154-independent rAb are more uniform. Thus, it may not necessarily be surprising if a stronger correlation between C1q binding and activation is observed with H151/L154-independent rAbs given a more similar starting platform. It would also be interesting to test if the various mAb used in other prior studies formed Ig assemblies that more closely resembled those formed by H151/L154 -independent rAb [162, 163]. If they are similar, it is possible that the reported correlations between C1q binding and activation accurately reflect the system biology. Adapting the STED imaging and ASA scoring algorithm for use in these models could test the hypothesis.

A limitation in our experimental approach is that the formation of multiple IgG platforms were inferred via a combination of super resolution STED nanoscopy findings and *in vitro* binding and activation data. Alternate imaging approaches are likely required to better resolve IgG platform structure. Atomic force microscopy has imaged IgG hexamers over mica substrate, although the resolution would not be sufficient to directly visualize Fc-

Fc amino acid contacts [331]. Cryo-EM modeled C1q engaging an IgG hexamer, but required the superimposition of IgG crystal structures and assumed structural parameters [163]. A more recent study achieved atomic resolution with cryo-EM [371]; it would be interesting to test if similar resolution could be obtained for AQP4 rAb.

One application of the structural characterizations would be to guide the design of more optimal small molecule therapeutics. Beyond the previously discussed considerations of the Fc-domain peptide inhibition experiments, an alternate possibility for the variable efficacy of peptide inhibition is that the bound surface area does not inhibit the full array of possible CH3 amino acid contacts (Figure 5.1, compare A vs. C). The amino acids mutagenized to both promote and inhibit Fc interaction were not covered by the Fc binding peptide; thus amino acid interactions may nevertheless be driving platform assembly in the presence of peptide. More rigorous platform disruption via a peptide that covers a larger surface area may be required for optimal therapeutic efficacy. The peptide chosen was selected based on binding affinity to the Fc-CH3 domain [341]; studies specifically examining how well this peptide or others block Fc domain interactions for multiple IgG platforms have not been performed.

As a brief aside, a novel application of the STED imaging algorithm could be to quantify how a small library of peptides may block AQP4-IgG assembly and/or rAb binding. Larger screens to recognize candidate molecules do not necessarily examine functional consequences of peptide binding, as the assays are often labor intensive. CDC activation studies at a larger scale require significant time and effort, and are not ideal for screening purposes. Application of super resolution imaging approaches, such as the STED imaging algorithm developed here (Chapter 2), may offer a quicker screening approach to identify

candidate peptides that could significantly impact Ig assembly, regardless of whether the peptide targeted AQP4 or IgG.

Indeed, modeling approaches that also resolve AQP4 extracellular loop amino acids in addition to Ig platforms would be valuable. If the AQP4 extracellular loop surfaces were resolved, peptides could also be designed that bind AQP4 but disrupt IgG assembly. An interesting implication of this approach would be that classical pathway activation would be inhibited but specifically for AQP4-IgG, leaving all other innate complement pathways intact. Depending on the amino acids contacted, the peptides could also compete with AQP4-IgG binding to limit complement activation via multiple mechanisms.

An alternate utility for novel small peptides could be to probe specific IgG platform structural pockets to understand how the pocket influences C1q activation. Therapeutic targeting of the pockets may also represent an alternate approach to limit classical pathway activation by IgG. Furthermore, mapping how pockets influence C1q activation on multiple Ig platforms may propose novel hypotheses into how specific IgG platforms may incite a mechanical stress to C1q. Studies in the laboratory have mapped additional amino acid contacts that influence C1q activation beyond the AEFTE combination and K322 (data not shown), which could assist in constructing a model. Perhaps higher resolution structures would also resolve the C1r2:C1s2 complex, allowing for the differentiation of activated vs. inactivated C1q molecules which has otherwise posed considerable historical challenges [192, 372]. An alternate approach would be to adapt a single-molecule PALM/STORM imaging approach to use a 3 color system (IgG, C1q, and C4d). The approach was partially developed as an alternate to STED AQP4 rAb imaging but not further pursued. The local deposition of activated complement proteins (C4d) neighboring C1q molecules would

indicate activated molecules; superimposing PALM/STORM images over cryo-EM models could provide insight into which Ig platforms represent ideal activation surfaces and may pose novel hypotheses regarding the mechanism inciting mechanical stress.

Crystal structures of AQP4 and IgG are available [107, 188]; and the epitopes recognized by AQP4 rAb have been mapped [299]. An alternate approach to understand the variety of AQP4 rAb platforms could be to first model OAP assembly using the AQP4 crystal structure. IgG binding to known epitopes could then be simulated to understand how the antibodies interact with AQP4 [299], and how the epitopes may impose geometric structural constraints on IgG platform assembly. C1q interactions could also be modeled over any platforms [163]. Thus, multiple approaches could be undertaken that use AQP4 rAb as a platform to better understand many aspects of classical pathway activation.

Using Other Nervous System Diseases as Additional Experimental Tests

Finally, the proposed model was arrived at using antibodies known to activate complement at high levels. An interesting test would be to introduce the molecular drivers into a system where antibodies do not activate complement at high levels. For example, anti-NMDAR antibodies are IgG1 but do not activate complement *in vivo* [345, 346]. Establishing "NMDAR rAb," similar to AQP4 rAb, with Fc-Fc enhancing point mutations would offer a novel test of the model. As receptor binding generally stimulates antigenic modulation, the experiment may also offer insight into how complement activation and receptor internalization may compete with each other to drive or limit cellular cytotoxicity. A competition model has been proposed in a variety of autoimmune disorders including myasthenia gravis (MG) [347]. Generating "anti-nAChR rAbs" may offer an alternate test of

the hypothesis as polyclonal antibodies stimulate both receptor internalization and complement activation in MG. The two disorders may therefore offer complementary approaches to test the proposed model of classical pathway activation in a broader autoimmune context.

NMO and AQP4 Membrane Organization

AQP4 membrane organization plays a key role in regulating classical pathway activation by AQP4 rAb [306]. Potential variables regulating AQP4 membrane availability have been proposed based on hypothetical considerations (Figure 3.6); experimental testing is required. The experiments may offer novel insight into the anatomic predilection of NMO. A mechanistic explanation as to why peripheral involvement is absent, and why CNS pathology aligns with sites of higher OAP formation is lacking. An intriguing hypothesis is that the ability of AQP4 OAPs to support Ig platform assembly directs pathology towards sites where OAPs are expressed at high levels. Studies that examine how AQP4 rAb pathogenicity is influenced by various AQP4 membrane organization variables would offer initial tests of the hypothesis.

One experimental modulation would be to develop a pure M1-AQP4 and a pure M23-AQP4 transgenic rat. The generation of these animals has been historically limited by a poor understanding of the regulation of M1- vs. M23-AQP4 isoform expression [124]. However, it is possible that the animals could be generated via application of recent technologic and scientific discoveries. Regarding a pure M23-AQP4 model, CRISPR-CAS technology could effectively replace the full genomic AQP4 sequence with a shortened sequence missing the DNA encoding amino acids 1-22. Thus, all AQP4 expressed will begin translation at M23-

AQP4. A pure M1-AQP4 animal is harder to generate as regulation of the unknown splicing machinery needs to be overcome. AQP4 crystallization studies suggest that Arg108 and Tyr250 are required amino acid contacts for OAP formation [127]; mutagenesis destroyed array formation as demonstrated by a Fourier transform. Confirmation of the organizational impact on live cell membranes could provide an approach to generate a pure M1-AQP4 animal regardless of isoform RNA expression. Other AQP4 point mutations closer to M23 may offer alternative mutagenesis candidates [330]. The models could also be used to investigate the functional consequences of AQP4 membrane organization.

AQP4 rAb peripheral injections into the genetic rat models may be particularly interesting, as AQP4 rAb can activate rat complement [257, 258]. Historically, peripheral injections into murine models did not produce pathology but lesion development may be limited by an unknown endogenous complement inhibitor [368]. The experiment would provide insight into whether peripheral membrane AQP4 organization alone limits lesion pathology. Injection of AQP4 rAb with CH3 domain Fc-Fc enhancing mutations into a wild type rat offers a complementary experimental approach. A larger screen of possible mutations may be required to identify an optimal mutation combination for injection [163, 193].

The model may suggest an alternate possibility for the lack of peripheral involvement: that that absolute level of AQP4 expressed may not be sufficient to overcome the local expression of complement inhibitors. AQP4 is most strongly expressed in the CNS, and is expressed at lower levels in the periphery. Curiosuly, AQP4 is largely organized into OAPs in some peripheral organs despite the absence of lesion development upon AQP4-IgG binding [260, 373, 374]. Injecting a virus encoding constitutive AQP4 expression into rat

muscle or kidney, and comparing lesion development to control-injected tissues, could test the hypothesis. Approaching the question from the alternate perspective by inhibiting complement inhibitors poses significant technical challenges given the large number of potential inhibitors. A better understanding of the differences in complement inhibitor expression in CNS vs. peripheral tissues is also needed. Notably, however, destructive levels of complement activation can occur in organs where AQP4 is expressed [147]. A promising approach to direct peripheral studies may therefore be to isolate an organ of interest, understand the initial potential for AQP4-IgG mediated complement pathology, and then experimentally manipulate the AQP4-IgG/AQP4 variables prior to modifying complement inhibitor levels.

A PALM/STORM super-resolution imaging approach was pursued to resolve AQP4-IgG clusters. The approach was confounded regarding application to Chapter 3 studies, but may offer an alternate model to develop peripheral pathology. The genetically-encoded fluorophore (mGeos [375]) introduced onto the AQP4 rAb CH3 domain disrupted antibody binding yet enhanced complement activation to levels not obtainable via any other experimental manipulation. One possible explanation is that the fluorophore itself, despite having introduced mutations to limit aggregation, nevertheless aggregates at low enough levels to stabilize IgG assembly. It is also possible that the fluorophore is accidentally inciting a direct mechanical stress onto C1q due to the size and/or position of the fluorophore. Thus, all rAb that bind C1q may cause activation, which would explain why only a low level of bound rAb is required for high level activation. An interesting test would be to see if the mGeos-tagged antibodies activate CDC on M1-AQP4. Super resolution imaging of C1q and IgG over M1-AQP4 tetramers, with the above mentioned C4d co-stain,

may provide insight into whether the activation was IgG assembly-dependent or more dependent on mGeos itself. The mGeos-tagged rAb may therefore represent an alternate approach to explore hypotheses regarding how local complement regulation may limit peripheral NMO involvement.

Experimentally dissecting the CNS predilection for spinal cord and optic nerve pathology is more difficult to approach. Significant unknown variables include unknown *in vivo* regional AQP4 expression levels and organizational differences at the protein level, and poorly characterized complement inhibitor expression. A promising approach may be to manipulate these variables using *ex vivo* models and primary culture lines. Indeed, preliminary studies have demonstrated that the CNS tissue source used to generate primary cultures (cerebellar vs. cortical) influences the maximal level of CDC activation by AQP4 rAb. Quantifying total levels of AQP4 and membrane organization patterns in the models, and comparing how toxicity changes with the modulation of AQP4 membrane organization, would offer an initial experiment. S-palmitoylation, calcium signaling, and PKC activation are proposed to modulate AQP4 surface expression and represent potential experimental manipulations [112]. Regulation of AQP4 organization via altered s-palmitoylation (induced by treatment with 2-bromopalmitate) is the most ideal approach of the 3; both calcium signaling and PKC activation change membrane organization without impacting OAP size or number presumably by modulating the available pool of M1-AQP4. A more rigorous understanding of calcium-dependent mechanisms could potentially assist in developing optogenetic models to regulate AQP4 membrane organization.

A particularly interesting experiment would be to breed a pure M1-AQP4 or M23-AQP4 rat with a rat lacking CD59. A spinal infusion of IgG and human complement

produced longitudinally extensive spinal lesions in rats lacking CD59 [256]. The genetic approach may offer a means of observing how AQP4 isoform expression may promote or limit pathology; spontaneous lesions may not develop or be significantly less extensive in the pure M1-AQP4 rat. Direct intra-cerebral injections could also be performed, however, the injections may introduce more variability than desired and make quantifications more challenging. Thus, experimental investigations that test how AQP4 membrane organization influences lesion development may offer significant insight into the unappreciated roles that AQP4 itself may play in regulating NMO pathology.

Complement and Lesion Propagation

A Model

Classical pathway activation initiated CNS damage in multiple experimental lesion models (Chapter 4). *Ex vivo and in vitro models* suggested that classical pathway cross-activation of the alternative pathway could cause CNS injury. However, classical pathway activation was sufficient for lesion propagation *in vivo*. Additional experiments suggested that the *in vivo* disparity could at least partially reflect an artifact of the experimental approach. A model of lesion propagation was realized whereby full CNS injury is dependent on a sufficient level of common pathway activation (Figure 4.7). Environments that supported lower levels of classical pathway activation required alternative activation to sufficiently fuel common pathway activity, while classical pathway activity alone could fuel the common pathway in environments that support high level classical pathway activation.

Translational Significance

The originally proposed experimental goals are significant to guide the introduction of safer complement therapeutics into the clinic. Eculizumab has demonstrated early successes in slowing NMO clinical progression, however, the mechanism of activation (common pathway inhibition) is associated with a high risk of adverse outcomes including fatal meningococcal infection [103, 352]. More targeted inhibition of the classical and/or alternative pathways would leave the cytotoxic capabilities of lectin pathway activation intact, possibly alleviating some risk. Although the results favor classical and alternative activation as the cytotoxic complement contributors to CNS damage, the contributions of the lectin pathway remain unclear as the pathway has not been specifically studied *in vitro* or *ex vivo*, and overwhelming *in vivo* classical pathway activation may be confounding. Given the translational significance, the revised interpretation calls for a full *in vivo* test using injection approaches that introduce decreased levels of classical pathway proteins.

Levels of various complement proteins have been quantified in the NMO patient serum and CSF [36-38, 376-379]. The translational utility for the assays is that the levels could serve as a biomarker of disease activity, or indicate attack severity. To date, studies have varied in both detection approach, proteins/pathways targeted, and analysis approaches. The finding that classical pathway alone, or classical and alternative pathway proteins may cause CNS damage poses considerable challenges in using either activation pathway as a marker of disease activity. The reported variation may indeed reflect differing dependencies on pathway activation in humans, or may simply reflect the heterogeneity of analyses approaches. Levels of activated complement fragments may have a more useful utility in predicting attack outcome. For example, CNS levels of MAC and CD59 may correlate with

attack severity [377]. The titers could reflect complement activation occurring over a larger CNS tissue surface area (potentially impacting attack severity) or larger total activation levels independent of lesion area. A mechanism linking activation with attack severity could be enhanced neuronal damage; the relationship between levels of complement activation and neuronal damage or dysfunction is not well studied. Nevertheless, the revised model may emphasize a stronger utility in using common pathway proteins as biomarkers of disease activity.

In Vivo Model Variation and Human NMO

The change in experimental lesion pathology from a relatively homogenous lesion phenotype to a more heterogeneous phenotype after reducing the introduced level of human C1q protein, replicated when lower levels of total complement proteins were injected, raises questions as to 1) what the available source(s) of C1q is in human disease, 2) how variation in C1q availability influences lesion molecular pathogenesis, and 3) how cross-activation of additional pathogenic mechanisms emanates from C1q activation and contributes to lesion heterogeneity and/or clinical progression. The optimized model also offers significant insight into how next-generation lesion models may be designed to molecularly dissect the heterogeneity observed in human lesions [47].

C1q may be produced directly within the CNS, or flux into the CNS from the periphery [202, 258]. Assuming the C1q-depleted serum was fully depleted, AQP4 rAb mediated complement-dependent pathology in a C1q-deficient mouse with C1q-deficient serum may also indicate that an uncharacterized C1q-like CNS molecule may stimulate lesion initiation [202, 206]. A better understanding of how and when the BBB breaks down

during lesion formation, and the contributions of peripheral vs. central C1q sources is needed to better understand how lesion models may recapitulate human CNS lesion environment(s).

The question of local C1q availability also requires considering the potential for C1q activation. In this regard, the AQP4 antibodies themselves may influence the activation of C1q (Chapter 3). To date, *in vivo* models have largely used rAb #53, a His151/Leu154 independent rAb, to initiate lesion formation. Comparing lesion phenotypes between His151/Leu154 dependent and independent rAb, and how lesions change upon introduction of the Fc-Fc enhancing E345R mutation to drive classical pathway activation, may be valuable in understanding both how environmental C1q availability and AQP4-IgG may influence complement activation and/or the requirement of alternative pathway activation to produce CNS damage. These experiments would also provide an *in vivo* test of the proposed classical pathway activation model.

The experiments may also assist in better dissecting the molecular heterogeneity observed in human lesions. Human NMO lesions may display considerable heterogeneity within and between lesions [47]. The clinical significance and a molecular explanation are unknown. Complement-dependent vs. complement-independent pathogenic mechanisms is an attractive hypothesis, and has both clinical and therapeutic implications. The use of the optimized murine model in conjunction with rat models may allow for a finer molecular dissection of the potential interplay between the various cytotoxic mechanisms proposed to participate in lesion propagation [257, 258]. A second key question is how the activation of each putative mechanism may influence clinical onset or progression. Ideally, experimental lesion sites would cause clinical deficit. A readily accessible target is the optic nerve, however vision deficits are difficult to quantify in rodents [255]. An attractive alternative

would to adapt current models to target the spinal cord as motor deficits have been associated with spinal cord lesions [256]. *In vivo* action potentials could also be stimulated (for example, optogenetically) upstream of the lesion site, with neuronal activity recorded past the lesion to correlate neuronal activity with various lesion pathology findings and/or behavior. Multiple molecular mechanisms could be targeted for investigation using a combination of injection parameters, AQP4 rAb +/- Fc mutations, and genetic approaches. *Ex vivo* models (optic nerve, cerebellum) may also allow the study of neuronal function during lesion formation [380, 381]. The optimized experimental models may therefore serve to further advance our understanding of the cytotoxic roles that complement plays in the CNS, as well as provide an experimental tool to investigate how the activation of additional cytotoxic molecular mechanisms may emanate from initial classical pathway activation.

C1q -/- Mice: A Novel NMO Model?

The development of a lesion dependent on AQP4 rAb effector complement activation in the C1q -/- mouse co-injected with C1q-deficient serum was unexpected (Figure 4.3L). A key question is what the source of complement protein was in the experiment. The genetic modification may have somehow bypassed a murine complement inhibitor that otherwise limits high-level endogenous complement activation by AQP4-IgG [368]. If this hypothesis was correct, the strain may offer a novel model of experimental lesion formation.

Prior work to characterize the murine complement inhibitor identified that the inhibitor bound to the IgG fraction of human serum, but did not test if the mouse complement could then activate CDC by AQP4 rAb [368]. The inhibitor may be absent in C1q deficient mice if inhibitor expression directly responds to circulating levels of C1q, which would

explain the potential for even low levels of C1q or a C1q-like protein to interact with AQP4 rAb and serve as an activating complement source. An injection of AQP4 rAb alone in the absence of human complement, and a series of *in vitro* CDC assays using purified murine serum from C1q -/- vs. WT mice could investigate this hypothesis. *Ex vivo*/primary culture models may further evaluate the potential for a CNS C1q-like protein to activate complement, and offer novel models to study the functional roles of these proteins and/or cerebellins [206, 214].

It is also possible that C1q-depleted serum is not fully depleted of C1q, or that the co-injection functions through an unappreciated mechanism. While human C1q may directly participate in lesion pathogenesis, it remains possible that a non-complement protein in the injected human serum permits lesion initiation. For example, it is possible that the murine complement inhibitor binds to the human serum Ig, outcompeting inhibitor binding to allow murine and/or human C1q to bind tissue-bound AQP4 rAb and activate complement. Testing this possibility may be valuable in designing better murine lesion models. If any MBL-IgG interactions are occurring, the possibility of a major cytotoxic potential are low.

Regardless, the observed rescue in lesion pathology when complement-null AQP4 rAb was injected strongly supports that our classical pathway inhibition approach did not fully inhibit classical pathway activation. Although pursuing an explanation is valuable to advance our understanding of the complement system, developing the C1q -/- strain as a novel NMO lesion model may ultimately introduce too many confounding variables to be of significant use: C1q -/- mice have altered synaptic structure, and frequent short seizures [211].

NMO Models as a Tool to Understand CNS Complement System Functions

The *ex vivo* model may provide a platform to better understand the endogenous functions of the CNS complement system. The culture design provides easy access for experimental manipulations, and system activation can be regulated at either sub-lytic or lytic levels. A spinal cord model may be limiting as neuronal architecture is not preserved [268]; a cerebellar slice culture model offers an attractive model as the neuronal and glial architecture is preserved [381]. Studying the cellular responses to specific pathway proteins or more global pathway activation would provide significant insight into how sublytic activation plays various roles in CNS homeostasis. Models could also be developed that dysregulate specific proteins to understand how the cross-activation of endogenous CNS complement protein mechanisms may contribute to neurodegenerative disorders [202, 204]. More global pathway activation could also be achieved via fluid-phase activation after hexamerizing an isotype control antibody, exposing all CNS cells to activated fragments without having any specific cell type serve as a complement-activating surface [163].

The model may be particularly useful to study how chronic activation may alter CNS physiology. Slices can be kept alive for days; the cellular responses to long-term protein accumulation may reveal novel insight into microglial interactions and the impact of chronic activation on synaptic remodeling [204]. Studying repair responses to complement damage may also be interesting. Given the role of C1q in removing apoptotic cells [382], even low levels of activation may significantly cross-activate endogenous homeostatic mechanisms. In this direction, unappreciated roles for complement activation may promote or limit NMO lesion repair. Perhaps a full understanding for the utility of complement therapeutics requires

considering the range of endogenous processes specific proteins play in the CNS at multiple stages during lesion formation.

Epilogue

To conclude, my studies have contributed to our understanding of NMO and the complement system. What a magical world biology is: each discovery reflects a fundamental truth, yet the illusions cast by its shadow blind us from the larger picture and ultimately keep the world hidden. I hope the proposed models inspire thoughtful reflection into both the truths they reveal and the illusions they cast. Although we are ultimately blind to the reality of the biologic world, we only need to know where to shine a light to alleviate the burden of one disease's shadow. After all, one doesn't need to see the sunset to feel the warmth of its colors.

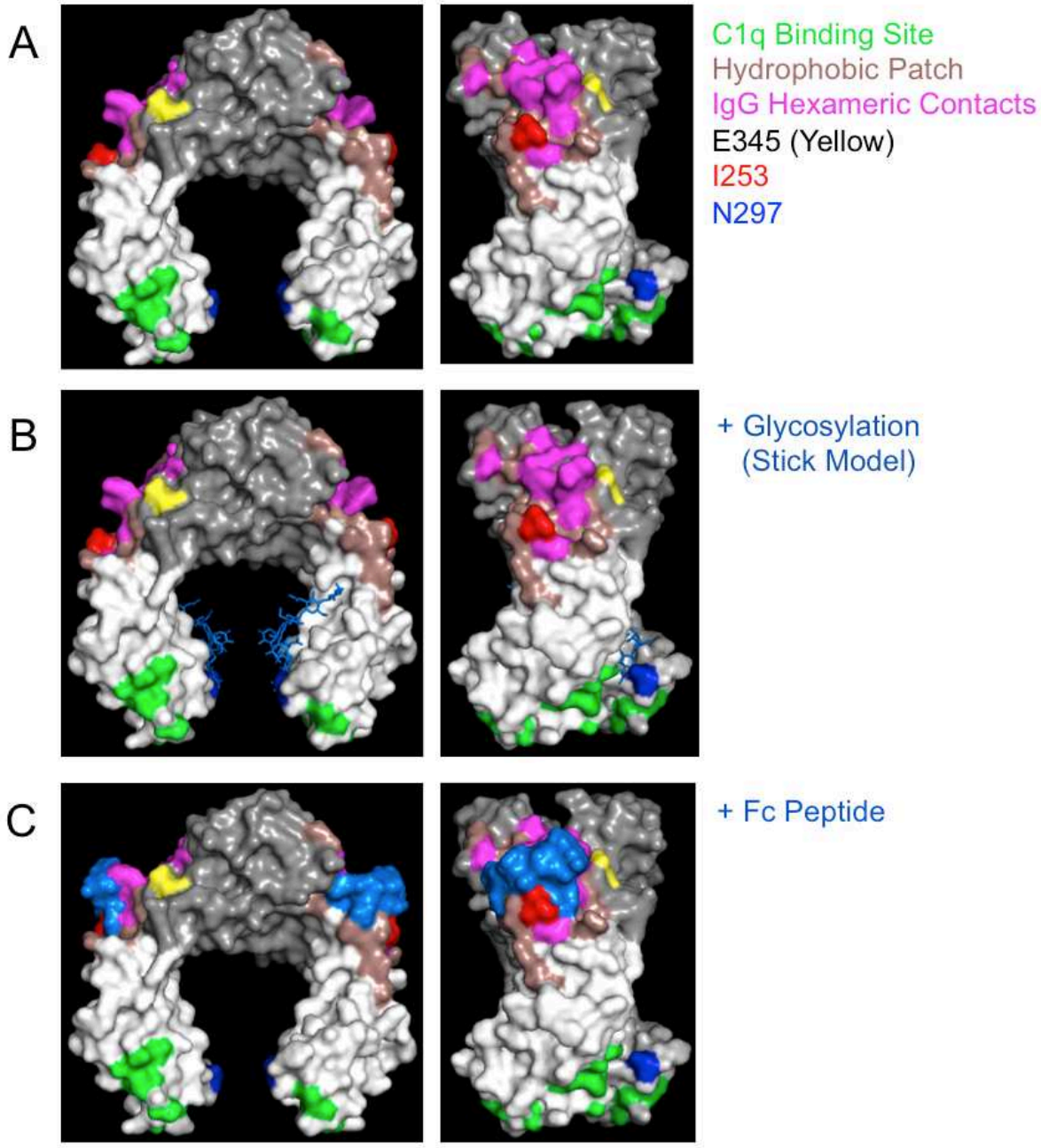

Figure 5.1: IgG schematics inspire novel hypothesis generation
(A-C): Front (left) and side (right) surface depictions of the IgG Fc domain crystal structure (PBD: 1DN2). A: The C1q binding site (green), Fc domain hydrophobic patch (light brown) and amino acid contacts in IgG hexamers (maroon) are colored respectively, as are amino acids N297 (glycosylation site, blue), and E345 (yellow) and I253 (red) which were mutagenized to respectively promote or limit Fc-Fc interactions. B: Attached sugar moieties are depicted as amino acid backbone structures in light blue. C: The Fc peptide (light blue) is shown when bound to IgG. The figure was generated using MacPyMol software.

REFERENCES

1. Devic E: Myélite aiguë dorso-lombaire avec névrite optique. - Autopsie. Congrès rançais de médecine (Premiere Session; Lyon, 1894; procès-verbaux, mémoires et discussions; publiés par M. le Dr L. Bard). 1895, Paris: Lyon: Asselin et Houzeau, Louis Savy, 434-439.

2. Wildemann, B., S. Jarius, and F. Paul, *[Neuromyelitis optica]*. Nervenarzt, 2013. **84**(4): p. 436-41.

3. Gault F: De la neuromyélite optique aiguë. 1894, Thése: Faculté de Médecine et de Pharmacie

4. Jarius, S. and B. Wildemann, *On the contribution of Thomas Clifford Allbutt, F.R.S., to the early history of neuromyelitis optica.* J Neurol, 2013. **260**(1): p. 100-4.

5. Jarius, S. and B. Wildemann, *'Spinal amaurosis' (1841). On the early contribution of Edward Hocken to the concept of neuromyelitis optica.* J Neurol, 2014. **261**(2): p. 400-4.

6. Jarius, S. and B. Wildemann, *Devic's disease before Devic: Bilateral optic neuritis and simultaneous myelitis in a young woman (1874).* J Neurol Sci, 2015. **358**(1-2): p. 419-21.

7. Acchiote, *Sur un cas de neuromyélite subaiguë ou maladie de Devic. Bulletin officiels de la Société de neurologie de Paris.* 1907.

8. Abercrombie J: Pathological and Practical Researches on Diseases of the Brain and Spinal Cord. 1829, Edinburgh: Waugh and Innes, 2

9. Sakuta, M., *[One hundred books which built up neurology (29)-John Abercrombie "Pathological and practical researches on diseases of the brain and spinal cord" (1828)]*. Brain Nerve, 2009. **61**(5): p. 618-9.

10. Jarius, S. and B. Wildemann, *The case of the Marquis de Causan (1804): an early account of visual loss associated with spinal cord inflammation.* J Neurol, 2012. **259**(7): p. 1354-7.

11. Cree, B, et al. Neuromyelitis optica, 2003. Semin Neurol 22:2 105-22

12. WR, B., *Critical review: disseminated sclerosis.* 1930.

13. O'Riordan, J.I., et al., *Clinical, CSF, and MRI findings in Devic's neuromyelitis optica.* J Neurol Neurosurg Psychiatry, 1996. **60**(4): p. 382-7.

14. Stansbury FC. Neuromyelitis optica (Devic's disease): presentation of five cases with pathologic study, and review of literature. Arch Ophthmol 1949;42:292-335, 465-501

15. Scott GI. Neuromyelitis optica. Am J Ophthalmol 1952;35:755-764

16. Peters G. Neuromyelitis optica. In: Lubarsche O, Henke F, Rossle R, eds. Handbuch der speziellen pathologischen Anatomie und Histologie, Bd XIII. IIA: Erkrankungen des zentralen Nerven Systems. Berlin: Springer 1958: 630-644

17. Wingerchuk, D.M., et al., *The clinical course of neuromyelitis optica (Devic's syndrome).* Neurology, 1999. **53**(5): p. 1107-14.

18. Lennon, V.A., et al., *A serum autoantibody marker of neuromyelitis optica: distinction from multiple sclerosis.* Lancet, 2004. **364**(9451): p. 2106-12.

19. Lennon, V.A., et al., *IgG marker of optic-spinal multiple sclerosis binds to the aquaporin-4 water channel.*, in *J. Exp. Med.* 2005. p. 473-477.

20. Wingerchuk, D.M., et al., *Revised diagnostic criteria for neuromyelitis optica.* Neurology, 2006. **66**(10): p. 1485-9.

21. Matà, S. and F. Lolli, *Neuromyelitis optica: an update.*, in *J. Neurol. Sci.* 2011. p. 13-21.

22. Kim, H.J., et al., *MRI characteristics of neuromyelitis optica spectrum disorder: an international update.* Neurology, 2015. **84**(11): p. 1165-73.

23. Misu, T., et al., *Intractable hiccup and nausea with periaqueductal lesions in neuromyelitis optica.* Neurology, 2005. **65**(9): p. 1479-82.

24. Takahashi, T., et al., *Intractable hiccup and nausea in neuromyelitis optica with anti-aquaporin-4 antibody: a herald of acute exacerbations.* J Neurol Neurosurg Psychiatry, 2008. **79**(9): p. 1075-8.

25. Apiwattanakul, M., et al., *Intractable vomiting as the initial presentation of neuromyelitis optica.* Ann Neurol, 2010. **68**(5): p. 757-61.

26. Pittock, S.J., et al., *Brain abnormalities in neuromyelitis optica.* Arch Neurol, 2006. **63**(3): p. 390-6.

27. Kremer, L., et al., *Brainstem manifestations in neuromyelitis optica: a multicenter study of 258 patients.*, in *Mult. Scler.* 2013.

28. Poppe, A.Y., et al., *Neuromyelitis optica with hypothalamic involvement.*, in *Mult. Scler.* 2005. p. 617-621.

29. Vernant, J.C., et al., *Recurrent optic neuromyelitis with endocrinopathies: a new syndrome.* Neurology, 1997. **48**(1): p. 58-64.

30. Kim, W., et al., *Brain abnormalities as an initial manifestation of neuromyelitis optica spectrum disorder.* Mult Scler, 2011. **17**(9): p. 1107-12.

31. Magana, S.M., et al., *Posterior reversible encephalopathy syndrome in neuromyelitis optica spectrum disorders.* Neurology, 2009. **72**(8): p. 712-7.

32. Tan, C.T., et al., *International consensus diagnostic criteria for neuromyelitis optica spectrum disorders.* Neurology, 2016. **86**(5): p. 491-2.

33. Melamed, E., et al., *Update on biomarkers in neuromyelitis optica.* Neurol Neuroimmunol Neuroinflamm, 2015. **2**(4): p. e134.

34. Jarius, S., et al., *Mechanisms of disease: aquaporin-4 antibodies in neuromyelitis optica.* Nat Clin Pract Neurol, 2008. **4**(4): p. 202-14.

35. Levy, M., et al., *Immunopathogenesis of neuromyelitis optica.* Adv Immunol, 2014. **121**: p. 213-42.

36. Veszeli, N., et al., *A systematic analysis of the complement pathways in patients with neuromyelitis optica indicates alteration but no activation during remission.*, in *Mol. Immunol.* 2014. p. 200-209.

37. Nytrova, P., et al., *Complement activation in patients with neuromyelitis optica.*, in *J. Neuroimmunol.* 2014. p. 185-191.

38. Tüzün, E., et al., *Enhanced complement consumption in neuromyelitis optica and Behçet's disease patients*, in *Journal of neuroimmunology*. 2011. p. 211-215.

39. Bennett, J.L., et al., *B lymphocytes in neuromyelitis optica.*, in *Neurol Neuroimmunol Neuroinflamm*. 2015. p. e104.

40. Matsushita, T., et al., *Characteristic cerebrospinal fluid cytokine/chemokine profiles in neuromyelitis optica, relapsing remitting or primary progressive multiple sclerosis*, in *PLoS ONE*. 2013.

41. Wang, H.H., et al., *Interleukin-17-secreting T cells in neuromyelitis optica and multiple sclerosis during relapse.* J Clin Neurosci, 2011. **18**(10): p. 1313-7.

42. Lucchinetti, C.F., et al., *A role for humoral mechanisms in the pathogenesis of Devic's neuromyelitis optica.* Brain, 2002. **125**(Pt 7): p. 1450-61.

43. Mandler, R.N., et al., *Devic's neuromyelitis optica: a clinicopathological study of 8 patients.* Ann Neurol, 1993. **34**(2): p. 162-8.

44. Parratt, J.D.E. and J.W. Prineas, *Neuromyelitis optica: a demyelinating disease characterized by acute destruction and regeneration of perivascular astrocytes.*, in *Mult. Scler.* 2010. p. 1156-1172.

45. Misu, T., et al., *Loss of aquaporin 4 in lesions of neuromyelitis optica: distinction from multiple sclerosis.*, in *Brain*. 2007. p. 1224-1234.

46. Roemer, S.F., et al., *Pattern-specific loss of aquaporin-4 immunoreactivity distinguishes neuromyelitis optica from multiple sclerosis.*, in *Brain*. 2007. p. 1194-1205.

47. Misu, T., et al., *Presence of six different lesion types suggests diverse mechanisms of tissue injury in neuromyelitis optica.*, in *Acta Neuropathol.* 2013. p. 815-827.

48. Popescu, B.F., et al., *Neuromyelitis optica unique area postrema lesions: nausea, vomiting, and pathogenic implications.* Neurology, 2011. **76**(14): p. 1229-37.

49. Walker-Caulfield, M.E., et al., *NFκB signaling drives pro-granulocytic astroglial responses to neuromyelitis optica patient IgG*, in *J Neuroinflammation*. 2015, BioMed Central. p. 7.

50. Saadoun, S., et al., *Paucity of natural killer and cytotoxic T cells in human neuromyelitis optica lesions.* Neuroreport, 2012. **23**(18): p. 1044-7.

51. Hinson, S.R., et al., *Pathogenic potential of IgG binding to water channel extracellular domain in neuromyelitis optica.*, in *Neurology*. 2007. p. 2221-2231.

52. Hinson, S.R., et al., *Molecular outcomes of neuromyelitis optica (NMO)-IgG binding to aquaporin-4 in astrocytes.*, in *Proc. Natl. Acad. Sci. U.S.A.* 2012. p. 1245-1250.

53. Weinshenker, B.G., et al., *Neuromyelitis optica IgG predicts relapse after longitudinally extensive transverse myelitis.* Ann Neurol, 2006. **59**(3): p. 566-9.

54. Bizzoco, E., et al., *Prevalence of neuromyelitis optica spectrum disorder and phenotype distribution.*, in *J. Neurol.* 2009. p. 1891-1898.

55. Merle, H., et al., *Natural history of the visual impairment of relapsing neuromyelitis optica.* Ophthalmology, 2007. **114**(4): p. 810-5.

56. Collongues, N., et al., *Neuromyelitis optica in France: a multicenter study of 125 patients.* Neurology, 2010. **74**(9): p. 736-42.

57. Jiao, Y., et al., *Updated estimate of AQP4-IgG serostatus and disability outcome in neuromyelitis optica.*, in *Neurology*. 2013. p. 1197-1204.

58. Wingerchuk, D.M., et al., *The spectrum of neuromyelitis optica.* Lancet Neurol, 2007. **6**(9): p. 805-15.

59. Kuroiwa, Y., et al., *Nationwide survey of multiple sclerosis in Japan. Clinical analysis of 1,084 cases.* Neurology, 1975. **25**(9): p. 845-51.

60. Asgari, N., et al., *A population-based study of neuromyelitis optica in Caucasians.* Neurology, 2011. **76**(18): p. 1589-95.

61. Rivera, J.F., et al., *Characteristics of Devic's disease (neuromyelitis optica) in Mexico.* J Neurol, 2008. **255**(5): p. 710-5.

62. Cabre, P., et al., *MS and neuromyelitis optica in Martinique (French West Indies).* Neurology, 2001. **56**(4): p. 507-14.

63. Mealy, M.A., et al., *Epidemiology of neuromyelitis optica in the United States: a multicenter analysis.* Arch Neurol, 2012. **69**(9): p. 1176-80.

64. Wingerchuk, D.M., et al., *The spectrum of neuromyelitis optica.*, in *Lancet Neurol*. 2007. p. 805-815.

65. Wingerchuk, D.M., et al., *International consensus diagnostic criteria for neuromyelitis optica spectrum disorders.*, in *Neurology*. 2015.

66. Collongues, N., et al., *Long-term follow-up of neuromyelitis optica with a pediatric onset.*, in *Neurology*. 2010. p. 1084-1088.

67. Banwell, B., et al., *Neuromyelitis optica-IgG in childhood inflammatory demyelinating CNS disorders.*, in *Neurology*. 2008. p. 344-352.

68. McKeon, A., et al., *CNS aquaporin-4 autoimmunity in children.* Neurology, 2008. **71**(2): p. 93-100.

69. Wingerchuk, D.M. and B.G. Weinshenker, *The emerging relationship between neuromyelitis optica and systemic rheumatologic autoimmune disease.* Mult Scler, 2012. **18**(1): p. 5-10.

70. Pittock, S.J., et al., *Neuromyelitis optica and non organ-specific autoimmunity.* Arch Neurol, 2008. **65**(1): p. 78-83.

71. Iyer, A., et al., *A review of the current literature and a guide to the early diagnosis of autoimmune disorders associated with neuromyelitis optica.* Autoimmunity, 2014. **47**(3): p. 154-61.

72. Chuquilin, M., N. Mullaguri, and B. Weinshenker, *Pediatric familial neuromyelitis optica in two sisters with long term follow-up.* J Clin Neurosci, 2016.

73. Yoshimine, S., et al., *Anti-aquaporin-4 antibody-positive familial neuromyelitis optica in mother and daughter.* Jpn J Ophthalmol, 2011. **55**(6): p. 647-50.

74. Matiello, M., et al., *Familial neuromyelitis optica.* Neurology, 2010. **75**(4): p. 310-5.

75. Braley, T. and D.D. Mikol, *Neuromyelitis optica in a mother and daughter.* Arch Neurol, 2007. **64**(8): p. 1189-92.

76. Yamakawa, K., et al., *Familial neuromyelitis optica (Devic's syndrome) with late onset in Japan.* Neurology, 2000. **55**(2): p. 318-20.

77. McALPINE, D., *FAMILIAL NEUROMYELITIS OPTICA: ITS OCCURRENCE IN IDENTICAL TWINS.* Brain, 1938. **61**(4): p. 430-448.

78. Rose N, Schur P, Romain P. Overview of autoimmunity. UpToDate (05/22/2015)

79. Haase, C.G. and S. Schmidt, *Detection of brain-specific autoantibodies to myelin oligodendrocyte glycoprotein, S100beta and myelin basic protein in patients with Devic's neuromyelitis optica.* Neurosci Lett, 2001. **307**(2): p. 131-3.

80. Yamasaki, K., et al., *HLA-DPB1*0501-associated opticospinal multiple sclerosis: clinical, neuroimaging and immunogenetic studies.* Brain, 1999. **122 (Pt 9)**: p. 1689-96.

81. Matsushita, T., et al., *Association of the HLA-DPB1*0501 allele with anti-aquaporin-4 antibody positivity in Japanese patients with idiopathic central nervous system demyelinating disorders.* Tissue Antigens, 2009. **73**(2): p. 171-6.

82. Brum, D.G., et al., *HLA-DRB association in neuromyelitis optica is different from that observed in multiple sclerosis.* Mult Scler, 2010. **16**(1): p. 21-9.

83. Deschamps, R., et al., *Different HLA class II (DRB1 and DQB1) alleles determine either susceptibility or resistance to NMO and multiple sclerosis among the French Afro-Caribbean population.* Mult Scler, 2011. **17**(1): p. 24-31.

84. Zephir, H., et al., *Is neuromyelitis optica associated with human leukocyte antigen?* Mult Scler, 2009. **15**(5): p. 571-9.

85. Kowarik, M.C., J. Soltys, and J.L. Bennett, *The treatment of neuromyelitis optica.*, in *J Neuroophthalmol*. 2014. p. 70-82.

86. Papadopoulos, M.C., J.L. Bennett, and A.S. Verkman, *Treatment of neuromyelitis optica: state-of-the-art and emerging therapies.*, in *Nat Rev Neurol*. 2014.

87. Harris, C.L., et al., *The complotype: dictating risk for inflammation and infection.* Trends Immunol, 2012. **33**(10): p. 513-21.

88. Heurich, M., et al., *Common polymorphisms in C3, factor B, and factor H collaborate to determine systemic complement activity and disease risk.* Proc Natl Acad Sci U S A, 2011. **108**(21): p. 8761-6.

89. Matiello M, Schaefer-Klein J, Hebrink D, Kingsbury D, Lennon V, Weinshenker B. Genetic analysis of neuromyelitis optica: two different Arg19 mutations in the N-terminus of aquaporin-4 suggest a molecular mechanism for susceptibility to NMO. Mult Scler. 2009b;15:S69.

90. Matiello M, Kim HJ, Kim W, Brum DG, Barreira AA, Kingsbury DJ, et al. Familial neuromyelitis optica. Neurology. 2010;75:310–315.

91. Crane, J.M., et al., *Orthogonal array formation by human aquaporin-4: examination of neuromyelitis optica-associated aquaporin-4 polymorphisms.* J Neuroimmunol, 2011. **236**(1-2): p. 93-8.

92. Opdal, S.H., et al., *Aquaporin-4 gene variation and sudden infant death syndrome.* Pediatr Res, 2010. **68**(1): p. 48-51.

93. Rubino, E., et al., *Investigating the genetic role of aquaporin4 gene in migraine.* J Headache Pain, 2009. **10**(2): p. 111-4.

94. Heuser, K., et al., *Variants of the genes encoding AQP4 and Kir4.1 are associated with subgroups of patients with temporal lobe epilepsy.* Epilepsy Res, 2010. **88**(1): p. 55-64.

95. Kleffner, I., et al., *The role of aquaporin-4 polymorphisms in the development of brain edema after middle cerebral artery occlusion.* Stroke, 2008. **39**(4): p. 1333-5.

96. Sorani, M.D., et al., *Novel variants in human Aquaporin-4 reduce cellular water permeability.* Hum Mol Genet, 2008. **17**(15): p. 2379-89.

97. Varrin-Doyer, M., et al., *Aquaporin 4-specific T cells in neuromyelitis optica exhibit a Th17 bias and recognize Clostridium ABC transporter.* Ann Neurol, 2012. **72**(1): p. 53-64.

98. Lindstrom, M., et al., *Novel insights into the epidemiology of Clostridium perfringens type A food poisoning.* Food Microbiol, 2011. **28**(2): p. 192-8.

99. Jeffery, A.R. and J.R. Buncic, *Pediatric Devic's neuromyelitis optica.* J Pediatr Ophthalmol Strabismus, 1996. **33**(5): p. 223-9.

100. Graves, J., et al., *Protective environmental factors for neuromyelitis optica.* Neurology, 2014. **83**(21): p. 1923-9.

101. Yoshimura, S., et al., *Distinct genetic and infectious profiles in Japanese neuromyelitis optica patients according to anti-aquaporin 4 antibody status.* J Neurol Neurosurg Psychiatry, 2013. **84**(1): p. 29-34.

102. Levy, M. and M.A. Mealy, *Purified human C1-esterase inhibitor is safe in acute relapses of neuromyelitis optica.*, in *Neurol Neuroimmunol Neuroinflamm*. 2014. p. e5.

103. Pittock, S.J., et al., *Eculizumab in AQP4-IgG-positive relapsing neuromyelitis optica spectrum disorders: an open-label pilot study.*, in *Lancet Neurol*. 2013. p. 554-562.

104. Hasegawa, H., et al., *Molecular cloning of a mercurial-insensitive water channel expressed in selected water-transporting tissues.* J Biol Chem, 1994. **269**(8): p. 5497-500.

105. Frigeri, A., et al., *Localization of MIWC and GLIP water channel homologs in neuromuscular, epithelial and glandular tissues.* J Cell Sci, 1995. **108 (Pt 9)**: p. 2993-3002.

106. Frigeri, A., et al., *Immunolocalization of the mercurial-insensitive water channel and glycerol intrinsic protein in epithelial cell plasma membranes.* Proc Natl Acad Sci U S A, 1995. **92**(10): p. 4328-31.

107. Ho, J.D., et al., *Crystal structure of human aquaporin 4 at 1.8 Å and its mechanism of conductance*, in *Proceedings of the ….* 2009.

108. Furman, C.S., et al., *Aquaporin-4 square array assembly: opposing actions of M1 and M23 isoforms.*, in *Proc. Natl. Acad. Sci. U.S.A.* 2003. p. 13609-13614.

109. Neely, J.D., et al., *Syntrophin-dependent expression and localization of Aquaporin-4 water channel protein.* Proc Natl Acad Sci U S A, 2001. **98**(24): p. 14108-13.

110. Verkman, A.S., et al., *Aquaporin-4: orthogonal array assembly, CNS functions, and role in neuromyelitis optica.* Acta Pharmacol Sin, 2011. **32**(6): p. 702-10.

111. Neely, J.D., et al., *Heterotetrameric composition of aquaporin-4 water channels.* Biochemistry, 1999. **38**(34): p. 11156-63.

112. Crane, J.M., J.L. Bennett, and A.S. Verkman, *Live cell analysis of aquaporin-4 m1/m23 interactions and regulated orthogonal array assembly in glial cells*, in *J. Biol. Chem.* 2009. p. 35850-35860.

113. Jung, J.S., et al., *Molecular characterization of an aquaporin cDNA from brain: candidate osmoreceptor and regulator of water balance.* Proc Natl Acad Sci U S A, 1994. **91**(26): p. 13052-6.

114. Lu, M., et al., *The human AQP4 gene: definition of the locus encoding two water channel polypeptides in brain.* Proc Natl Acad Sci U S A, 1996. **93**(20): p. 10908-12.

115. Yang, B., T. Ma, and A.S. Verkman, *cDNA cloning, gene organization, and chromosomal localization of a human mercurial insensitive water channel. Evidence for distinct transcriptional units.* J Biol Chem, 1995. **270**(39): p. 22907-13.

116. Rossi, A., J.M. Crane, and A.S. Verkman, *Aquaporin-4 Mz isoform: brain expression, supramolecular assembly and neuromyelitis optica antibody binding*, in *Glia*. 2011. p. 1056-1063.

117. Furman, C.S., et al., *Aquaporin-4 square array assembly: opposing actions of M1 and M23 isoforms.* Proc Natl Acad Sci U S A, 2003. **100**(23): p. 13609-14.

118. Papadopoulos, M.C. and A.S. Verkman, *Aquaporin water channels in the nervous system*, in *Nat. Rev. Neurosci.* 2013. p. 265-277.

119. Crane, J.M., et al., *Aquaporin-4 dynamics in orthogonal arrays in live cells visualized by quantum dot single particle tracking.* Mol Biol Cell, 2008. **19**(8): p. 3369-78.

120. Crane, J.M., M. Tajima, and A.S. Verkman, *Live-cell imaging of aquaporin-4 diffusion and interactions in orthogonal arrays of particles.* Neuroscience, 2010. **168**(4): p. 892-902.

121. Verkman, A.S., A. Rossi, and J.M. Crane, *Live-cell imaging of aquaporin-4 supramolecular assembly and diffusion*, in *Meth Enzymol*. 2012. p. 341-354.

122. Rossi, A., et al., *Super-resolution imaging of aquaporin-4 orthogonal arrays of particles in cell membranes*, in *J Cell Sci*. 2012. p. 4405-4412.

123. Papadopoulos, M.C. and A.S. Verkman, *Aquaporin water channels in the nervous system.* Nat Rev Neurosci, 2013. **14**(4): p. 265-77.

124. Verkman, A.S., et al., *Aquaporin-4: orthogonal array assembly, CNS functions, and role in neuromyelitis optica*, in *Acta Pharmacol Sin*. 2011. p. 702-710.

125. Matiello, M., et al., *Aquaporin 4 expression and tissue susceptibility to neuromyelitis optica.*, in *JAMA Neurol*. 2013. p. 1118-1125.

126. Fenton, R.A., et al., *Differential water permeability and regulation of three aquaporin 4 isoforms.* Cell Mol Life Sci, 2010. **67**(5): p. 829-40.

127. Hiroaki, Y., et al., *Implications of the aquaporin-4 structure on array formation and cell adhesion.* J Mol Biol, 2006. **355**(4): p. 628-39.

128. Rossi, A., et al., *Neuromyelitis optica IgG does not alter aquaporin-4 water permeability, plasma membrane M1/M23 isoform content, or supramolecular assembly.* Glia, 2012. **60**(12): p. 2027-39.

129. Zhang, H. and A.S. Verkman, *Evidence against involvement of aquaporin-4 in cell-cell adhesion.* J Mol Biol, 2008. **382**(5): p. 1136-43.

130. Ma, T., et al., *Generation and phenotype of a transgenic knockout mouse lacking the mercurial-insensitive water channel aquaporin-4.* J Clin Invest, 1997. **100**(5): p. 957-62.

131. Manley, G.T., et al., *Aquaporin-4 deletion in mice reduces brain edema after acute water intoxication and ischemic stroke.* Nat Med, 2000. **6**(2): p. 159-63.

132. Papadopoulos, M.C., et al., *Aquaporin-4 facilitates reabsorption of excess fluid in vasogenic brain edema.* Faseb j, 2004. **18**(11): p. 1291-3.

133. Saadoun, S., et al., *AQP4 gene deletion in mice does not alter blood-brain barrier integrity or brain morphology.* Neuroscience, 2009. **161**(3): p. 764-72.

134. Li, J., R.V. Patil, and A.S. Verkman, *Mildly abnormal retinal function in transgenic mice without Muller cell aquaporin-4 water channels.* Invest Ophthalmol Vis Sci, 2002. **43**(2): p. 573-9.

135. Li, J. and A.S. Verkman, *Impaired hearing in mice lacking aquaporin-4 water channels.* J Biol Chem, 2001. **276**(33): p. 31233-7.

136. Lu, D.C., et al., *Impaired olfaction in mice lacking aquaporin-4 water channels.* Faseb j, 2008. **22**(9): p. 3216-23.

137. Bloch, O., et al., *Accelerated progression of kaolin-induced hydrocephalus in aquaporin-4-deficient mice.* J Cereb Blood Flow Metab, 2006. **26**(12): p. 1527-37.

138. Saadoun, S., et al., *Greatly improved neurological outcome after spinal cord compression injury in AQP4-deficient mice.* Brain, 2008. **131**(Pt 4): p. 1087-98.

139. Binder, D.K., et al., *Increased seizure threshold in mice lacking aquaporin-4 water channels.* Neuroreport, 2004. **15**(2): p. 259-62.

140. Li, L., et al., *Proinflammatory role of aquaporin-4 in autoimmune neuroinflammation.* Faseb j, 2011. **25**(5): p. 1556-66.

141. Saadoun, S., et al., *Involvement of aquaporin-4 in astroglial cell migration and glial scar formation.* J Cell Sci, 2005. **118**(Pt 24): p. 5691-8.

142. Nesargikar, P.N., B. Spiller, and R. Chavez, *The complement system: history, pathways, cascade and inhibitors.* Eur J Microbiol Immunol (Bp), 2012. **2**(2): p. 103-11.

143. Buchner H: Zur nomenklatur der schutzenden Eiweisskorper. Centr Bakteriol Parasitenk 10, 699-701 (1891)

144. Ehrlich P et al: Zur Theorie der Lysenwirkung. Berlin Klin Woch 36, 6 (1899)

145. Morgan BP: Complement: Clinical Aspects and Relevance to Disease. Academic Press, UK (1990)

146. Kaufmann SH: Immunology's foundation: the 100-year anniversary of the Nobel Prize to Paul Ehrlich and Elie Metchnikoff. Nat Immunol 9, 705-712 (2008)

147. Holers, V.M., *Complement and its receptors: new insights into human disease.*, in *Annu. Rev. Immunol.* 2014. p. 433-459.

148. Nonaka, M. and A. Kimura, *Genomic view of the evolution of the complement system.* Immunogenetics, 2006. **58**(9): p. 701-13.

149. Andrades, J.A., et al., *Complement proteins are present in developing endochondral bone and may mediate cartilage cell death and vascularization.* Exp Cell Res, 1996. **227**(2): p. 208-13.

150. Bora, P.S., et al., *Role of complement and complement membrane attack complex in laser-induced choroidal neovascularization.* J Immunol, 2005. **174**(1): p. 491-7.

151. Ratajczak, M.Z., et al., *Transplantation studies in C3-deficient animals reveal a novel role of the third complement component (C3) in engraftment of bone marrow cells.* Leukemia, 2004. **18**(9): p. 1482-90.

152. Markiewski, M.M., et al., *The regulation of liver cell survival by complement.* J Immunol, 2009. **182**(9): p. 5412-8.

153. Kimura, Y., et al., *Expression of complement 3 and complement 5 in newt limb and lens regeneration.* J Immunol, 2003. **170**(5): p. 2331-9.

154. Botto, M., *Links between complement deficiency and apoptosis.* Arthritis Res, 2001. **3**(4): p. 207-10.

155. Holers, V.M., *Complement receptors and the shaping of the natural antibody repertoire.* Springer Semin Immunopathol, 2005. **26**(4): p. 405-23.

156. Janeway CA Jr, Travers P, Walport M, et al. Immunobiology: The Immune System in Health and Disease. 5th edition. New York: Garland Science; 2001. The complement system and innate immunity.

157. Zipfel, P.F. and C. Skerka, *Complement regulators and inhibitory proteins*, in *Nat Rev Immunol*. 2009. p. 729-740.

158. Thurman, J.M. and V.M. Holers, *The central role of the alternative complement pathway in human disease.*, in *J. Immunol.* 2006. p. 1305-1310.

159. Merle, N.S., S.E. Church, and V. Fremeaux-Bacchi, *Complement system part I– molecular mechanisms of activation and regulation*, in *Front ….* 2015.

160. Gaboriaud, C., et al., *Structure and activation of the C1 complex of complement: unraveling the puzzle.*, in *Trends Immunol.* 2004. p. 368-373.

161. Wallis, R., et al., *Paths reunited: Initiation of the classical and lectin pathways of complement activation.*, in *Immunobiology*. 2010. p. 1-11.

162. Gregory L Moore, H.C.S.K. and G.A. Lazar, *Engineered Fc variant antibodies with enhanced ability to recruit complement and mediate effector functions*, in *mAbs*. 2010, Landes Bioscience. p. 181-189.

163. Diebolder, C.A., et al., *Complement is activated by IgG hexamers assembled at the cell surface.*, in *Science*. 2014. p. 1260-1263.

164. Thommesen, J.E., et al., *Lysine 322 in the human IgG3 C(H)2 domain is crucial for antibody dependent complement activation.*, in *Mol. Immunol.* 2000. p. 995-1004.

165. Duncan, A.R. and G. Winter, *The binding site for C1q on IgG.* Nature, 1988. **332**(6166): p. 738-40.

166. Morgan, A., et al., *The N-terminal end of the CH2 domain of chimeric human IgG1 anti-HLA-DR is necessary for C1q, Fc gamma RI and Fc gamma RIII binding.* Immunology, 1995. **86**(2): p. 319-24.

167. Tao, M.H., R.I. Smith, and S.L. Morrison, *Structural features of human immunoglobulin G that determine isotype-specific differences in complement activation.* J Exp Med, 1993. **178**(2): p. 661-7.

168. Idusogie, E.E., et al., *Engineered antibodies with increased activity to recruit complement.*, in *J. Immunol.* 2001. p. 2571-2575.

169. Idusogie, E.E., et al., *Mapping of the C1q binding site on rituxan, a chimeric antibody with a human IgG1 Fc.* J Immunol, 2000. **164**(8): p. 4178-84.

170. Schneider, S. and M. Zacharias, *Atomic resolution model of the antibody Fc interaction with the complement C1q component*, in *Molecular Immunology*. 2012.

171. Saphire, E.O., et al., *Crystal structure of a neutralizing human IGG against HIV-1: a template for vaccine design.*, in *Science*. 2001. p. 1155-1159.

172. Schroeder, H.W. and L. Cavacini, *Structure and function of immunoglobulins*, in *J Allergy Clin Immunol*. 2010. p. S41-52.

173. Borsos, T. and H.J. Rapp, *Complement fixation on cell surfaces by 19S and 7S antibodies.* Science, 1965. **150**(3695): p. 505-6.

174. Rosse, W.F., H.J. Rapp, and T. Borsos, *Structural characteristics of hemolytic antibodies as determined by the effects of ionizing radiation.* J Immunol, 1967. **98**(6): p. 1190-5.

175. Manderson, A.P., et al., *Continual low-level activation of the classical complement pathway.* J Exp Med, 2001. **194**(6): p. 747-56.

176. Hughes-Jones, N.C. and B. Gardner, *Reaction between the isolated globular sub-units of the complement component C1q and IgG-complexes.*, in *Mol. Immunol.* 1979. p. 697-701.

177. Feinstein, A., N. Richardson, and M.I. Taussig, *Immunoglobulin flexibility in complement activation.*, in *Immunol. Today*. 1986. p. 169-174.

178. Teeling, J.L., et al., *Characterization of new human CD20 monoclonal antibodies with potent cytolytic activity against non-Hodgkin lymphomas.* Blood, 2004. **104**(6): p. 1793-800.

179. de Weers, M., et al., *Daratumumab, a novel therapeutic human CD38 monoclonal antibody, induces killing of multiple myeloma and other hematological tumors.* J Immunol, 2011. **186**(3): p. 1840-8.

180. Cragg, M.S., et al., *Complement-mediated lysis by anti-CD20 mAb correlates with segregation into lipid rafts.* Blood, 2003. **101**(3): p. 1045-52.

181. Parce, J.W., D. Kelley, and K. Heinzelmann, *Measurement of antibody-dependent binding, proteolysis, and turnover of C1s on liposomal antigens localizes the fluidity-dependent step in C1 activation.* Biochim Biophys Acta, 1983. **736**(1): p. 92-8.

182. Hughes-Jones, N.C., et al., *Antibody density on rat red cells determines the rate of activation of the complement component C1.* Eur J Immunol, 1985. **15**(10): p. 976-80.

183. Teeling, J.L., et al., *The biological activity of human CD20 monoclonal antibodies is linked to unique epitopes on CD20.* J Immunol, 2006. **177**(1): p. 362-71.

184. Xia, M.Q., G. Hale, and H. Waldmann, *Efficient complement-mediated lysis of cells containing the CAMPATH-1 (CDw52) antigen.* Mol Immunol, 1993. **30**(12): p. 1089-96.

185. Pawluczkowycz, A.W., et al., *Binding of submaximal C1q promotes complement-dependent cytotoxicity (CDC) of B cells opsonized with anti-CD20 mAbs ofatumumab (OFA) or rituximab (RTX): considerably higher levels of CDC are induced by OFA than by RTX.* J Immunol, 2009. **183**(1): p. 749-58.

186. Dechant, M., et al., *Complement-dependent tumor cell lysis triggered by combinations of epidermal growth factor receptor antibodies.* Cancer Res, 2008. **68**(13): p. 4998-5003.

187. Kushihata, F., et al., *Human leukocyte antigen antibodies and human complement activation: role of IgG subclass, specificity, and cytotoxic potential.* Transplantation, 2004. **78**(7): p. 995-1001.

188. Saphire, E.O., et al., *Crystallization and preliminary structure determination of an intact human immunoglobulin, b12: an antibody that broadly neutralizes primary isolates of HIV-1.* Acta Crystallogr D Biol Crystallogr, 2001. **57**(Pt 1): p. 168-71.

189. Reidler, J., Uzgiris, E. E. and Kornberg, R. D. (1986) in *Handbook of Experimental Immunology* 4th Edn (Weir, DM ed.), C 17 Blackwell.

190. Pinteric, L., R.H. Painter, and G.E. Connell, *Ultrastructure of the Fc fragment of human immunoglobulin G.*, in *Immunochemistry*. 1971. p. 1041-1045.

191. Burton, D.R., *Is IgM-like dislocation a common feature of antibody function?* Immunol Today, 1986. **7**(6): p. 165-7.

192. Gaboriaud, C., et al., *Deciphering the fine details of c1 assembly and activation mechanisms: "mission impossible"?*, in *Front Immunol*. 2014. p. 565.

193. de Jong, R.N., et al., *A Novel Platform for the Potentiation of Therapeutic Antibodies Based on Antigen-Dependent Formation of IgG Hexamers at the Cell Surface.* PLoS Biol, 2016. **14**(1): p. e1002344.

194. Gaboriaud, C., et al., *The Crystal Structure of the Globular Head of Complement Protein C1q Provides a Basis for Its Versatile Recognition Properties*, in *Journal of Biological Chemistry*. 2003. p. 46974-46982.

195. Nilsson, B. and K. Nilsson Ekdahl, *The tick-over theory revisited: is C3 a contact-activated protein?* Immunobiology, 2012. **217**(11): p. 1106-10.

196. Ehrnthaller, C., et al., *New insights of an old defense system: structure, function, and clinical relevance of the complement system.* Mol Med, 2011. **17**(3-4): p. 317-29.

197. Kawasaki, T., R. Etoh, and I. Yamashina, *Isolation and characterization of a mannan-binding protein from rabbit liver.* Biochem Biophys Res Commun, 1978. **81**(3): p. 1018-24.

198. Matsushita, M. and T. Fujita, *Ficolins and the lectin complement pathway.* Immunol Rev, 2001. **180**: p. 78-85.

199. Hansen, S., et al., *Collectin 11 (CL-11, CL-K1) is a MASP-1/3-associated plasma collectin with microbial-binding activity.* J Immunol, 2010. **185**(10): p. 6096-104.

200. Gadjeva, M., K. Takahashi, and S. Thiel, *Mannan-binding lectin--a soluble pattern recognition molecule.* Mol Immunol, 2004. **41**(2-3): p. 113-21.

201. Malhotra, R., et al., *Glycosylation changes of IgG associated with rheumatoid arthritis can activate complement via the mannose-binding protein.* Nat Med, 1995. **1**(3): p. 237-43.

202. Veerhuis, R., H.M. Nielsen, and A.J. Tenner, *Complement in the brain*, in *Mol. Immunol.* 2011. p. 1592-1603.

203. Beek, J., K. Elward, and P. Gasque, *Activation of complement in the central nervous system*, in *... of the New York Academy of ...*. 2003.

204. Orsini, F., et al., *Versatility of the complement system in neuroinflammation, neurodegeneration and brain homeostasis.* Front Cell Neurosci, 2014. **8**: p. 380.

205. Rutkowski, M.J., et al., *Complement and the central nervous system: emerging roles in development, protection and regeneration.* Immunol Cell Biol, 2010. **88**(8): p. 781-6.

206. Eiberger, B. and K. Schilling, *Cerebellins: capstones to bridge the synaptic cleft.* J Neurochem, 2012. **121**(5): p. 697-9.

207. Yuzaki, M., *Cbln and C1q family proteins: new transneuronal cytokines.* Cell Mol Life Sci, 2008. **65**(11): p. 1698-705.

208. Gendrel, M., et al., *A secreted complement-control-related protein ensures acetylcholine receptor clustering.* Nature, 2009. **461**(7266): p. 992-6.

209. Rogers, C.A., et al., *Expression and function of membrane regulators of complement on rat astrocytes in culture*, in .... 1996.

210. Stevens, B., et al., *The classical complement cascade mediates CNS synapse elimination*, in *Cell*. 2007. p. 1164-1178.

211. Chu, Y., et al., *Enhanced synaptic connectivity and epilepsy in C1q knockout mice.* Proc Natl Acad Sci U S A, 2010. **107**(17): p. 7975-80.

212. Stephan, A.H., B.A. Barres, and B. Stevens, *The complement system: an unexpected role in synaptic pruning during development and disease.* Annu Rev Neurosci, 2012. **35**: p. 369-89.

213. Bolliger, M.F., D.C. Martinelli, and T.C. Sudhof, *The cell-adhesion G protein-coupled receptor BAI3 is a high-affinity receptor for C1q-like proteins.* Proc Natl Acad Sci U S A, 2011. **108**(6): p. 2534-9.

214. Ressl, S., et al., *Structures of C1q-like proteins reveal unique features among the C1q/TNF superfamily.* Structure, 2015. **23**(4): p. 688-99.

215. Rahpeymai, Y., et al., *Complement: a novel factor in basal and ischemia-induced neurogenesis.* Embo j, 2006. **25**(6): p. 1364-74.

216. Pisalyaput, K. and A.J. Tenner, *Complement component C1q inhibits beta-amyloid- and serum amyloid P-induced neurotoxicity via caspase- and calpain-independent mechanisms.* J Neurochem, 2008. **104**(3): p. 696-707.

217. Benoit, M.E. and A.J. Tenner, *Complement protein C1q-mediated neuroprotection is correlated with regulation of neuronal gene and microRNA expression.* J Neurosci, 2011. **31**(9): p. 3459-69.

218. Heese, K., C. Hock, and U. Otten, *Inflammatory signals induce neurotrophin expression in human microglial cells.* J Neurochem, 1998. **70**(2): p. 699-707.

219. Tegla, C.A., et al., *Neuroprotective effects of the complement terminal pathway during demyelination: implications for oligodendrocyte survival.* J Neuroimmunol, 2009. **213**(1-2): p. 3-11.

220. Yin, W., et al., *Classical pathway complement activation on human endothelial cells.* Mol Immunol, 2007. **44**(9): p. 2228-34.

221. Bossi, F., R. Bulla, and F. Tedesco, *Endothelial cells are a target of both complement and kinin system.* Int Immunopharmacol, 2008. **8**(2): p. 143-7.

222. Lozada, C., et al., *Identification of C1q as the heat-labile serum cofactor required for immune complexes to stimulate endothelial expression of the adhesion molecules E-selectin and intercellular and vascular cell adhesion molecules 1.* Proc Natl Acad Sci U S A, 1995. **92**(18): p. 8378-82.

223. van den Berg, R.H., et al., *The first subcomponent of complement, C1q, triggers the production of IL-8, IL-6, and monocyte chemoattractant peptide-1 by human umbilical vein endothelial cells.* J Immunol, 1998. **161**(12): p. 6924-30.

224. Orsini, F., et al., *Targeting mannose-binding lectin confers long-lasting protection with a surprisingly wide therapeutic window in cerebral ischemia.* Circulation, 2012. **126**(12): p. 1484-94.

225. Longhi, L., et al., *Mannose-binding lectin is expressed after clinical and experimental traumatic brain injury and its deletion is protective.* Crit Care Med, 2014. **42**(8): p. 1910-8.

226. Collard, C.D., et al., *Endothelial oxidative stress activates the lectin complement pathway: role of cytokeratin 1.* Am J Pathol, 2001. **159**(3): p. 1045-54.

227. Jani, P.K., et al., *MASP-1 induces a unique cytokine pattern in endothelial cells: a novel link between complement system and neutrophil granulocytes.* PLoS One, 2014. **9**(1): p. e87104.

228. Monsinjon, T., et al., *Regulation by complement C3a and C5a anaphylatoxins of cytokine production in human umbilical vein endothelial cells.* Faseb j, 2003. **17**(9): p. 1003-14.

229. Van Beek, J., et al., *Expression of receptors for complement anaphylatoxins C3a and C5a following permanent focal cerebral ischemia in the mouse.* Exp Neurol, 2000. **161**(1): p. 373-82.

230. Schraufstatter, I.U., et al., *Complement c3a and c5a induce different signal transduction cascades in endothelial cells.* J Immunol, 2002. **169**(4): p. 2102-10.

231. Lister, K.J., W.G. James, and M.J. Hickey, *Immune complexes mediate rapid alterations in microvascular permeability: roles for neutrophils, complement, and platelets.* Microcirculation, 2007. **14**(7): p. 709-22.

232. Bossi, F., et al., *Cross-talk between the complement and the kinin system in vascular permeability.* Immunol Lett, 2011. **140**(1-2): p. 7-13.

233. Bossi, F., et al., *Platelet-activating factor and kinin-dependent vascular leakage as a novel functional activity of the soluble terminal complement complex.* J Immunol, 2004. **173**(11): p. 6921-7.

234. Tedesco, F., et al., *The cytolytically inactive terminal complement complex activates endothelial cells to express adhesion molecules and tissue factor procoagulant activity.* J Exp Med, 1997. **185**(9): p. 1619-27.

235. Jarius, S. and B. Wildemann, *Aquaporin-4 antibodies (NMO-IgG) as a serological marker of neuromyelitis optica: a critical review of the literature.* Brain Pathol, 2013. **23**(6): p. 661-83.

236. Waters, P.J., et al., *Serologic diagnosis of NMO: a multicenter comparison of aquaporin-4-IgG assays.*, in *Neurology*. 2012. p. 665-71- discussion 669.

237. Waters, P., et al., *Multicentre comparison of a diagnostic assay: aquaporin-4 antibodies in neuromyelitis optica.* J Neurol Neurosurg Psychiatry, 2016.

238. Jarius, S. and B. Wildemann, *Aquaporin-4 antibodies (NMO-IgG) as a serological marker of neuromyelitis optica: a critical review of the literature.*, in *Brain Pathol*. 2013. p. 661-683.

239. Nishiyama, S., et al., *A case of NMO seropositive for aquaporin-4 antibody more than 10 years before onset.* Neurology, 2009. **72**(22): p. 1960-1.

240. Wingerchuk, D.M., et al., *International consensus diagnostic criteria for neuromyelitis optica spectrum disorders.* Neurology, 2015. **85**(2): p. 177-89.

241. Rodriguez, M., *Have we finally identified an autoimmune demyelinating disease?* Ann Neurol, 2009. **66**(5): p. 572-3.

242. Rose, N.R. and C. Bona, *Defining criteria for autoimmune diseases (Witebsky's postulates revisited).* Immunol Today, 1993. **14**(9): p. 426-30.

243. Bona, C.A., *Postulates defining pathogenic autoantibodies and T cells.* Autoimmunity, 1991. **10**(3): p. 169-72.

244. Drachman, D.B., *How to recognize an antibody-mediated autoimmune disease: criteria.* Res Publ Assoc Res Nerv Ment Dis, 1990. **68**: p. 183-6.

245. Witebsky, E., et al., *Chronic thyroiditis and autoimmunization.* J Am Med Assoc, 1957. **164**(13): p. 1439-47.

246. Gomori, E., et al., *Fetal development of membrane water channel proteins aquaporin-1 and aquaporin-4 in the human brain.* Int J Dev Neurosci, 2006. **24**(5): p. 295-305.

247. Saadoun, S., et al., *Neuromyelitis optica IgG causes placental inflammation and fetal death.* J Immunol, 2013. **191**(6): p. 2999-3005.

248. Nour, M.M., et al., *Pregnancy outcomes in aquaporin-4-positive neuromyelitis optica spectrum disorder.* Neurology, 2016. **86**(1): p. 79-87.

249. Fallier-Becker, P., et al., *Onset of aquaporin-4 expression in the developing mouse brain.* Int J Dev Neurosci, 2014. **36**: p. 81-9.

250. Bradl, M., et al., *Neuromyelitis optica: pathogenicity of patient immunoglobulin in vivo.*, in *Ann. Neurol.* 2009. p. 630-643.

251. Bennett, J.L., et al., *Intrathecal pathogenic anti-aquaporin-4 antibodies in early neuromyelitis optica.* Ann Neurol, 2009. **66**(5): p. 617-29.

252. Saadoun, S., et al., *Intra-cerebral injection of neuromyelitis optica immunoglobulin G and human complement produces neuromyelitis optica lesions in mice.* Brain, 2010. **133**(Pt 2): p. 349-61.

253. Ratelade, J., et al., *Neuromyelitis optica IgG and natural killer cells produce NMO lesions in mice without myelin loss*, in *Acta Neuropathol.* 2012. p. 861-872.

254. Ratelade, J., et al., *Involvement of antibody-dependent cell-mediated cytotoxicity in inflammatory demyelination in a mouse model of neuromyelitis optica.*, in *Acta Neuropathol.* 2013. p. 699-709.

255. Asavapanumas, N., et al., *Experimental mouse model of optic neuritis with inflammatory demyelination produced by passive transfer of neuromyelitis optica-immunoglobulin G.* J Neuroinflammation, 2014. **11**: p. 16.

256. Zhang, H. and A.S. Verkman, *Longitudinally extensive NMO spinal cord pathology produced by passive transfer of NMO-IgG in mice lacking complement inhibitor CD59.*, in *J. Autoimmun.* 2014.

257. Asavapanumas, N., J. Ratelade, and A.S. Verkman, *Unique neuromyelitis optica pathology produced in naïve rats by intracerebral administration of NMO-IgG.*, in *Acta Neuropathol.* 2014. p. 539-551.

258. Asavapanumas, N. and A.S. Verkman, *Neuromyelitis optica pathology in rats following intraperitoneal injection of NMO-IgG and intracerebral needle injury.*, in *Acta Neuropathol Commun*. 2014. p. 48.

259. Giraudon, P., *In vivo CNS chronic infusion of AQP4-IgG induces NMO-like lesions and motor behavioral changes in rat via astrocytopathy and glutamate homeostasis disturbance.* Journal of Neuroimmunology. **275**(1): p. 99.

260. Ratelade, J., J.L. Bennett, and A.S. Verkman, *Intravenous neuromyelitis optica autoantibody in mice targets aquaporin-4 in peripheral organs and area postrema*, in *PLoS ONE*. 2011. p. e27412.

261. Rowley, M.J., et al., *Differing epitope selection of experimentally-induced and natural antibodies to a disease-specific autoantigen, the E2 subunit of pyruvate dehydrogenase complex (PDC-E2).* Int Immunol, 1992. **4**(11): p. 1245-53.

262. Kurosawa, K., et al., *Severely exacerbated neuromyelitis optica rat model with extensive astrocytopathy by high affinity anti-aquaporin-4 monoclonal antibody.* Acta Neuropathol Commun, 2015. **3**(1): p. 82.

263. McGonagle, D. and M.F. McDermott, *A proposed classification of the immunological diseases.* PLoS Med, 2006. **3**(8): p. e297.

264. Bonnan, M., et al., *Plasma exchange in severe spinal attacks associated with neuromyelitis optica spectrum disorder.* Mult Scler, 2009. **15**(4): p. 487-92.

265. Takahashi, T., et al., *Anti-aquaporin-4 antibody is involved in the pathogenesis of NMO: a study on antibody titre.* Brain, 2007. **130**(Pt 5): p. 1235-43.

266. Jarius, S., et al., *Antibody to aquaporin-4 in the long-term course of neuromyelitis optica.* Brain, 2008. **131**(Pt 11): p. 3072-80.

267. Bennett, J.L., et al., *Intrathecal pathogenic anti-aquaporin-4 antibodies in early neuromyelitis optica*, in *Ann. Neurol.* 2009. p. 617-629.

268. Zhang, H., J.L. Bennett, and A.S. Verkman, *Ex vivo spinal cord slice model of neuromyelitis optica reveals novel immunopathogenic mechanisms*, in *Ann. Neurol.* 2011. p. 943-954.

269. Levy, M., *Does aquaporin-4-seronegative neuromyelitis optica exist?* JAMA Neurol, 2014. **71**(3): p. 271-2.

270. Kowarik, M.C., et al., *The cerebrospinal fluid immunoglobulin transcriptome and proteome in neuromyelitis optica reveals central nervous system-specific B cell populations.*, in *J Neuroinflammation*. 2015. p. 19.

271. Dujmovic, I., et al., *Temporal dynamics of cerebrospinal fluid anti-aquaporin-4 antibodies in patients with neuromyelitis optica spectrum disorders.* J Neuroimmunol, 2011. **234**(1-2): p. 124-30.

272. Klawiter, E.C., et al., *NMO-IgG detected in CSF in seronegative neuromyelitis optica.* Neurology, 2009. **72**(12): p. 1101-3.

273. Sato, D.K., et al., *Cerebrospinal fluid aquaporin-4 antibody levels in neuromyelitis optica attacks.* Ann Neurol, 2014. **76**(2): p. 305-9.

274. Majed, M., et al., *Clinical utility of testing AQP4-IgG in CSF: Guidance for physicians.* Neurology® Neuroimmunology & Neuroinflammation, 2016. **3**(3): p. e231.

275. Kitley, J., et al., *Myelin-oligodendrocyte glycoprotein antibodies in adults with a neuromyelitis optica phenotype.* Neurology, 2012. **79**(12): p. 1273-7.

276. Kitley, J., et al., *Prognostic factors and disease course in aquaporin-4 antibody-positive patients with neuromyelitis optica spectrum disorder from the United Kingdom and Japan.* Brain, 2012. **135**(Pt 6): p. 1834-49.

277. Sato, D.K., et al., *Distinction between MOG antibody-positive and AQP4 antibody-positive NMO spectrum disorders.*, in *Neurology*. 2014. p. 474-481.

278. Saadoun, S., et al., *Neuromyelitis optica MOG-IgG causes reversible lesions in mouse brain.* Acta Neuropathol Commun, 2014. **2**: p. 35.

279. Kitley, J., et al., *Longitudinally extensive transverse myelitis with and without aquaporin 4 antibodies.* JAMA Neurol, 2013. **70**(11): p. 1375-81.

280. Bruck, W., et al., *Neuromyelitis optica lesions may inform multiple sclerosis heterogeneity debate.* Ann Neurol, 2012. **72**(3): p. 385-94.

281. Lucchinetti, C., et al., *Heterogeneity of multiple sclerosis lesions: implications for the pathogenesis of demyelination.* Ann Neurol, 2000. **47**(6): p. 707-17.

282. Jarius, S., et al., *Antibody to aquaporin-4 in the long-term course of neuromyelitis optica.*, in *Brain*. 2008. p. 3072-3080.

283. Hinson, S.R., et al., *Prediction of neuromyelitis optica attack severity by quantitation of complement-mediated injury to aquaporin-4-expressing cells*, in *Arch. Neurol.* 2009. p. 1164-1167.

284. Pellkofer, H.L., et al., *Long-term follow-up of patients with neuromyelitis optica after repeated therapy with rituximab.* Neurology, 2011. **76**(15): p. 1310-5.

285. Quast, I., et al., *Sialylation of IgG Fc domain impairs complement-dependent cytotoxicity*, in *J. Clin. Invest.* 2015. p. 4160-4170.

286. Nimmerjahn, F., R.M. Anthony, and J.V. Ravetch, *Agalactosylated IgG antibodies depend on cellular Fc receptors for in vivo activity.* Proc Natl Acad Sci U S A, 2007. **104**(20): p. 8433-7.

287. Dashivets, T., et al., *Multi-Angle Effector Function Analysis of Human Monoclonal IgG Glycovariants.* PLoS One, 2015. **10**(12): p. e0143520.

288. Arnold, J.N., et al., *The impact of glycosylation on the biological function and structure of human immunoglobulins.* Annu Rev Immunol, 2007. **25**: p. 21-50.

289. Crane, J.M., et al., *Binding affinity and specificity of neuromyelitis optica autoantibodies to aquaporin-4 m1/m23 isoforms and orthogonal arrays*, in *J. Biol. Chem.* 2011. p. 16516-16524.

290. Glennie, M.J., et al., *Mechanisms of killing by anti-CD20 monoclonal antibodies.* Mol Immunol, 2007. **44**(16): p. 3823-37.

291. Tradtrantip, L., et al., *Enzymatic deglycosylation converts pathogenic neuromyelitis optica anti-aquaporin-4 immunoglobulin G into therapeutic antibody*, in *Ann. Neurol.* 2012.

292. Owens, G.P., et al., *Measles virus-specific plasma cells are prominent in subacute sclerosing panencephalitis CSF.* Neurology, 2007. **68**(21): p. 1815-9.

293. Cepok, S., et al., *Short-lived plasma blasts are the main B cell effector subset during the course of multiple sclerosis.* Brain, 2005. **128**(Pt 7): p. 1667-76.

294. Winges, K.M., et al., *Analysis of multiple sclerosis cerebrospinal fluid reveals a continuum of clonally related antibody-secreting cells that are predominantly plasma blasts*, in *Journal of neuroimmunology*. 2007. p. 226-234.

295. Mader, S., et al., *Patterns of antibody binding to aquaporin-4 isoforms in neuromyelitis optica.*, in *PLoS ONE*. 2010. p. e10455.

296. Nicchia, G.P., et al., *Aquaporin-4 orthogonal arrays of particles are the target for neuromyelitis optica autoantibodies.* Glia, 2009. **57**(13): p. 1363-73.

297. Pisani, F., et al., *Identification of Two Major Conformational Aquaporin-4 Epitopes for Neuromyelitis Optica Autoantibody Binding*, in *J. Biol. Chem.* 2011. p. 9216-9224.

298. Iorio, R., et al., *Astrocytic autoantibody of neuromyelitis optica (NMO-IgG) binds to aquaporin-4 extracellular loops, monomers, tetramers and high order arrays*, in *Journal of Autoimmunity*. 2013. p. 21-27.

299. Owens, G.P., et al., *Mutagenesis of the aquaporin 4 extracellular domains defines restricted binding patterns of pathogenic neuromyelitis optica IgG.*, in *J. Biol. Chem.* 2015. p. 12123-12134.

300. Tradtrantip, L., et al., *Anti-aquaporin-4 monoclonal antibody blocker therapy for neuromyelitis optica*, in *Ann. Neurol.* 2012. p. 314-322.

301. Jarius, S. and B. Wildemann, *AQP4 antibodies in neuromyelitis optica: diagnostic and pathogenetic relevance.*, in *Nat Rev Neurol*. 2010. p. 383-392.

302. Kalluri, S.R., et al., *Quantification and functional characterization of antibodies to native aquaporin 4 in neuromyelitis optica.* Arch Neurol, 2010. **67**(10): p. 1201-8.

303. Owens, G.P., et al., *Antibodies produced by clonally expanded plasma cells in multiple sclerosis cerebrospinal fluid*, in *Ann. Neurol.* 2009. p. 639-649.

304. Kowarik, M.C., et al., *The cerebrospinal fluid immunoglobulin transcriptome and proteome in neuromyelitis optica reveals central nervous system-specific B cell populations.* J Neuroinflammation, 2015. **12**: p. 19.

305. Bradl, M., et al., *Neuromyelitis optica: pathogenicity of patient immunoglobulin in vivo.* Ann Neurol, 2009. **66**(5): p. 630-43.

306. Phuan, P.-W., et al., *Complement-dependent cytotoxicity in neuromyelitis optica requires aquaporin-4 protein assembly in orthogonal arrays*, in *J. Biol. Chem.* 2012. p. 13829-13839.

307. Ratelade, J., J.L. Bennett, and A.S. Verkman, *Evidence against cellular internalization in vivo of NMO-IgG, aquaporin-4, and excitatory amino acid transporter 2 in neuromyelitis optica*, in *J. Biol. Chem.* 2011. p. 45156-45164.

308. Saadoun, S., et al., *Intra-cerebral injection of neuromyelitis optica immunoglobulin G and human complement produces neuromyelitis optica lesions in mice*, in *Brain*. 2010. p. 349-361.

309. Wrzos, C., et al., *Early loss of oligodendrocytes in human and experimental neuromyelitis optica lesions.*, in *Acta Neuropathol.* 2013.

310. Zhang, H. and A.S. Verkman, *Eosinophil pathogenicity mechanisms and therapeutics in neuromyelitis optica.* J Clin Invest, 2013. **123**(5): p. 2306-16.

311. Saadoun, S., et al., *Neutrophil protease inhibition reduces neuromyelitis optica-immunoglobulin G-induced damage in mouse brain.* Ann Neurol, 2012. **71**(3): p. 323-33.

312. Saadoun, S., et al., *T cell deficiency does not reduce lesions in mice produced by intracerebral injection of NMO-IgG and complement.* J Neuroimmunol, 2011. **235**(1-2): p. 27-32.

313. Zhang, H., J.L. Bennett, and A.S. Verkman, *Ex vivo spinal cord slice model of neuromyelitis optica reveals novel immunopathogenic mechanisms.* Ann Neurol, 2011. **70**(6): p. 943-54.

314. Hinson, S.R., et al., *Aquaporin-4-binding autoantibodies in patients with neuromyelitis optica impair glutamate transport by down-regulating EAAT2.* J Exp Med, 2008. **205**(11): p. 2473-81.

315. Kolaczkowska, E. and P. Kubes, *Neutrophil recruitment and function in health and inflammation.* Nat Rev Immunol, 2013. **13**(3): p. 159-75.

316. Beyrau, M., J.V. Bodkin, and S. Nourshargh, *Neutrophil heterogeneity in health and disease: a revitalized avenue in inflammation and immunity.* Open Biol, 2012. **2**(11): p. 120134.

317. Mestas, J. and C.C. Hughes, *Of mice and not men: differences between mouse and human immunology.* J Immunol, 2004. **172**(5): p. 2731-8.

318. Abbe, E., *Beiträge zur Theorie des Mikroskops und der mikroskopischen Wahrnehmung*, in *Archiv f. mikrosk. Anatomie*. 1873. p. 413-418.

319. Hell, S.W., *Far-field optical nanoscopy.*, in *Science*. 2007. p. 1153-1158.

320. Hell, S.W. and J. Wichmann, *Breaking the diffraction resolution limit by stimulated emission: stimulated-emission-depletion fluorescence microscopy*, in *Opt. Lett., OL*. 1994, Optical Society of America. p. 780-782.

321. Willig, K.I., et al., *STED microscopy reveals that synaptotagmin remains clustered after synaptic vesicle exocytosis.*, in *Nature*. 2006. p. 935-939.

322. Chojnacki, J., et al., *Maturation-dependent HIV-1 surface protein redistribution revealed by fluorescence nanoscopy.*, in *Science*. 2012. p. 524-528.

323. Heller, I., et al., *STED nanoscopy combined with optical tweezers reveals protein dynamics on densely covered DNA.*, in *Nat. Methods*. 2013. p. 910-916.

324. Lau, L., et al., *STED microscopy with optimized labeling density reveals 9-fold arrangement of a centriole protein.*, in *Biophys. J.* 2012. p. 2926-2935.

325. Silberstein, C., R. Bouley, and Y. Huang, *Membrane organization and function of M1 and M23 isoforms of aquaporin-4 in epithelial cells*, in *American Journal of ….* 2004.

326. Okuyama, K., et al., *High-resolution structures of collagen-like peptides [(Pro-Pro-Gly) 4-Xaa-Yaa-Gly-(Pro-Pro-Gly) 4]: Implications for triple-helix hydration and Hyp(X) puckering*, in *Biopolymers*. 2009. p. 361-372.

327. Rainey, J.K. and M.C. Goh, *A statistically derived parameterization for the collagen triple‐helix*, in *Protein Science*. 2002.

328. Fahmy, M.F., et al., *A New Fast Iterative Blind Deconvolution Algorithm*, in *Journal of Signal and Information Processing*. 2012, Scientific Research Publishing. p. 98.

329. Fish DA, B.A., Pike ER, Walker JG, *Blind Deconvolution by Means of the Richardson-Lucy Algorithm.* Journal of the Optical Society of America a-Optics Image Science and Vision, 1995(12).

330. Crane, J.M. and A.S. Verkman, *Determinants of aquaporin-4 assembly in orthogonal arrays revealed by live-cell single-molecule fluorescence imaging*, in *J Cell Sci*. 2009. p. 813-821.

331. Ido, S., et al., *Immunoactive two-dimensional self-assembly of monoclonal antibodies in aqueous solution revealed by atomic force microscopy.*, in *Nat Mater*. 2014. p. 264-270.

332. Preiner, J., et al., *IgGs are made for walking on bacterial and viral surfaces*, in *Nature*. 2014.

333. Göttfert, F., et al., *Coaligned dual-channel STED nanoscopy and molecular diffusion analysis at 20 nm resolution.*, in *Biophys. J.* 2013. p. L01-3.

334. Westphal, V. and S.W. Hell, *Nanoscale resolution in the focal plane of an optical microscope.*, in *Phys. Rev. Lett.* 2005. p. 143903.

335. Ratelade, J. and A.S. Verkman, *Neuromyelitis optica: Aquaporin-4 based pathogenesis mechanisms and new therapies*, in *Int J Biochem Cell Biol*. 2012. p. 1519-1530.

336. Lachmann, P.J. and N.C. Hughes-Jones, *Initiation of complement activation*, in *Springer Semin Immunopathol*. 1984. p. 143-162.

337. Ricklin, D., et al., *Complement: a key system for immune surveillance and homeostasis.*, in *Nat. Immunol.* 2010. p. 785-797.

338. Phuan, P.-W., et al., *C1q-targeted monoclonal antibody prevents complement-dependent cytotoxicity and neuropathology in in vitro and mouse models of neuromyelitis optica*, in *Acta Neuropathol.* 2013. p. 829-840.

339. Nytrova, P., et al., *Complement activation in patients with neuromyelitis optica*, in *Journal of ...*. 2014.

340. Lucchinetti, C.F., et al., *A role for humoral mechanisms in the pathogenesis of Devic's neuromyelitis optica.*, in *Brain*. 2002. p. 1450-1461.

341. DeLano, W.L., et al., *Convergent solutions to binding at a protein-protein interface*, in *Science*. 2000. p. 1279-1283.

342. Pittock, S.J., et al., *Neuromyelitis optica brain lesions localized at sites of high aquaporin 4 expression.*, in *Arch. Neurol.* 2006. p. 964-968.

343. Verkman, A.S., *Aquaporins in clinical medicine*, in *Annu Rev Med*. 2012. p. 303-316.

344. McCullough, J.W., B. Renner, and J.M. Thurman, *The role of the complement system in acute kidney injury.*, in *Semin. Nephrol.* 2013. p. 543-556.

345. Martinez-Hernandez, E., et al., *Analysis of complement and plasma cells in the brain of patients with anti-NMDAR encephalitis.*, in *Neurology*. 2011. p. 589-593.

346. Hughes, E.G., et al., *Cellular and synaptic mechanisms of anti-NMDA receptor encephalitis.*, in *J. Neurosci.* 2010. p. 5866-5875.

347. Engel, A.G. and G. Fumagalli, *Mechanisms of acetylcholine receptor loss from the neuromuscular junction*, in *Receptors*. 1982.

348. Drachman, D.B., C.W. Angus, and R.N. Adams, *Myasthenic antibodies cross-link acetylcholine receptors to accelerate degradation*, in *... England Journal of ...*. 1978.

349. Tüzün, E. and P. Christadoss, *Complement associated pathogenic mechanisms in myasthenia gravis.*, in *Autoimmun Rev*. 2013. p. 904-911.

350. Tradtrantip, L., N. Asavapanumas, and A.S. Verkman, *Therapeutic cleavage of anti-aquaporin-4 autoantibody in neuromyelitis optica by an IgG-selective proteinase*, in *Mol Pharmacol*. 2013. p. 1268-1275.

351. Thurman, J.M., et al., *Detection of complement activation using monoclonal antibodies against C3d.*, in *J. Clin. Invest.* 2013. p. 2218-2230.

352. Lewis, L.A. and S. Ram, *Meningococcal disease and the complement system*, in *Virulence*. 2014.

353. Trouw, L.A., et al., *Anti-C1q autoantibodies deposit in glomeruli but are only pathogenic in combination with glomerular C1q-containing immune complexes.*, in *J. Clin. Invest.* 2004. p. 679-688.

354. Owens, G.P., et al., *Screening random peptide libraries with subacute sclerosing panencephalitis brain-derived recombinant antibodies identifies multiple epitopes in the C-terminal region of the measles virus nucleocapsid protein.*, in *J. Virol.* 2006. p. 12121-12130.

355. Jarius, S., et al., *Testing for antibodies to human aquaporin-4 by ELISA: sensitivity, specificity, and direct comparison with immunohistochemistry.* J Neurol Sci, 2012. **320**(1-2): p. 32-7.

356. Kowarik, M.C., J. Soltys, and J.L. Bennett, *The treatment of neuromyelitis optica.* J Neuroophthalmol, 2014. **34**(1): p. 70-82.

357. Bruck, W., et al., *Neuromyelitis optica lesions may inform multiple sclerosis heterogeneity debate.*, in *Ann. Neurol.* 2012. p. 385-394.

358. Asavapanumas, N., J. Ratelade, and A.S. Verkman, *Unique neuromyelitis optica pathology produced in naive rats by intracerebral administration of NMO-IgG.* Acta Neuropathol, 2014. **127**(4): p. 539-51.

359. Mallon, B.S., et al., *Proteolipid promoter activity distinguishes two populations of NG2-positive cells throughout neonatal cortical development.* J Neurosci, 2002. **22**(3): p. 876-85.

360. Blauth, K., et al., *Antibodies produced by clonally expanded plasma cells in multiple sclerosis cerebrospinal fluid cause demyelination of spinal cord explants.*, in *Acta Neuropathol.* 2015. p. 765-781.

361. Thurman, J.M., et al., *A novel inhibitor of the alternative complement pathway prevents antiphospholipid antibody-induced pregnancy loss in mice.* Mol Immunol, 2005. **42**(1): p. 87-97.

362. Ratelade, J., A.J. Smith, and A.S. Verkman, *Human immunoglobulin G reduces the pathogenicity of aquaporin-4 autoantibodies in neuromyelitis optica.*, in *Exp. Neurol.* 2014. p. 145-153.

363. Tradtrantip, L., et al., *Potential therapeutic benefit of C1-esterase inhibitor in neuromyelitis optica evaluated in vitro and in an experimental rat model.* PLoS One, 2014. **9**(9): p. e106824.

364. Parekh, R.B., et al., *Association of rheumatoid arthritis and primary osteoarthritis with changes in the glycosylation pattern of total serum IgG.* Nature, 1985. **316**(6027): p. 452-7.

365. Tradtrantip, L., et al., *Anti-aquaporin-4 monoclonal antibody blocker therapy for neuromyelitis optica.* Ann Neurol, 2012. **71**(3): p. 314-22.

366. Crane, J.M., et al., *Binding affinity and specificity of neuromyelitis optica autoantibodies to aquaporin-4 M1/M23 isoforms and orthogonal arrays.* J Biol Chem, 2011. **286**(18): p. 16516-24.

367. Weil, M.T., et al., *Loss of Myelin Basic Protein Function Triggers Myelin Breakdown in Models of Demyelinating Diseases.* Cell Rep, 2016. **16**(2): p. 314-22.

368. Ratelade, J. and A.S. Verkman, *Inhibitor(s) of the classical complement pathway in mouse serum limit the utility of mice as experimental models of neuromyelitis optica.*, in *Mol. Immunol.* 2014. p. 104-113.

369. Lux, A. and F. Nimmerjahn, *Impact of differential glycosylation on IgG activity.* Adv Exp Med Biol, 2011. **780**: p. 113-24.

370. Lux, A., et al., *Impact of immune complex size and glycosylation on IgG binding to human FcgammaRs.* J Immunol, 2013. **190**(8): p. 4315-23.

371. Bai, X.-c., et al., *An atomic structure of human [ggr]-secretase.* Nature, 2015. **525**(7568): p. 212-217.

372. Bally, I., et al., *Identification of the C1q-binding Sites of Human C1r and C1s: a refined three-dimensional model of the C1 complex of complement.*, in *J. Biol. Chem.* 2009. p. 19340-19348.

373. Verkman, A.S., et al., *Biology of AQP4 and anti-AQP4 antibody: therapeutic implications for NMO.* Brain Pathol, 2013. **23**(6): p. 684-95.

374. Papadopoulos, M.C. and A.S. Verkman, *Aquaporin 4 and neuromyelitis optica.*, in *Lancet Neurol*. 2012. p. 535-544.

375. Chang, H., et al., *A unique series of reversibly switchable fluorescent proteins with beneficial properties for various applications.* Proceedings of the National Academy of Sciences, 2012. **109**(12): p. 4455-4460.

376. Doi, H., et al., *Hypercomplementemia at relapse in patients with anti-aquaporin-4 antibody.* Mult Scler, 2009. **15**(3): p. 304-10.

377. Wang, H., et al., *Increased soluble C5b-9 in CSF of neuromyelitis optica.* Scand J Immunol, 2014. **79**(2): p. 127-30.

378. Kuroda, H., et al., *Increase of complement fragment C5a in cerebrospinal fluid during exacerbation of neuromyelitis optica.* J Neuroimmunol, 2013. **254**(1-2): p. 178-82.

379. Chen, Y., et al., *The complement and immunoglobulin levels in NMO patients.* Neurol Sci, 2014. **35**(2): p. 215-20.

380. Brown, A.M., et al., *Astrocyte glycogen metabolism is required for neural activity during aglycemia or intense stimulation in mouse white matter*, in *J. Neurosci. Res.* 2005. p. 74-80.

381. Harlow, D.E., et al., *Myelin Proteolipid Protein Complexes with αv Integrin and AMPA Receptors In Vivo and Regulates AMPA-Dependent Oligodendrocyte Progenitor Cell Migration through the Modulation of Cell-Surface GluR2 Expression.* The Journal of Neuroscience, 2015. **35**(34): p. 12018-12032.

382. Mitchell, D.A., et al., *C1q deficiency and autoimmunity: the effects of genetic background on disease expression.* J Immunol, 2002. **168**(5): p. 2538-43.